University of Kentucky
UKnowledge

Theses and Dissertations--Civil Engineering

Civil Engineering

2013

Unsaturated Soil Parameters From Field Stiffness Measurements

Jason M. Curd
University of Kentucky, jmcurd2@gmail.com

Click here to let us know how access to this document benefits you.

Recommended Citation

Curd, Jason M., "Unsaturated Soil Parameters From Field Stiffness Measurements" (2013). *Theses and Dissertations--Civil Engineering*. 11.
https://uknowledge.uky.edu/ce_etds/11

This Master's Thesis is brought to you for free and open access by the Civil Engineering at UKnowledge. It has been accepted for inclusion in Theses and Dissertations--Civil Engineering by an authorized administrator of UKnowledge. For more information, please contact UKnowledge@lsv.uky.edu.

STUDENT AGREEMENT:

I represent that my thesis or dissertation and abstract are my original work. Proper attribution has been given to all outside sources. I understand that I am solely responsible for obtaining any needed copyright permissions. I have obtained and attached hereto needed written permission statements(s) from the owner(s) of each third-party copyrighted matter to be included in my work, allowing electronic distribution (if such use is not permitted by the fair use doctrine).

I hereby grant to The University of Kentucky and its agents the non-exclusive license to archive and make accessible my work in whole or in part in all forms of media, now or hereafter known. I agree that the document mentioned above may be made available immediately for worldwide access unless a preapproved embargo applies.

I retain all other ownership rights to the copyright of my work. I also retain the right to use in future works (such as articles or books) all or part of my work. I understand that I am free to register the copyright to my work.

REVIEW, APPROVAL AND ACCEPTANCE

The document mentioned above has been reviewed and accepted by the student's advisor, on behalf of the advisory committee, and by the Director of Graduate Studies (DGS), on behalf of the program; we verify that this is the final, approved version of the student's dissertation including all changes required by the advisory committee. The undersigned agree to abide by the statements above.

Jason M. Curd, Student

Dr. L. Sebastian Bryson, Major Professor

Dr. Y Wang, Director of Graduate Studies

UNSATURATED SOIL PARAMETERS FROM FIELD STIFFNESS MEASUREMENTS

THESIS

A thesis submitted in partial fulfillment of the
requirements for the degree of Master of Science in
Civil Engineering in the
College of Engineering
at the University of Kentucky

By

Jason Michael Curd

Lexington, Kentucky

Director: Dr. L. Sebastian Bryson, Associate Professor of Civil Engineering

Lexington, Kentucky

2013

Copyright© Jason Michael Curd 2013

ABSTRACT OF THESIS

UNSATURATED SOIL PARAMETERS FROM FIELD STIFFNESS MEASUREMENTS

The behavior of unsaturated soils depends heavily on material properties and soil conditions. In Geotechnical Engineering, compacted soils are frequently used as fill material, and quality control is vital to the construction process. There are few methods available to estimate the parameters associated with unsaturated soils based on field measurements, and a relationship between these factors could reduce testing time and lower construction costs.

Undrained triaxial tests were performed on four clays representing a range of material properties in an effort to reach the maximum dry density, which provides the highest bearing capacity. Each clay was compacted at optimum moisture content, as well as wet and dry of optimum. Measurements were taken using the GeoGauge and shear wave velocities. An empirical approach was used to estimate the effect of a density gradient on soil suction.

A relationship between the normal stress and matric suction produced a strong trend when plotted against a function of stiffness and the void ratio, which represents a density gradient. Another relationship between the GeoGauge and shear wave stiffness measurements was found, but no relationship with the material properties of the samples was observed, indicating that more in-depth research is needed to find a stronger relationship.

KEYWORDS: Unsaturated Soil Mechanics, Shear Modulus, Soil Stiffness, Shear Wave Velocity, GeoGauge

UNSATURATED SOIL PARAMETERS FOR FIELD STIFFNESS MEASUREMENTS

By

Jason Michael Curd

Dr. L. Sebastian Bryson

Director of Thesis

Dr. Yi-Tin Wang

Director of Graduate Studies

To:
My Parents: Denise and Michael Curd
My Stepmother: Melissa Curd
My Grandparents: Jean Whitfield and JoAnn Curd

As well as the rest of my family and friends
for all of their constant love, encouragement, and support

And most importantly,

Thank the Lord, because without him, none of this would be possible

ACKNOWLEDGEMENTS

First of all, I would like to thank Dr. Sebastian Bryson, my graduate advisor, for his guidance and assistance throughout my undergraduate and graduate career at the University of Kentucky. His knowledge, continuous support, and encouragement gave me the self-confidence and personal drive to achieve this level of higher education. I am absolutely certain that the skills and knowledge I have obtained from Dr. Bryson will be a valuable asset as I transition into the working field as a Geotechnical Engineer.

I would like to give a special thanks to my professors, Dr. Michael Kalinski, and Dr. George Blandford, as well as the office staff in the Civil Engineering office, Suzy Wampler and Sheila Williams. Their assistance and dedication was extremely helpful and will always be appreciated. None of this would have been possible without the help of my colleague, Corrie Walton-Macauley, who co-conducted this research as a part of his Ph.D. dissertation. Thanks to his assistance, advanced knowledge, and dedication, the laboratory testing was conducted properly and efficiently. I would like to thank my classmates, Isabel Gomez-Gutierrez, Travis Greenwell, Joe Goodin, Amanda Loathes, Derrick Dennison, and Jordan Kirkendoll. These individuals were my classmates, and were always willing to lend a hand. I have been very fortunate to make so many friends during my career at The University of Kentucky.

Last, but not least, I would like to express my gratitude to my thesis defense committee, Dr. Bryson, Dr. Kalinski, and Dr. Woolery. I felt extremely fortunate to have these individuals take the time to review this material and provide invaluable feedback. It is an honor to have my work reviewed by such esteemed and experienced members of the Civil Engineering and Mining Engineering professions.

TABLE OF CONTENTS

LIST OF TABLES

LIST OF FIGURES

1 INTRODUCTION

1.1 Synopsis of Problem

The general behavior of unsaturated soils under various field conditions can be difficult to predict without soil sampling and laboratory testing. Within the past decade, the GeoGauge, manufactured by Humboldt, has been introduced for determining the shear modulus and stiffness of compacted soils. This device measures soil stiffness to a depth of approximately 230 mm, which is the thickness of a typical compacted soil layer. If a relationship between data produced from a portable device such as the GeoGauge, and data from controlled laboratory testing (e.g. unconfined compression testing, or triaxial testing), the construction process could potentially be drastically shortened by reducing the need for soil sampling and laboratory testing

Soil stiffness, k, is directly related to the shear modulus, G. Stiffness describes the tendency of a soil to deform under various loading conditions and is a vital component to the overall integrity of any geotechnical design. Inadequate evaluation of soil stiffness could result in failure, causing catastrophic damages and even loss of life. Today, the determination of soil stiffness requires extensive laboratory work which delays field work and is extremely expensive. The most common laboratory method to determine stiffness requires an evaluation of the stress-strain curve from triaxial testing. The slope of the stress-strain curve provides the elastic modulus (or Young's modulus), and can be used to calculate the shear modulus using Poisson's ratio. For this research, the shear modulus was also found by using the elastic theory equation, which is a function of soil density and the shear wave velocity.

From insitu shear wave velocity measurements taken from a soil sample subjected to simulated, real-time stress conditions could be simulated. A relationship between the insitu stiffness data and soil properties common in field conditions. The shear velocity measurements make it possible to analyze the effect of density and depth on stiffness. A relationship between GeoGauge and shear wave velocity stiffness values could allow the GeoGauge to be used on-site to determine stiffness. This could drastically cut back on laboratory costs and even shorten the overall construction process.

1.2 Proposed Concept

Comparing GeoGauge and shear wave stiffness data could yield a relationship used to decrease the need for some laboratory testing. Using the GeoGauge to provide stiffness data could also facilitate real-time predictions of geotechnical behavior. The proposed concept of this thesis is to evaluate the parameters (e.g. moisture and density) that influence the GeoGauge measurements of stiffness and identify relationships between GeoGauge and shear wave velocity measurements.

1.3 Objectives of Research

Since all of the material properties (e.g. plasticity index, liquid limit, clay fraction, percent fines, and specific gravity) were determined through previous research, further investigation was conducted in order to plot the state-dependent parameters for the soils (e.g. void ratio, degree of saturation, gravitational and volumetric water content, dry density, shear wave velocity, etc.) against their defining material properties (e.g. Atterberg limits). If a relationship were to be found between these two methods, and held true for multiple soils in various moisture conditions, a more generic expression could be used to predict soil suction and shear wave velocity based shear modulus based on GeoGauge

stiffness data. Furthermore, a relationship between tested data and soil material properties could be used with a much more broad range of soils in various soil conditions.

The primary goals of this research were to:

- Perform undrained triaxial load tests on four Kentucky clays at four various moisture contents which were at, above, and below the optimum moisture content. For each test, the clay was compacted as close as possible to the maximum dry density, MDD. This was the most critical objective due to the fact that soils exhibit the highest possible bearing capacity at the maximum dry density.
- Measure shear wave travel times at various stages of compaction in order to calculate the shear wave velocity and shear modulus of the soil. The shear wave velocities are required for determining the shear modulus, G, of a soil based on the elastic theory equation.
- Record GeoGauge stiffness and modulus readings after each load increment to analyze the changes in stiffness as a function of dry density. This will allow the GeoGauge stiffness to be compared to the shear wave stiffness at various stages of compaction, showing the relationship between soil stiffness and dry density.
- Use an empirical approach to estimate soil suction at a specific degree of saturation, void ratio, and net normal stress. Due to the fact that there was no live measurement to record the matric suction, an empirical approach was considered. This also would make it possible to predict the matric suction of a soil based on GeoGauge readings and other state-dependent parameters.

- Determine a possible correlation between the shear modulus derived from shear wave velocity measurements and GeoGauge shear modulus values. If found, this relationship could change the modern method for determining soil stiffness, bypassing extensive and costly laboratory testing.
- Develop a physical model which predicts the shear wave velocity (therefore shear modulus) of a soil based on GeoGauge readings. This would be incredibly beneficial, financially and in terms of project duration.
- Use the data acquired from laboratory testing on four Kentucky clays to derive a relationship which would allow constant values to be determined for any soil based on certain material properties. By using a relationship between the GeoGauge and shear wave velocities, the parameters could be related to soil material properties, which would make the relationship valid for many types of soil as opposed to only being reliable for the soils being tested.

1.4 Contents of Thesis

- Chapter 2 provides a technical background of the basic knowledge needed for a general understanding of unsaturated soil mechanics. These principles include the general concepts of unsaturated soils (e.g. the three zones of unsaturated soil particles, soil suction and the soil-water characteristic curve, and soil stiffness).
- Chapter 3 explains the methodology used for this research and laboratory testing. This chapter also provides a description of the equipment and materials used, along with a detailed description of the testing procedure. A detailed

description of the test soils and their respective material properties is provided as well.

- Chapter 4 describes the correction function used to determine the corrected dry density, and the effect of the dry density on soil parameters (e.g. the shear wave velocity and stiffness). A method for determining the suction based on an empirical approach introduced by Zhou et al. (2012) is also included, and the relationship between the matric suction and net normal stress is also discussed.
- Chapter 5 explains the method used to predict the matric suction based on GeoGauge stiffness data and other parameters. These suction values are compared to the values from Zhou et al. (2012) to check accuracy. This chapter also provides an equation to predict the stiffness from laboratory in situ testing (e.g. shear wave velocity readings) of a soil sample based on GeoGauge stiffness readings. The final section of Chapter 5 examines the fidelity of the relationship as well as an attempt to correlate the relationship to material properties. Recommendations for further research are provided at the end of this chapter.

2 TECHNICAL BACKGROUND

2.1 Soil Stiffness

Soil stiffness is an extremely critical parameter in the geotechnical aspect of the construction process. It provides ground deformation information to engineers for small strain levels (Salem et al. (2006). Several researchers have investigated the stiffness of unsaturated compacted clays at small strains. The general expression to derive soil stiffness is provided in Equation 1.

$$K = P / \delta \quad (1)$$

where P refers to the normal stress and δ is the deflection. The shear modulus, G, can be used to measure soil stiffness. The shear modulus (or modulus of rigidity) is defined as the ratio of shear stress to shear strain. The stiffness and shear modulus of a soil go hand in hand with one another, and the shear modulus can be calculated based on stiffness and known values of Poisson's ratio, ν, and Young's modulus (or elastic modulus), E.

Laboratory testing is a very efficient way to evaluate the strength and stiffness behavior of a soil in field conditions. Laboratory testing is non-destructive, and allows various situations to be simulated under controlled variables such as traffic (loading and unloading) and shaking (seismic) conditions. Current methods for determining the shear modulus and stiffness of soil include triaxial testing, cyclic triaxial testing, resonant column testing, and bender element testing. For cyclic triaxial testing, the shear modulus is determined by applying three to four stages of varying cyclic loading about an ambient load and a set frequency and applying around five loads at each stage. Resonant Column Testing (RC Testing) consists of a soil column in fixed-free conditions and is vibrated at

preset frequencies to determine the shear wave velocity. With the shear wave velocity, the shear modulus can be calculated as a function of the soil's density. Bender element testing is the most similar testing method to what was performed for this research. This method measures the shear modulus from shear wave velocity measurements traveling through a soil sample. (Takkabutr, 2006)

There are portable devices available to measure soil stiffness, such as the Humboldt GeoGauge, which measure soil stiffness and elastic modulus by placing the device on the soil surface. If the GeoGauge were to show a direct relationship with laboratory testing data, a great deal of efficiency could be added to the construction process by eliminating the financial and time restraints associated with laboratory testing and provide direct on-site measurements.

The GeoGauge weighs 10 kg and has a diameter of 280 mm. For application, the device is placed on the soil surface via the ring-shaped foot, which has an outside diameter of 114 mm and an inside diameter of 89 mm, providing an annular ring thickness of 13 mm. The foot comes in direct contact with the soil, and the weight of the GeoGauge is supported by rubber isolators, which is shown in Figure 2.1. There is also a shaker which drives the foot and sensors that measure the force and displacement frequency of the foot. Minimal preparation is needed for the soil surface to utilize the GeoGauge. However, a slight rotation of no more than 90 degrees is typically needed to obtain full contact between the foot and the soil surface.

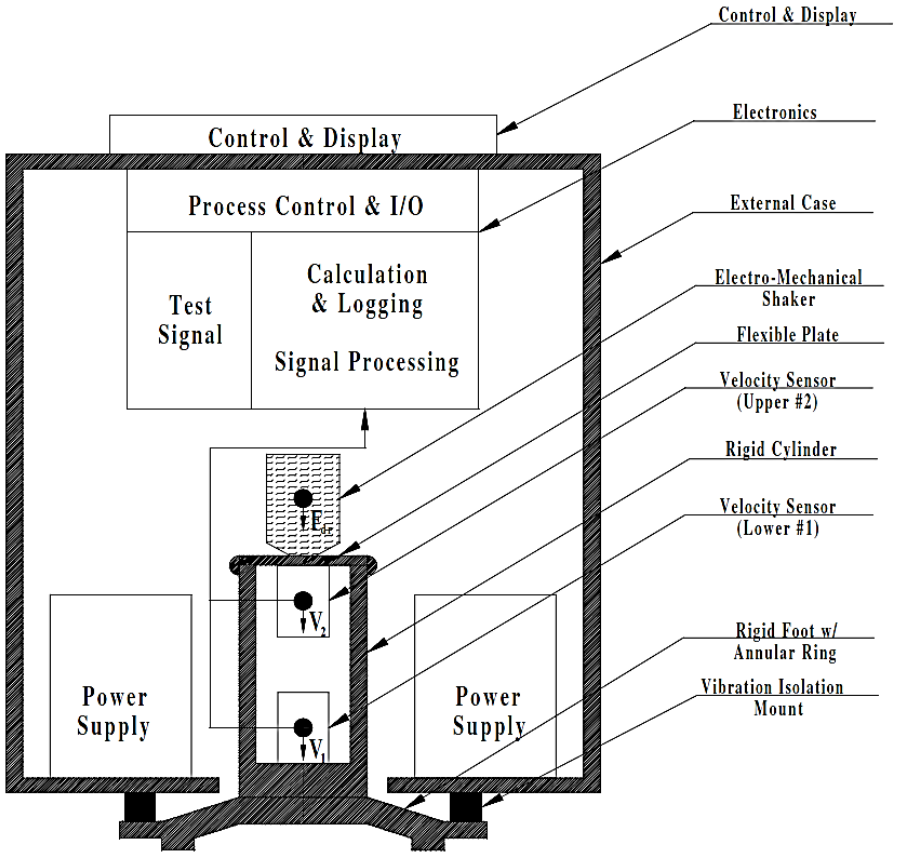

Figure 2.1: GeoGauge schematic and cross-section (Lenke et. al. 2003)

The GeoGauge vibrates and produces small changes in force causing very small deflections. The deflection resulting from the GeoGauge weight is not accounted for. The soil deflection, δ , is proportional to the outside radius of the ring foot, R (57 mm), Young's modulus, E , shear modulus, G , and Poisson's ratio, υ , of the soil. The stiffness is the ratio of the force to displacement, and was provided in Equation 1.

$$K = P / \delta \qquad (1)$$

The GeoGauge produces soil stress levels commonly encountered with pavement and foundation applications, which are around 27.6 kPa (Humboldt, 2007). Young's modulus and shear modulus can be determined from the GeoGauge measurements if a Poisson's

ratio is assumed, as shown in Figure 2.2. The “plate load” test setup, provided in Equation 2, shows how a Young’s modulus value could be calculated by measuring a given load placed on a soil sample via a round plate, and comparing it to the measured displacement. The “GeoGauge loading”, provided in Equation 3, also shows how a Young’s modulus value could be calculated by measuring a given load placed on a soil sample via a ring-shaped foot, and comparing it to a measured displacement.

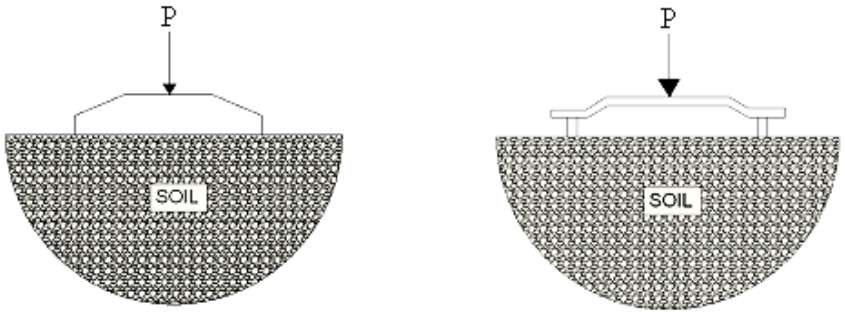

Figure 2.2: Loading setup: General plate load (L) and GeoGauge loading (R)

Plate load test (general):

$$P = \frac{2RE}{(1+\nu^2)}\delta = \frac{4RG}{(1-\nu)}\delta \qquad (2)$$

$$K = \frac{P}{\delta} = \frac{2RE}{(1-\nu^2)} \qquad (3)$$

GeoGauge loading (Humboldt, 2007):

$$P = \frac{1.77RE}{(1+\nu^2)}\delta \approx \frac{3.54RG}{(1-\nu)}\delta \quad (4)$$

$$K = \frac{P}{\delta} \approx \frac{1.77RE}{(1-\nu^2)} \quad (5)$$

Equation 4 and Equation 5 assume that the underlying soil is linear elastic, homogeneous, and isotropic. They also assume an infinite half-space. The assumptions of homogeneity, isotropy, and elasticity are frequently invoked in soil mechanics and pavement design when soil layers are analyzed. These assumptions can be roughly assumed to be valid for applications involving geomaterials under conditions of small operating strains. However, the assumption of an infinite half-space is questioned when the consideration that underlying pavement layers are generally of finite depth and are of increasing modulus with depth. However, the question of reliability is not accounted for due to the fact that GeoGauge vibrations are very small, and only affect a very small depth.

From Equation 4, the shear modulus, G_{SSG}, can be calculated based on the values of Poisson ratio, and Young's Modulus, since the radius, and displacement values cancel out when they are set equal to one another. Equation 6 provides the expression to determine the shear modulus based on the GeoGauge stiffness readings.

$$G_{SSG} = \frac{1.77*(1-v)*E}{3.54*(1+v)^2} \quad (6)$$

There is a need for additional research in obtaining soil stiffness and shear modulus in the field, especially for clayey soils. However, field methods used to develop stiffness profiles of soil layers are expensive and require heavy machinery. There are many assumptions made for laboratory work (e.g. isotropic, homogeneous soil), but previous studies have been conducted and suggest an agreement between laboratory results and field results. Schneider et al., (1999) conducted a study to compare field and laboratory measurements on piedmont residual silty sands. The findings from the study indicated that laboratory and field values for shear modulus matched closely. Also, overconsolidation ratios from laboratory data matched well with shear wave velocity data, and the shear wave data from the field matched well with laboratory data. However, according to Larsson et al., (1991), the shear modulus taken from laboratory testing tends to be smaller than direct field data for most clays. The reason for this is most likely caused by soil disturbance which occurs during the sampling process. For that reason, a strain-based correction factor could possibly be used for soft clays at strains greater than 10^{-6}. Therefore, laboratory work is appropriate and very much needed to evaluate the stiffness of clay soils and will provide a reasonable approximation of field conditions.

The effects of water content, degree of saturation, and density on the matric suction were analyzed. The relationships between stiffness, soil suction, and net stress were not determined to be unique, and outside factors such as the degree of compaction, saturation, and material properties played a heavy role in soil behavior. For soils compacted at similar densities, stiffness and matric suction both increased proportionally. Matric suction tends

to steadily decrease as compaction water content is increased, regardless of density or the degree of saturation, and shear wave velocities tend to decrease as the compaction water content increases. Soil fabric is the main determinant of the behavior of soil stiffness in relation to matric suction. The stiffness of soil depends primarily on the soil's state of stress. For all specimens tested by Salem et al. (2006), the matric suction steadily decreased as the compaction water content increased with no correlation to density or the degree of saturation.

The GeoGauge was evaluated as an alternative non-nuclear method for compaction control of highway materials, and it was concluded that the device performed very well for measuring stiffness. Tests showed that the moisture content of a cohesive soil had a substantial impact on stiffness, and that the optimum moisture content for maximum stiffness was not the same as the optimum moisture content for maximum density. The tests did not use a field target value for stiffness, and the results did not indicate that the GeoGauge could be used as a laboratory method for determining the target stiffness value. The recommendations for future research with the GeoGauge included careful control and monitoring of moisture content as well as monitoring soil stiffness with the GeoGauge throughout the compaction process in order to maximize the stiffness of subgrades. (Lenke et al., 2003)

An experiment was conducted using the GeoGauge to measure stiffness of a dry cohesion-less silica sand, and the results were compared to a computational estimate as a predicted stiffness value. The results showed an error of less than five percent, and it was concluded that the GeoGauge proved to be an excellent device for measuring the stiffness of underlying granular soil media. (Lenke et al., 1999)

Another test was conducted to evaluate the use of the GeoGauge as a non-destructive testing device to measure the stiffness/strength parameters of highway materials and embankment soils during and after construction. It was determined that the GeoGauge can indeed be used to evaluate the strength/stiffness properties of different pavement layers and embankments. The device was also able to determine the thickness of the soil layer being tested and detect weak points within compacted soil sections. (Nazzal, 2002)

2.2 Field methods for determining stiffness and shear modulus

Field measurements of shear wave velocity and shear modulus include crosshole tests (CHT), downhole tests (DHT), suspension logging, seismic reflection, seismic refraction, and spectral analysis of surface waves (SASW) Figure 2.3 provides details of the most common laboratory and field tests used to determine stiffness and shear modulus. (Schneider et al., 1999)

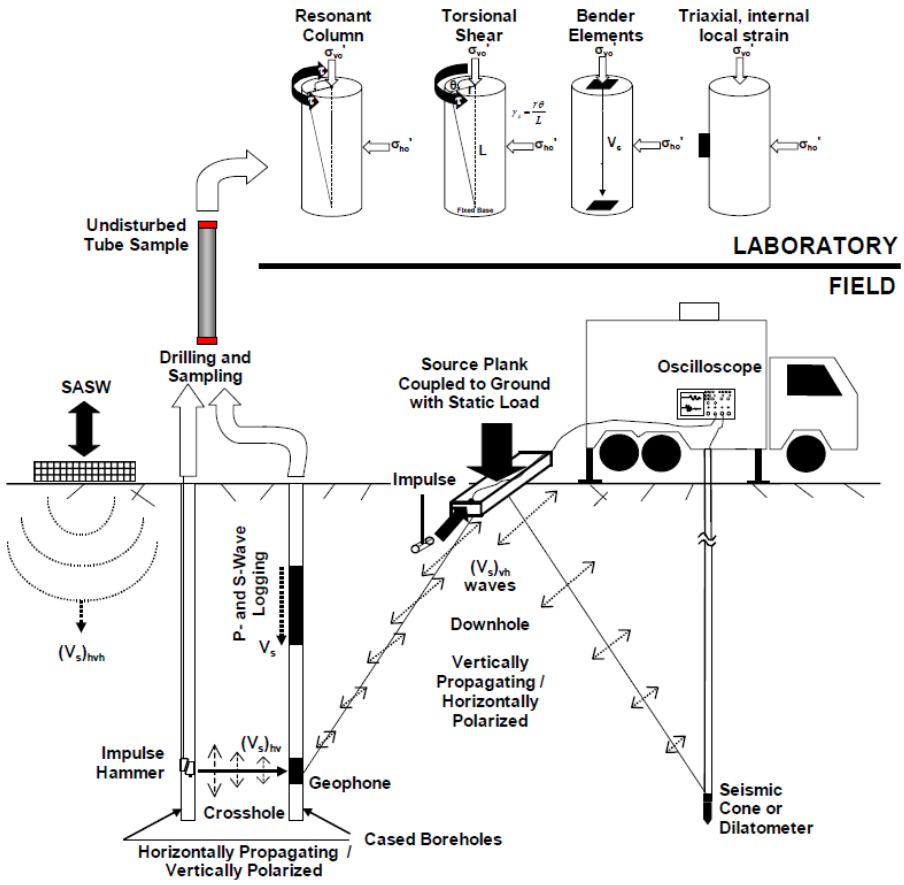

Figure 2.3: Common methods to determine stiffness (Schneider et al., 1999)

The SASW and crosshole seismic methods are the two methods which are closely related to the laboratory methods performed in this research. The GeoGauge operates solely at the surface of the soil, and is most closely related to the SASW method.

2.2.1 Crosshole Seismic Testing

Crosshole seismic testing is a technique which measures the travel times of body waves between adjacent boreholes in soil or rock. This method is most closely related to the laboratory testing which was conducted for this research. In accordance with ASTM D4428, this method is commonly used to analyze soil properties as a function of depth (e.g. a soil profile) when borehole drilling is allowed. Figure 2.4 provides a schematic diagram of the crosshole seismic testing method.

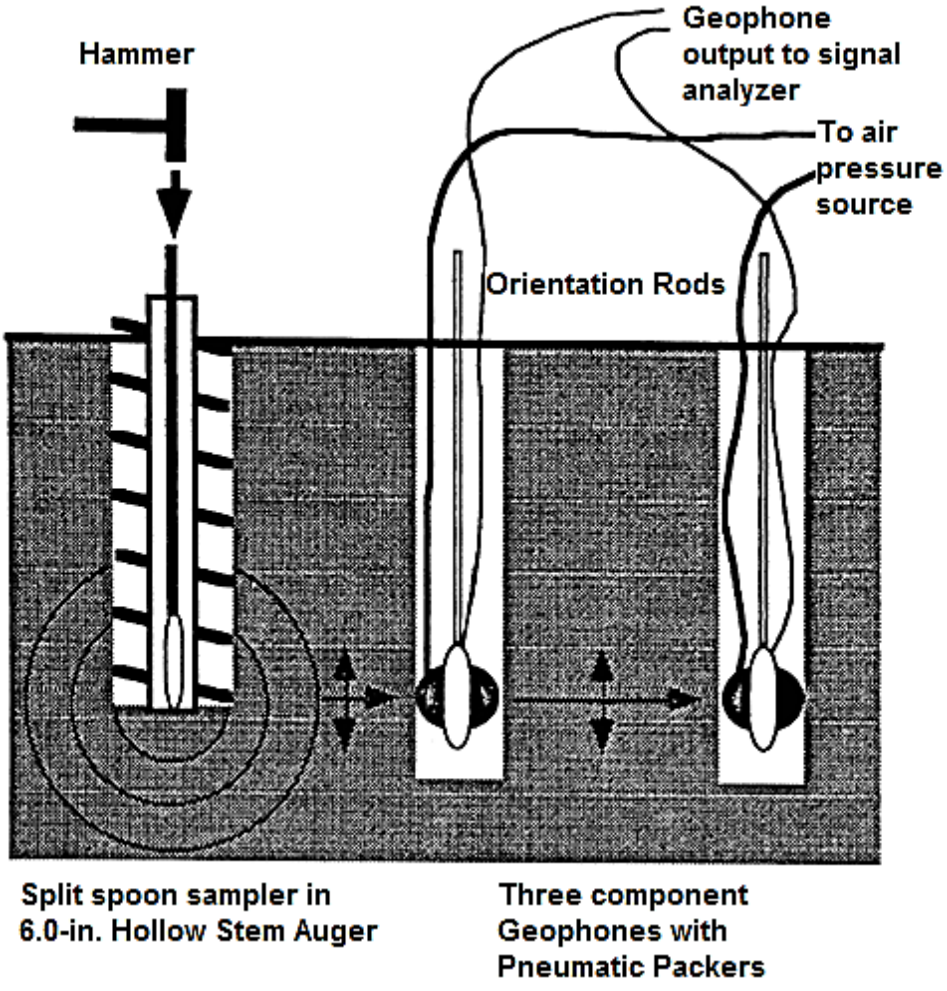

Figure 2.4: Crosshole Seismic Testing Method

Advantages of crosshole seismic testing include: (EPA, 2012)

- Allows a small amount of each layer to be sampled as far down as it is drilled, giving a more detailed seismic velocity profile.
- Makes it easier to determine the exact arrival times of the velocity waves.
- Obtain more detailed and specific geotechnical data (e.g. liquefaction, deformation, and strong motion characterization).
- Assess a complex layered velocity structure with alternating high and low relative velocities.

Disadvantages of crosshole seismic testing include: (EPA, 2012)

- Testing is usually related to the placement and testing of multiple drill locations. Many sites have strict regulations regarding drilling, sampling, and decontamination and require non-invasive techniques for reasons, such as hazardous surface conditions.
- Specialization in borehole completion is often required where P and S wave velocities are required, because drill hole completion must adhere to the ASTM procedures.
- Crosshole testing requires considerably more waveform analysis due to the refraction of high velocity layers when they reach the boundary of a higher or lower velocity layer.
- ASTM requirements are often costly to the construction budget.

2.2.2 Spectral Analysis of Surface Waves (SASW)

The Spectral Analysis of Surface Waves, or SASW is non-destructive method that utilizes the dispersion properties of surface waves in a layered system to quantify variations in stiffness with depth in accordance with ASTM D6758. This method is relatively new and provides an insitu method for determining shear wave velocity. It is most commonly used in situations where the variation of material properties needs to be analyzed with depth (e.g. soil profiles, landfills, road beds, etc.)

The SASW method is performed on the ground surface, which provides a much more cost efficient method than crosshole seismic testing. It utilizes a minimum of two receivers and one source which are equally spaced along a straight line. The basis of the SASW method is the dispersive characteristic of Rayleigh waves when traveling through a layered medium. Rayleigh wave velocity is determined by the material properties (primarily shear wave velocity, but also compression wave velocity and material density) of the subsurface to a depth of approximately 1 to 2 wavelengths (GeoVision, 2012). Figure 2.5 shows the wave source and equally spaced receivers used in the SASW method.

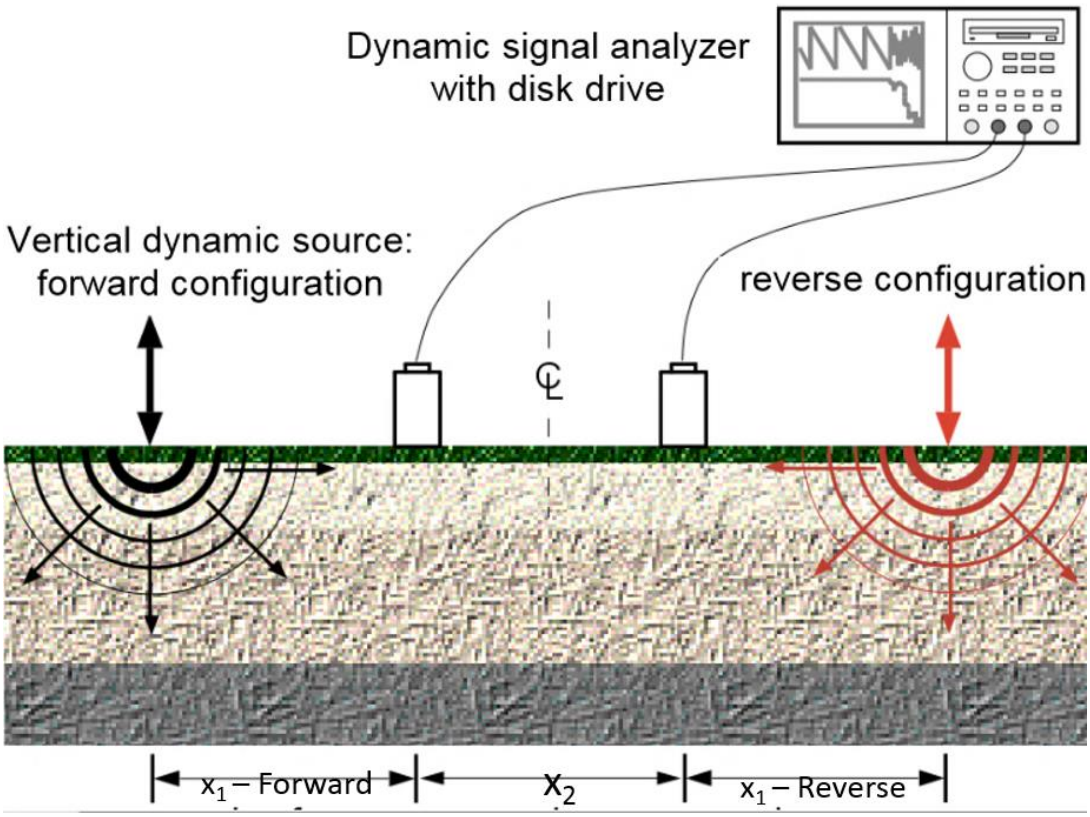

Figure 2.5: Components of the SASW method

Data is generated by measuring surface wave energy as it propagates starting at the source through the receiver locations. The data is transferred from a time domain to a frequency domain to determine the phase difference between the receivers at different frequencies. Compared to crosshole seismic testing, SASW allows for global measurements; meaning that a larger volume of a soil layer is sampled, since crosshole seismic tests use boreholes, which are considered point estimates. Because there are a number of inconsistencies and uncertainties associated with surface methods of geophysical analysis, but cannot ensure exact accuracy about the specific information about the subsurface based solely on surface testing. (EPA, 2012)

2.3 Unsaturated Soil Mechanics

Microscopically, there are three principle layers that exist in unsaturated soils. The vadose zone, which is located above the water table; the two phase zone, which is the capillary zone where water and air phases are idealized as continuous; and the dry zone, which is above the two phase zone where the soil becomes dryer and the water phase is discontinuous and the air phase remains continuous. Figure 2.6 shows a diagram of these zones in unsaturated soils.

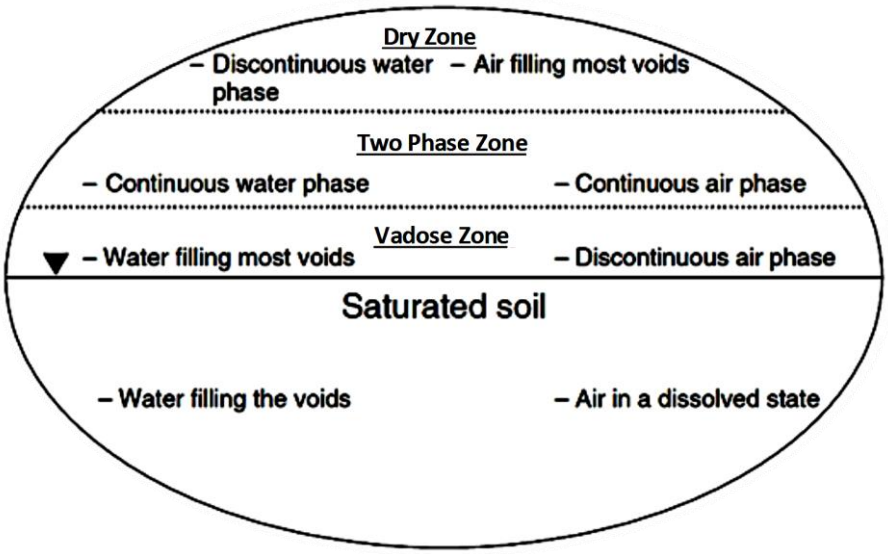

Figure 2.6: Components of an unsaturated soil particle (Fredlund, 1996)

Below the water table, pore pressures are positive and the soil is generally considered saturated. Above the water table, pore pressures are negative with respect to atmospheric pressures. In the vadose zone, the degree of saturation ranges between 20 and 90 percent. (Ng and Menzies, 2007).

2.3.1 Soil Suction

Soil matric suction, ψ, is considered to be the free energy state of soil-water, and is measured in partial vapor pressure. The general equation for soil matric suction is provided in Equation 7, and is simply the pore air pressure, u_a, minus the pore water pressure, u_w.

$$\psi = u_a - u_w \quad (7)$$

The relationship between matric suction and soil water content (gravimetric, w, or volumetric, θ) or saturation, S, is known as the soil-water characteristic curve (SWCC) (Fredlund and Xing, 1994). In geotechnical engineering, gravimetric water content (the ratio of the mass of water to the mass of solids) is most often used. Figure 2.7 provides a detailed generic soil water characteristic curve for impact of gravimetric water contents on a soil's matric suction.

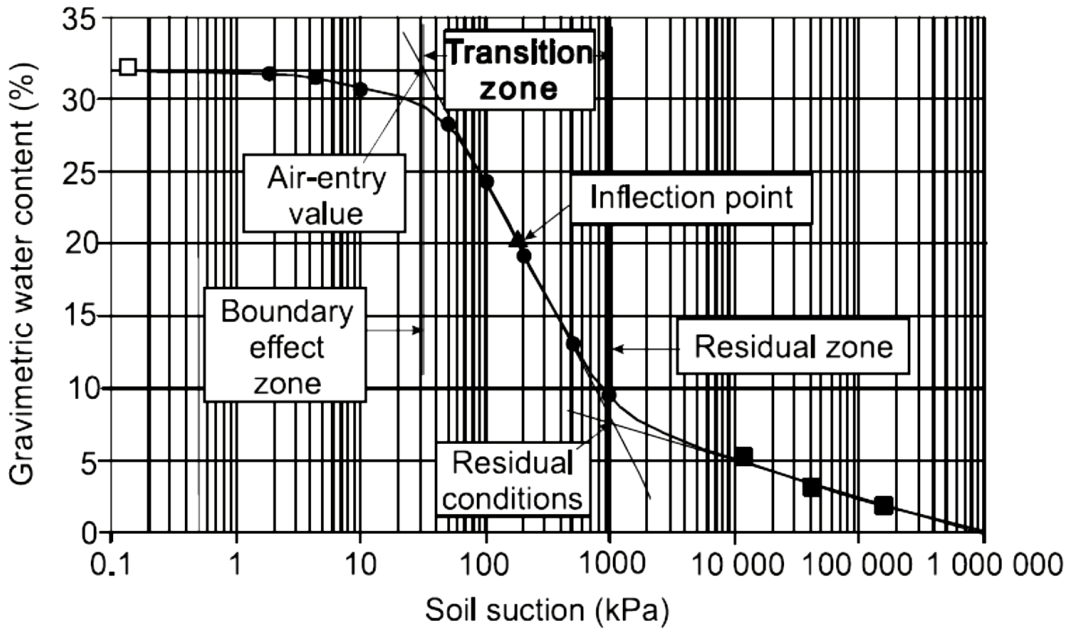

Figure 2.7: A typical Soil Water Characteristic Curve (Fredlund et al., 2011)

The three main stages of the SWCC are the boundary effect zone, the desaturation zone, and the residual zone. The boundary effect zone is where the pore-water is in tension but the soil remains saturated. This stage ends at the air entry value, ψ_a, where the applied suction overcomes the capillary water forces in the largest pore in the soil (Fredlund, 1999).

The desaturation zone is where water is displaced by air within the pore spaces. This stage ends at the residual water content, θ_R, or w, where the pore-water becomes discontinuous. The desaturation stage is also referred to as the transition stage (Vanapalli, 1994).

The residual saturation zone is the zone where water is tightly absorbed onto the soil particles and flow occurs in the form of vapor. A consistent way to define the residual water content is shown in Figure 2.7 where a tangent line is drawn from the inflection point of the SWCC; the curve in the high-suction range can be approximated by another line;

and the residual water content, θ, or w, can be approximated as the ordinate of the point at which the two lines intersect (Fredlund and Xing, 1994). Soil is defined to have zero water content and the soil suction is approximately 1 million kPa (Fredlund and Rahardjo, 1994). The total suction corresponding to zero water content appears to be essentially the same for all types of soils (Fredlund and Xing, 1994). To develop an unsaturated soil property function, an accurate and continuous representation of the soil-water characteristic curve is necessary. Fredlund and Xing (1994) developed the most applicable fit among other evaluated equations, which is provided in Equation 8.

$$\theta(\psi, a, n, m) = C(\psi)\left[\frac{\theta_s}{\left\{\ln\left[e + \left(\frac{\psi}{a}\right)^n\right]^m\right\}}\right] \quad (8)$$

The variable ψ is the matric suction; θ is the saturated volumetric water content; ψ_r is the residual suction; e is the natural irrational number equivalent to 2.7182; and the a, n, and m terms are fitting parameters. Saturated volumetric water content, θ_S, may be replaced with saturated gravimetric water content, w. $C(\psi)$ is a correction function and is defined in Equation 9.

$$C(\psi) = \frac{\left[-\ln\left(1 + \frac{\psi}{\psi_r}\right)\right]}{\ln\left[1 + \left(\frac{1{,}000{,}000}{\psi_r}\right)\right]} + 1 \quad (9)$$

3 LABORATORY TESTING

3.1 Test Soil Types and Preparation

Four clay soils were tested in the lab, all of which are native to the state of Kentucky. Samples from Henderson County, Lee County, Daviess County, and Fayette County, were tested. Figure 3.1 shows a map of Kentucky as well as the location of each county that each sample was taken from. These clays were chosen mainly due to the fact that they represent a broad range of the various clay soils throughout the state of Kentucky. According to ASTM 2487/2488, a fat clay is one with a liquid limit, LL, greater than 50. The Fayette County clay is a fat, highly plastic clay (LL=64.3) and the Lee County clay is also considered a fat clay (LL=55), while the other two soils are lean, and have a plasticity index lower than 10. Each of the clays possess unique characteristics which include a broad range of material properties such as the liquid limit, plasticity index, clay fraction, and percent fines value.

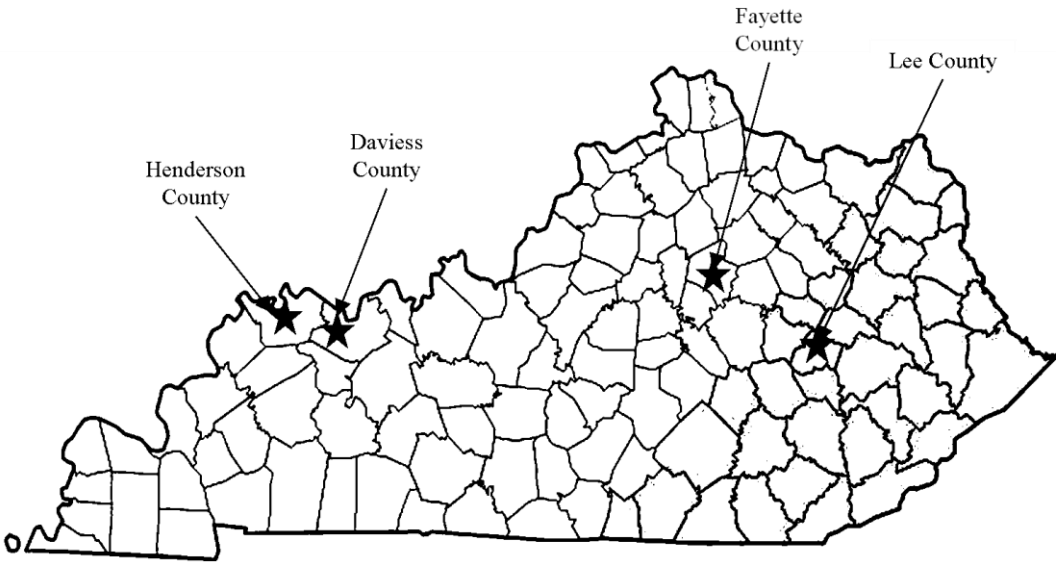

Figure 3.1: Map of Kentucky showing the location of the test soils

From previous research conducted by Huff (2010) and Kidd (2011), the Atterberg limits (LL and PI), percent fines, $\%F$, clay fraction, CF, specific gravity, G_S, optimum moisture contents, w_{opt}, and maximum dry density, MDD, had been determined in full accordance with ASTM D4318 and ASTM D558. It should be noted that for these tests, dry unit weight and dry density are synonymous. Two of the initial goals of this research were to compact each clay to reach its specific maximum dry density, and to test each soil at gravimetric moisture contents below, above, and as close to the optimum moisture content as possible. When the maximum dry density is reached, soils are said to be at their best behavior by providing the highest shear strength and bearing capacity, and the chance of unwanted settlement is at its lowest. The optimum moisture content is the water content at which a soil can be compacted to reach MDD. Moisture contents below optimum and wet of optimum were needed for this testing to analyze the behavior and effect of moisture content on soil density. Table 3.1 provides a summary of each of the four clay soils and their material-specific properties.

Table 3.1: Material Properties of the four Kentucky Clays

Parameter	Henderson County	Lee County	Daviess County	Fayette County
Liquid Limit (LL)	**28.2**	**55**	**23.3**	**64.3**
Plasticity Index (PI)	**8.5**	**23**	**3.9**	**29.3**
Specific Gravity (Gs)	**2.69**	**2.65**	**2.72**	**2.86**
Percent Fines (% Passing #200 sieve)	**99.4**	**66.5**	**95.6**	**86.8**
Clay Fraction (% smaller than 0.002 mm)	**20**	**88**	**21**	**74**
Optimum Moisture Content (%) (standard)	**14.6**	**22.8**	**16.4**	**31**
Maximum Dry Density (KN/m^3) (standard)	**16.45**	**15.85**	**17.39**	**13.89**

From Table 3.1, it can be seen that the clay fraction, which is the percent of soil particles smaller than the # 200 sieve, shows some correlation with the liquid limit and plasticity index. Lower Atterberg limit values indicate lower clay fractions, and vice versa. Also, lower Atterberg limit values are seen for high percent fines values.

Figure 3.2 shows the original SWCC for the Daviess County Clay derived by Kidd (2011) using the Fredlund and Xing Equation, provided in Equation 8 and the correction factor from Equation 9. The SWCCs were calculated in accordance with ASTM D6836. The parameters a, n, and m were determined using the optimization function in Microsoft Excel. The constraints for the parameters were taken from Fredlund and Xing (1999). To derive the SWCCs, saturated soil specimens were placed in contact with saturated high air

entry ceramic plates and an air pressure applied to a sealed chamber via an air compressor to induce matric suction. Upon application of an air pressure to a saturated sample, the equilibrium of internal pore-water and pore-air pressure was altered. The outflow of water from the pressure cell was monitored and once matric suction equilibrium was reached, the outflow of water ceased. The gravimetric water content at that corresponding matric suction provided one point on a drying soil-water characteristic curve. Several identical samples tested in this manner at different matric suctions collectively constructed a drying soil-water characteristic curve. (Kidd, 2011)

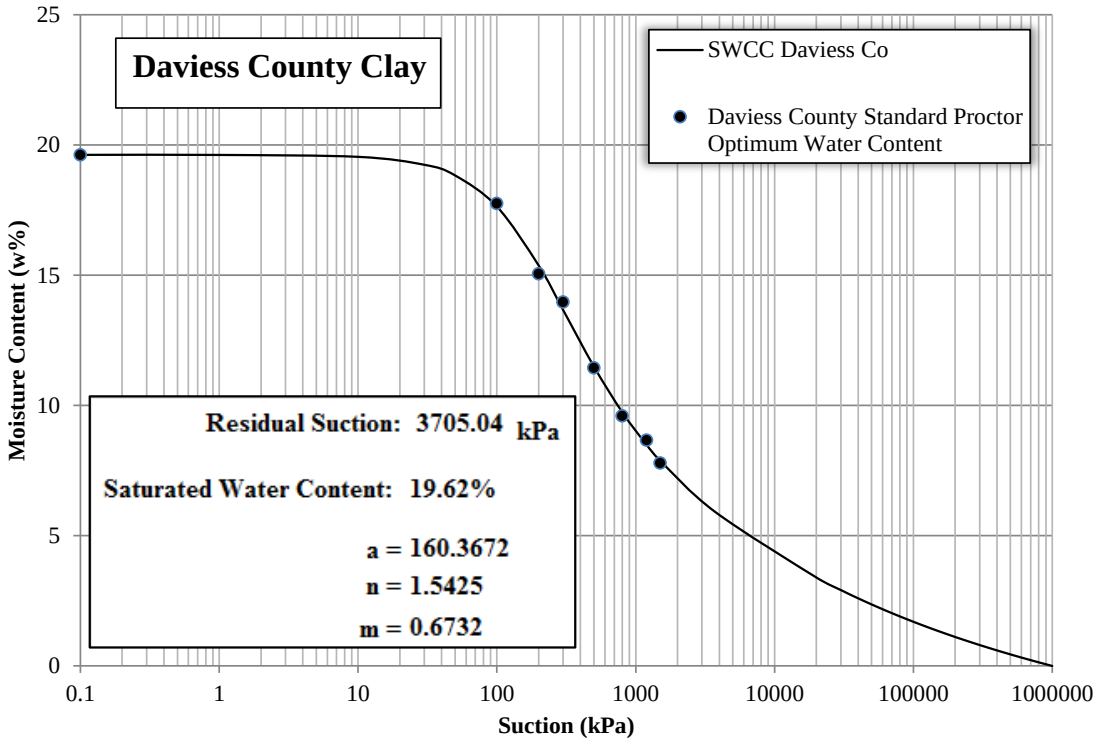

Figure 3.2: Original SWCC for the Daviess County Clay (Kidd, 2011)

These SWCCs were used as a reference point, representing the SWCC at maximum dry density. The SWCCs were also used to calculate the matric suction at various stages of compaction (using void ratios). The new matric suction values were calculated using the Zhou et al. (2012) method.

3.2 Testing Equipment

3.2.1 PicoScope Background Theory

The PicoScope 3200 is an Oscilloscope designed to measure and sample signal rates. The device is equipped with two analog channels and 16 digital channels. It is capable of measuring analog signals up to 200 MHz and digital signals up to 100 MHz and is equipped with a Pentium-class processor with a 256 MB memory and 10 MB of disk space. The device is connected to a computer via USB. The specifications of the PicoScope can be found in Appendix A of this thesis. Figure 3.3 provides an image of the PicoScope 3200 oscillator.

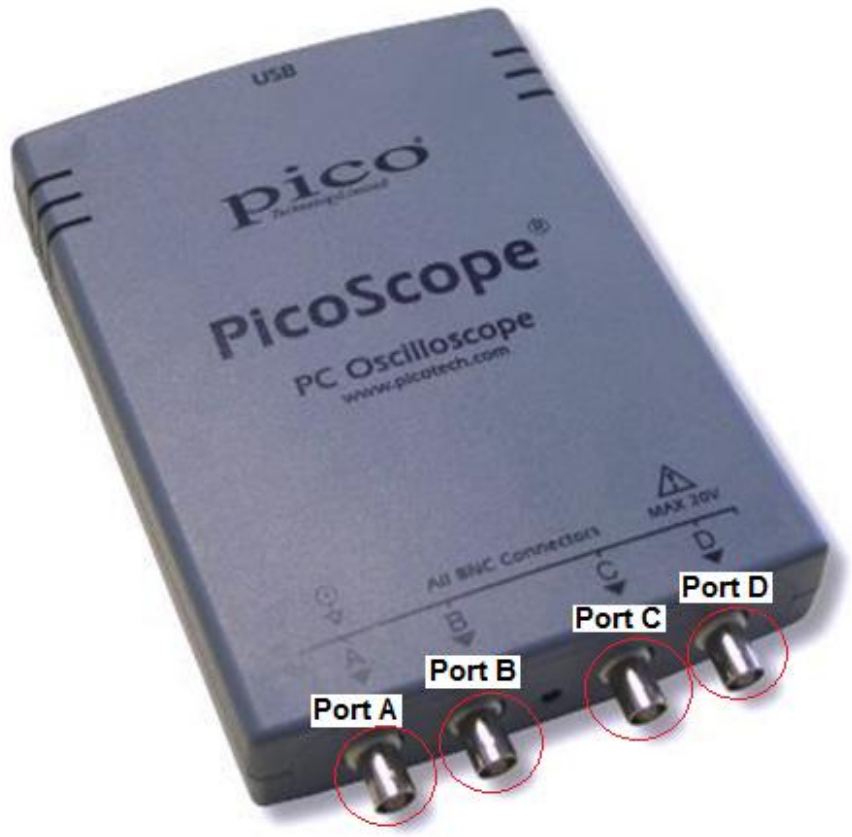

Figure 3.3: The PicoScope 3200 oscillator

The PicoScope was used to simulate cross-hole seismic testing in the laboratory. For this test specifically, a hammer was connected to port A (see Figure 3.3) on the PicoScope and used to generate the shear waves. The hammer was used to hit a steel rod with a wedge at the end which made it possible to control the depth of shear wave generation, and is shown in Figure 3.4.

Figure 3.4: Hammer used to create the source of the shear waves

At the opposite corner of the test box, an accelerometer was placed at the same depth at which the shear waves were generated, and connected to port B on the PicoScope. Figure 3.5 shows and image of the rod with the wedge at the end which was tightened at specific depths to control the various depths of the shear waves.

Figure 3.5: Rod with a wedge used send shear waves at a controlled depth

The PicoScope can be utilized to measure the shear wave velocity in a geotechnical engineering sense because the user can determine the shear wave travel times by examining the data in graphical form. If the travel distance is known, a velocity can easily be determined by dividing the travel time by the travel distance. Equation 10 provides the expression used to determine the shear wave velocity based on the travel distance of the wave and the travel time.

$$V_S = \frac{Wave\,Travel\,Length}{Travel\,Time} \qquad (10)$$

The portion of this research for determining shear wave velocities required a hammer instrument which had a sensor at the tip of the head, a wedge to accurately produce the signal at a specific depth in the copper rod, and an accelerometer, which was taped onto another steel rod and placed down inside the opposing copper pipe, and held at various depths which were calculated based on soil heights and layer thicknesses. The accelerometer was placed so that the waves were received at a shearing angle to avoid accidental P wave measurements.

Included with the PicoScope is the PicoScope 6 software, which allows the user manually input sampling settings to collect data. Figure 3.6 shows a screen shot from the PicoScope 6 software and provides a visual explanation of the blue line showing an initial spike caused from impact with the hammer, and the red line showing very noticeable yet significantly smaller spike within a matter of milliseconds, allowing the length of time the wave traveled through the soil to be determined.

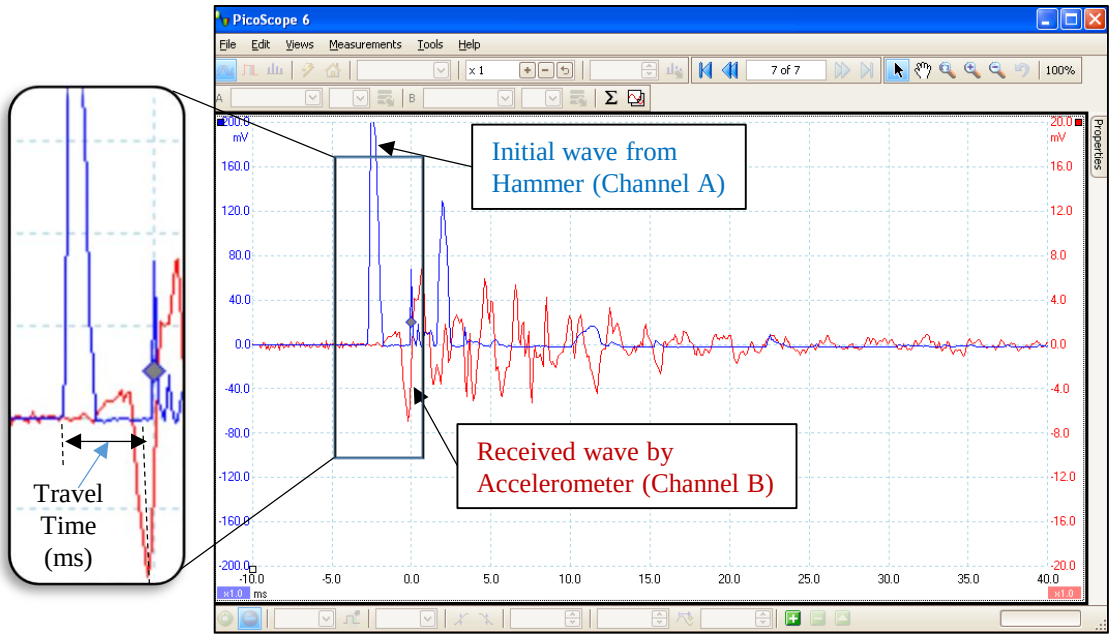

Figure 3.6: PicoScope software and the method used to record travel time

After the determining the shear wave velocity of a soil sample, the shear modulus, G_{VS}, can be determined using the elastic theory equation, which simply states that the shear modulus is equal to the shear wave velocity squared, V_S^2, multiplied by the density, ρ, and is presented in Equation 11.

$$G_{VS} = \rho * V_S^{\,2} \qquad (11)$$

3.2.2 GeoGauge Background Theory

The Humboldt GeoGauge was used to simulate on-site field measurements of stiffness, since it is a portable instrument which provides a user-friendly, rapid means for measuring the in-place and mechanical properties of compacted soil and aggregate. The GeoGauge is able to measure the stiffness and modulus at the surface of compacted soil by imparting very small displacements, less than 1.27×10^{-3} mm to the soil on an annularly loaded ring through a harmonic oscillator, which operates more than twenty five steady-state frequencies, ranging between 100 kHz to 196 kHz. Figure 3.7 shows an image of the Humboldt GeoGauge. (Humboldt, 2007)

Figure 3.7: The Humboldt GeoGauge (Humboldt, 2007)

3.3 Box Testing

In order to compact the test soils as close as possible to their maximum dry densities, a smaller wooden box was chosen so that less soil would be needed to run each test. Three 2 x 4 pieces of wood were used for each face of the box and were nailed down to the base. The inside of the box was coated with an impervious liner. The inside dimensions of the box are provided in Figure 3.8.

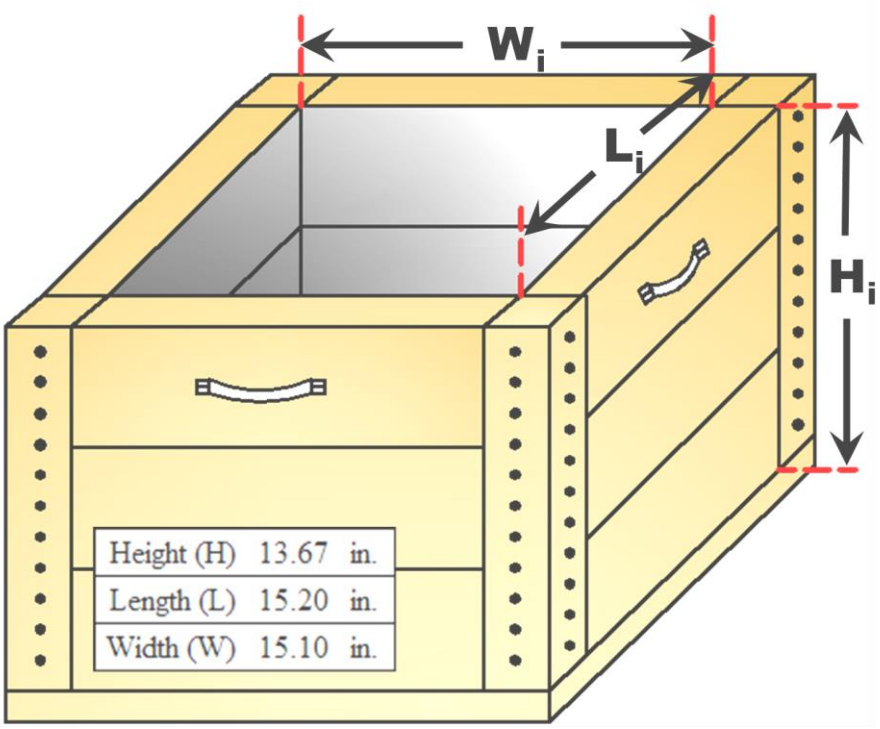

Figure 3.8: Test box interior dimensions

For each clay soil, two types of tests were performed at four various moisture contents that were above, at, and below the optimum moisture content for the particular soil. Figure 3.9 shows a detailed schematic diagram with all of the required connections to determine shear wave travel time.

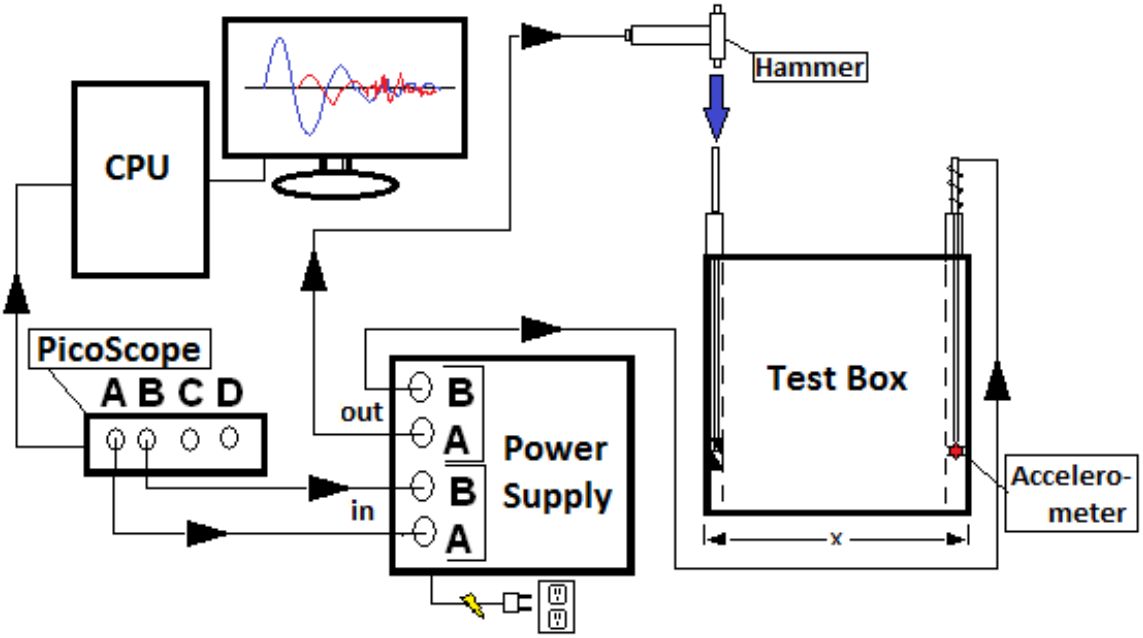

Figure 3.9: Schematic diagram of the PicoScope setup

The box was first modified to account for the specific needs of this test. Three pressure plates were used in the box. Two of the plates were placed against two adjacent walls of the box, and the third was placed at the bottom of the box, to account for loading pressures in each direction of a three dimensional axis. The two pressure plates on the side had a maximum pressure tolerance of 350 kPa and the plate placed at the bottom of the box had a maximum pressure tolerance of 1 MPa. A hole was drilled out in the front of the box so that the bottom pressure plate could be run though without damaging the cord or the soil sample during compaction. Figure 3.10 provides a photograph taken from an overhead view of the test box and the placement of each of the three pressure plates can be seen.

Figure 3.10: Overhead view of the test box showing the pressure plate placements

Bracing was applied so that the rigidity of the box would not be compromised. The bracing consisted of two steel bars on each side of the box that were connected by threaded rods that could be tightened and loosened as needed. Since each face of the text box was constructed from three separate pieces of wood, steel sheets of approximately 100 mm thickness were placed between the box and the bars so that the bracing would support the entire face of the box as opposed to the small area of the face that each bar covered. The extra support allowed the stresses imposed by compressed soil to be transferred evenly to the bracing rods, and provide extra strength for the vulnerable parts of the box that were not directly in contact with the steel bracing rods. Figure 3.11 shows an image of the test box placed in the load frame with the applied bracing.

Figure 3.11: Testing box with bracing

3.3.1 Testing Procedure

The four samples were individually prepped for each test. For each of the samples, four moisture contents were used, making sure that at least one was below the optimum moisture content, at least one was below, and one was as close to the optimum moisture content as possible. The ultimate goal was to compact the samples to their maximum dry densities, so two tests were performed for each of the four moisture contents, making a total of thirty two tests performed.

For both of these tests, the amount of water needed was calculated based on the initial moisture content of each sample, which was determined by placing a small sample in the oven for a minimum of 16 hours and the weights of the sample before and after were recorded. The total weight of the soil sample was recorded, and the amount of water needed to be added to each sample was then measured out, and added to the soil using a concrete

mixing drum. The sample was thoroughly mixed and promptly placed back in the buckets and covered so that no moisture was lost.

It was important that the box dimensions be measured at the beginning of each test. The dimensions of the box were measured with a precision of 1.59 centimeters (or one sixteenth of an inch) so that any minor volumetric changes could be accounted for if the box suffered any deformation during loading. This allowed for a more precise calculation of soil density based on the dimensions of the box and the soil compaction height. Approximately three buckets of each sample were used to fill the box, and each bucket was weighed while full of soil as well as after the bucket was emptied into the box so that the total weight of soil could be recorded. A small sample from each bucket as taken and placed into the oven to determine the initial water content, which was based on an average value form the three buckets.

The first test was referred to as the single compaction test, where the entire sample (enough to fill the box) was placed in the box prior to compaction. However, before anything was done, the pressure plates and two type M copper tubes were placed inside the box. The copper tubes were chosen for their high durability and compressive strength. Type M copper tubes are predominately used in many ASTM guidelines. These tubes ensured that the source of the shear waves and the receiver were unaffected by any deformations or disturbances that could have possibly been encountered with a weaker material due to the extremely high compressive loading.

A piece of wax paper was placed in the box after each bucket was unloaded in order to monitor the density gradient before and after compaction. The reason for monitoring the density gradient was take into account the possibility that the bottom soil layer (or first

bucket) may have been compacted to a higher density than the middle and top layers. At the end of each test, extreme caution was taken while removing the compacted soil so that the compacted height of the wax paper could be recorded. This allowed the initial and final heights of the wax paper to be evaluated for each layer, showing any gradation in soil density that may have occurred between layers of with soil depth. Figure 3.12 shows a photograph taken of the box as a soil sample was being unloaded into the box, after the copper tubes and pressure plates has been placed in their proper positions.

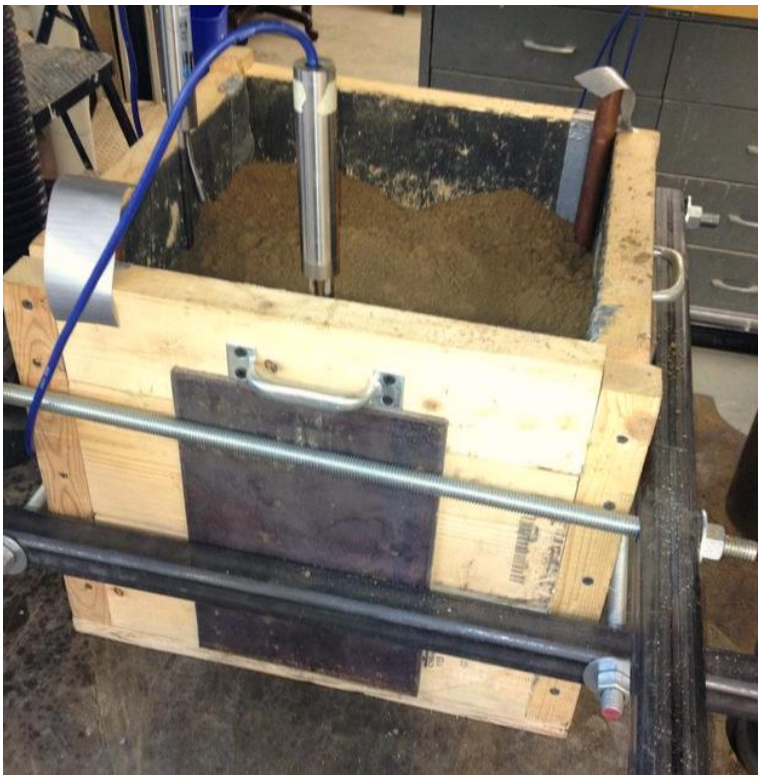

Figure 3.12: Partially loaded box with pressure plates and copper tubes in place

A combination of spacers were used to add enough height to the box so that the pressure head from the load frame could be able to make contact with the spacers without being lowered enough to damage the pressure plates, which were sticking out above the box. The box cover and spacers were placed on top of the soil. The soil height was

measured before compaction, and the depths for the shear wave measuring equipment were calculated based on the loose height of the soil and pre-determined compaction increments. The two steel rods were then marked accordingly. The pressure plates and load frame were then powered on, and the soil sample was compacted in increments of around one to one and a half inches. Figure 3.13 shows a soil sample undergoing compression from the load frame.

Figure 3.13: The test box filled with soil under load frame compression

After each compression increment, the load frame was disabled, and the spacers were removed. When a load, or stress, is removed from a soil after consolidation, the soil will rebound, expanding to regain a portion of the initial volume. For this reason, the soil samples were then given time to rebound until equilibrium was reached. After the soil had time to rebound, the GeoGauge was placed on top of the soil, and two readings for the

modulus of elasticity, and stiffness were taken. The GeoGauge was rotated 90 degrees each time for the second reading, which was recommended in the user manual. There was not a set time limit for the soil to rebound, but when the pressure plate readings did not change by more than .001 stress units, it was assumed that the soil had adequately rebounded. Figure 3.14 shows the GeoGauge placed on the top of the soil after all spacers were removed.

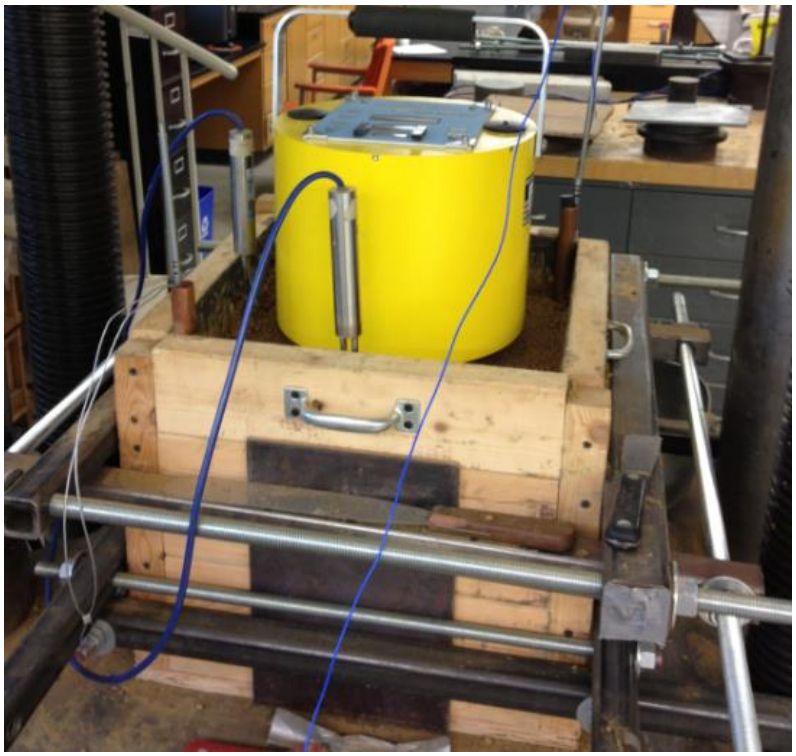

Figure 3.14: The GeoGauge placed on the soil surface taking stiffness readings

The accelerometer (shear wave receiver) was placed at the end of a steel rod and lowered into the copper tube at a pre-calculated depth, so that the accelerometer and the source of the shear wave were at the same elevation, or depth, which was the midpoint of the soil layer.

The shear wave source device was then assembled using another steel rod and a wedge, so that it could be lowered to the midpoint of the soil layer and tightened to ensure that no vertical movement occurred while the hammer was hitting the top of the steel rod. After the two steel rods were in the tubes, the hammer was used to hit the top of the wedged rod, and the shear wave data was recorded to the computer using the PicoScope software. Shear wave measurements were made while the sample was under compression by pausing the load frame at a constant maximum load, as well as after the load was completely removed and the soil was allowed to rebound.

The second test was referred to as the three layer compaction test, and each of the four samples were brought to the same gravimetric moisture contents that were used for the single compaction test. For this test, one bucket of each sample was unloaded into the box at a time, and compressed to a certain height which was calculated based on the box dimension and weight of the soil to achieve the desired density for each layer. After repeating this process, there were basically three separately compacted layers of soil in the box. A piece of wax paper was again placed on top of each layer in order to measure the density gradient. The GeoGauge was used to measure the stiffness and modulus for each individual layer, and after the final layer was compacted, the PicoScope was used to measure the shear wave travel time at the midpoint of each of the three layers. Again, similar to the single layer compaction test, shear waves were measured under a concentrated load and after the soil was fully rebounded. Three sets of shear wave measurements were recorded under loading and after rebound at three depths which were calculated to be at the midpoint of each of the three layers. To determine the required compaction depth needed for each layer, the soil volume and weight were used along with

the moisture content to come up with the needed compaction height to achieve the maximum dry density. For some of the tests, however, the pressure plates became too close to their maximum loading tolerance, and compaction had to be stopped before that height was reached. To attempt to make up for the loss in compaction, the extra compaction height that was not achieved during the intended compaction increment was added onto the next layers compression depth to try to reach the maximum dry density, and was successful in some cases and in others it continued to put too much pressure on the plates.

For both tests, after all data had been recorded, an undisturbed sample was taken to provide another measurement of the soil's density other than calculations from the box dimensions. A shelby tube was pushed into the compacted sample by placing it directly under the load frame head and pushed to a depth that was calculated based on the final compressed soil height. An extra 19 mm was subtracted from the depth at which the shelby tube was pushed to ensure that it did not make contact with the pressure plate, which could damage the plate or potentially ruin it or cause inaccurate readings. The dimensions and weights of each shelby tube sample were recorded and placed in the oven so that the final moisture content, wet density, and dry density could be calculated. For the layered test, the shelby tube sample was broken up all three layers since there was a clear sign inconsistency in each sample where each layer had been individually compressed. Each sample from the top, bottom, and middle layers were analyzed individually. Figure 3.15 provides an image of a shelby tube being driven into the compacted soil by the load frame.

Figure 3.15: A shelby tube being driven into the compressed soil by the load frame

The maximum dry density was achieved, or closely reached from the single layer compaction method, so the three layer compaction data was neglected for the data analysis portion of this report. For the single compaction test, more data was available due to the fact that there were 5 to 6 compression increments and only three for the three layer compaction tests. Comprehensive step-by-step summaries of the single lift compaction test and the layered compaction test are provided in Table 3.2 and Table 3.3.

Table 3.2: Testing procedure for the single lift compaction test

Single Lift Compaction	
i	The required amount of water needed to achieve the desired gravimetric moisture content, w, was calculated using the weight of the soil sample and the current moisture content
ii	The interior box dimensions (H_i, W_i, L_i) were measured to the precision of one sixteenth of an inch
iii	Bracing was applied to the test box, and place the testing materials (pressure plates and copper tubes) inside the box in their respective locations
iv	The soil samples were kept in three 5 gallon buckets (sometimes four buckets were needed) and the lids were tightly fastened at all times so that no moisture was lost
v	The first bucket was weighed, and carefully emptied into the box. The empty bucket was then weighed and subtracted from the initial weight
vi	A small sample was obtained from each bucket to determine the initial moisture content (per ASTM standards)
vii	After the first bucket was emptied into the box, the "loose height" was measured, by recording the height from the top of the test box to the top of the soil layer
viii	A piece of wax paper was placed on the surface of the first soil layer to show the effects of a possible density gradient
ix	The second bucket was then weighed, emptied into the box, and the empty bucket weight was recorded. Another moisture content sample was taken, and another piece of wax paper was applied to the surface.
x	The loose height was again measured from the height of the second bucket to the top of the box
xi	The third bucket was emptied into the box and the same procedures were taken for the sample weight, and moisture content. If there was any remaining soil in the third bucket after the box was full, it was weighed and subtracted from the initial weight, and promptly placed back in the bucket and sealed with a lid. The loose height was again recorded after the third bucket
xii	The load distribution and spacers were placed on top of the soil. These consisted of a wooden "cover" which is placed directly over the soil, followed by four steel rectangular bars. A steel plate was then placed on top, followed by a circular steel plate, and a swivel head, two circular metal pieces, and lastly, a cone shaped head that comes in contact with the actual load frame.

Table 3.2, continued

xiii	**The height of the soil was again recorded to account for any consolidation induced by the load distribution and spacing materials**
xiv	The pressure plates and load frame were then powered on
xv	The loading was applied and based on the material properties of the clay being tested; increments of 1 to 2 inches of compaction were observed. The load was always monitored, and was quickly stopped if the pressure plate readings were close to their respective maximum thresholds.
xvi	After each compaction increment, the load was paused, and the shear wave travel time measurements were taken using the PicoScope. The shear waves were recorded at the midpoint of the soil layer, which was calculated using the compacted heights of the soil.
xvii	The load was then released, and the soil was given adequate time to rebound after the spacing materials had been removed
xviii	After the soil had rebounded, shear wave travel times were again recorded, and the GeoGauge was used to record stiffness measurements
xix	The spacers were placed back on the soil, and loading was applied again until the desired compaction increment was reached, or until the pressure plates reached their maximum tolerance
xx	The same procedure was repeated by applying the load, pausing the load, and stopping the load while recording shear wave travel times while under loading, and after rebound, and measuring stiffness with the GeoGauge after round
xxi	After the final compaction increment, a shelby tube was driven into the soil sample, so that an undisturbed sample could be obtained for density calculations

Table 3.3: Testing procedure for the layered compaction test

Three Lift Compaction	
i	The required amount of water needed to achieve the desired gravimetric moisture content, w, was calculated using the weight of the soil sample and the current moisture content
ii	The interior box dimensions (H_i, W_i, L_i) were measured to the precision of one sixteenth of an inch
iii	Bracing was applied to the test box, and place the testing materials (pressure plates and copper tubes) inside the box in their respective locations
iv	The soil samples were kept in three 5 gallon buckets (sometimes four buckets were needed) and the lids were tightly fastened at all times so that no moisture was lost
v	The first bucket was weighed, and carefully emptied into the box. The empty bucket was then weighed and subtracted from the initial weight
vi	A small sample was obtained from each bucket to determine the initial moisture content (per ASTM standards)
vii	After the first bucket was emptied into the box, the "loose height" was measured, by recording the height from the top of the test box to the top of the soil layer
viii	The pressure plates and load frame were then powered on
ix	The loading was applied and the soil was compacted to previously calculated heights based on the moisture content, maximum dry density, and box dimensions. The load was always monitored, and was quickly stopped if the pressure plate readings were close to their respective maximum thresholds.
x	When the loading was stopped (not paused) the spacers were removed, and GeoGauge readings were taken after the soil had rebounded
xi	The compacted height was recorded for the first layer, and a piece of wax paper was placed on the surface of the compacted first layer
xii	The second bucket was weighed, and emptied into the box. A moisture content sample was taken, and the soil was again compacted to a specific height. (If the previous height was not reached due to pressure plate tolerance, it was added on to the next compaction height)

Table 3.3, continued

xiii	**Loading was applied and removed, and another GeoGauge reading was recorded after rebound. Wax paper was again placed on the surface after the second bucket, and the compacted heights were recorded.**
xiv	The same procedure was done for the third bucket, except that the loading was paused after the final compaction increment and shear wave travel times were recorded under loading. After the load was released, shear wave travel times and GeoGauge readings were recorded after rebound.
xv	Shear waves were measured at pre-determined depths, at the midpoint of each of the three layers
xvi	After the final compaction increment, a shelby tube was driven into the soil sample, so that an undisturbed sample could be obtained for density calculations

4 TEST RESULTS AND DISCUSSION

4.1 Soil Behavior and Reaction to Loading

To account for the variation between the measured density of the soil and the density from the Shelby tube sample, a correction factor was used and determined by plotting the measured density values from the load frame and the box dimensions against the shelby tube densities. The load frame density was calculated by taking the total weight of the soil in the box divided by the soil volume. The soil volume was determined by multiplying the length and width of the box by the final compacted soil height.

A linear trend line in the form of $y = mx + b$ was then created through the points, and the linear equation given by the trend line was then used to determine the corrected density values. Figure 4.1 shows the plots used to determine a corrected dry density value based on the dry densities that were yielded by the shelby tube tests, γ_{ST}, versus those calculated based on the box volume and depth of compaction, γ_{Meas}, and the dry density given by the load frame readings, γ_{LF}. The corrected dry density values were used in all comparisons and data analyses. The density factors were found in English units of pounds per cubic foot, and then converted to kilograms per cubic meter.

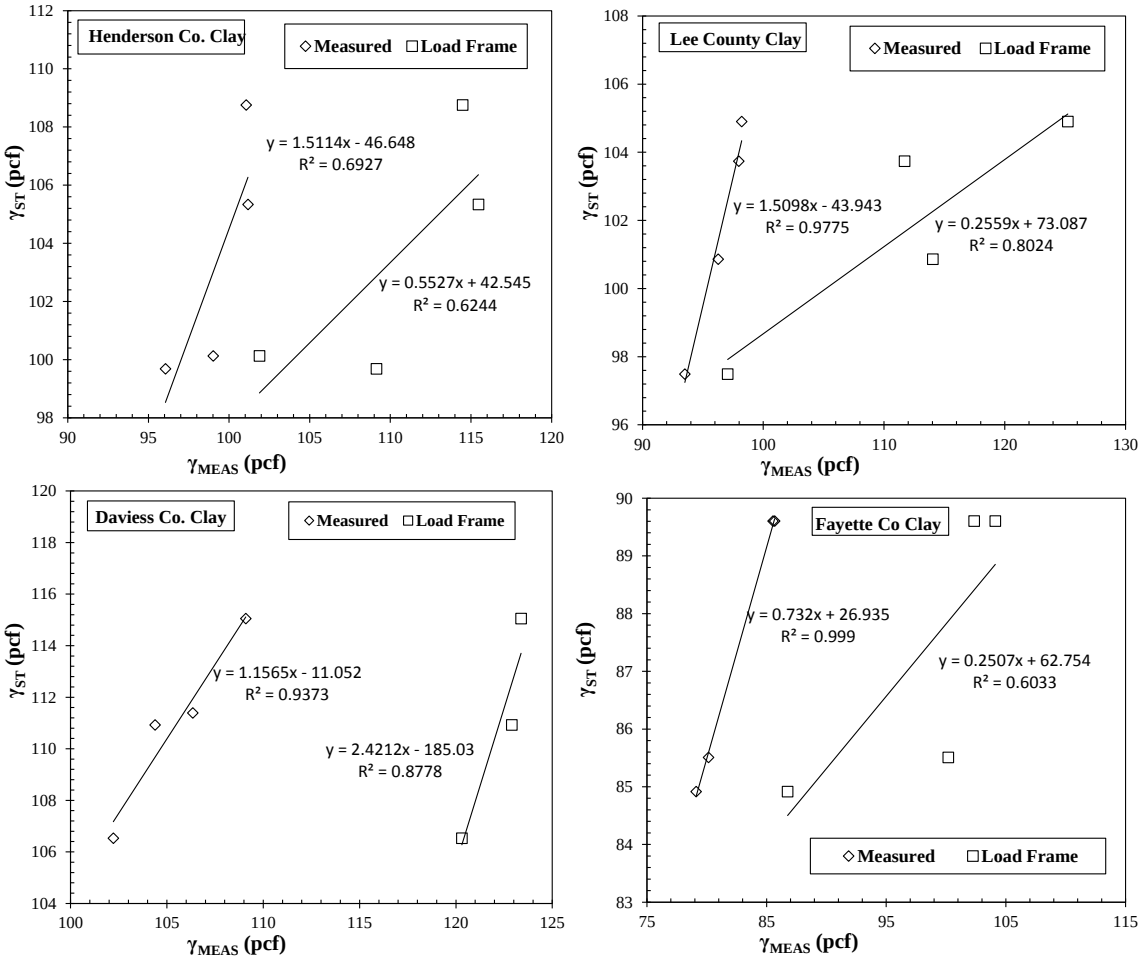

Figure 4.1: Plots used to derive correction factors

The measured density values had a higher R squared value than the load frame density values, so the m and b values from the measured equation were used to calibrate the corrected density values with the final shelby tube density after the soil had been fully compacted. Table 4.1 provides a summary of all of the factors given by the calibration equations which were used to determine the corrected dry density.

Table 4.1: Calibration function used to determine the corrected dry density

	Measured		Load Frame	
	m	**b**	**m**	**b**
Henderson County	1.5114	-46.648	0.5527	42.545
Lee County	1.5098	-43.943	0.2559	73.087
Daviess County	1.1565	-11.052	2.4212	-185.03
Fayette County	0.732	26.935	0.2507	62.754

4.2 Effect of Density on Shear Wave Velocities and Soil Stiffness

Due to the fact that the box used did not allow any drainage, the gravimetric moisture content of the sample was presumed to stay constant throughout the entire test for each sample. It was assumed that no loss of moisture occurred due to evaporation. To verify this assumption, three small samples were taken before each test was conducted and compared to the shelby tube sample which was taken after the test was competed. The initial and final moisture contents showed little to no change in gravimetric moisture content. In Figure 4.2, the dry density is plotted against the shear wave velocity that was measured after the soil was allowed adequate time to rebound. Each plot in Figure 4.2 accounts for all four tests on each soil at four different moisture contents.

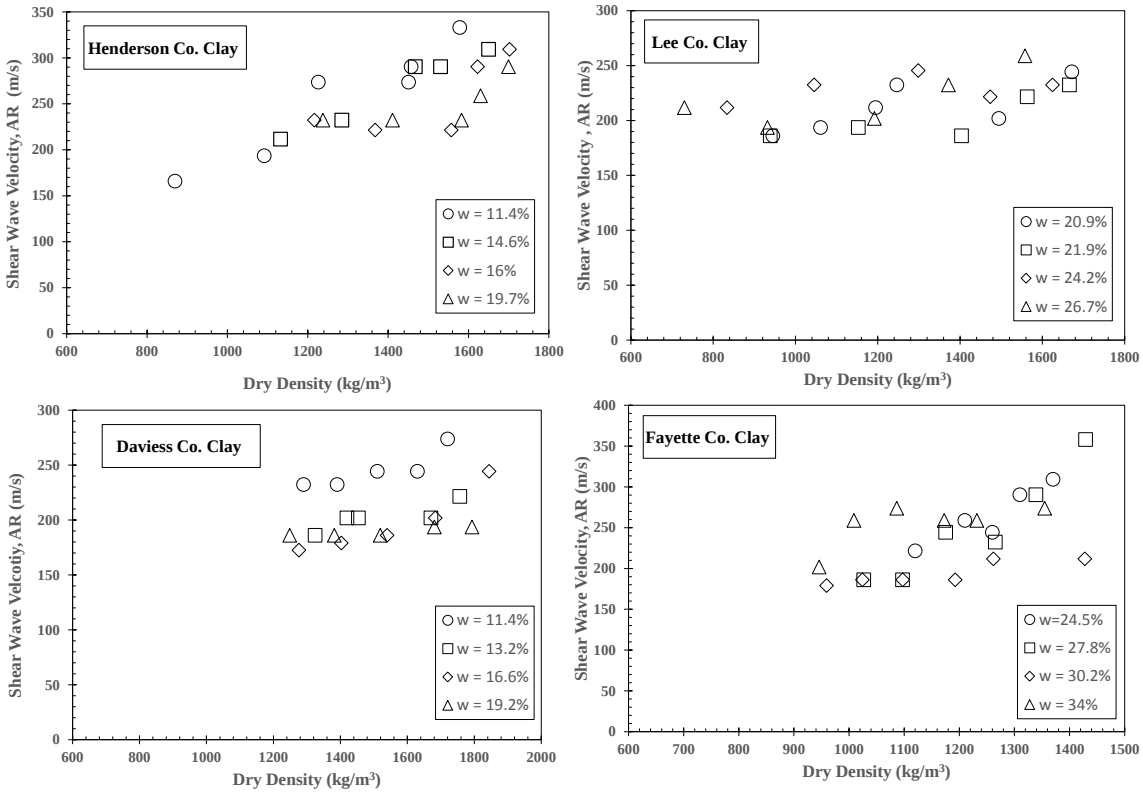

Figure 4.2: Shear wave velocity versus dry density

Although there is a variation in the values, a clear and somewhat constant trend can be seen which shows that the shear wave velocity increases with density. This shows that the dry density has a larger effect on shear wave velocity than other parameters such as the gravitational water content. The Henderson County clay shows the most uniform trend, using a logarithmic trend line, and the Daviess County clay shows the least reliable trend. The Daviess, Lee, and Fayette County equations were found with linear trend lines. It can be seen from observation that a definite relationship exists between shear wave velocity and dry density. Figure 4.3 shows the GeoGauge stiffness, k , plotted against the dry density, γ_{dry}.

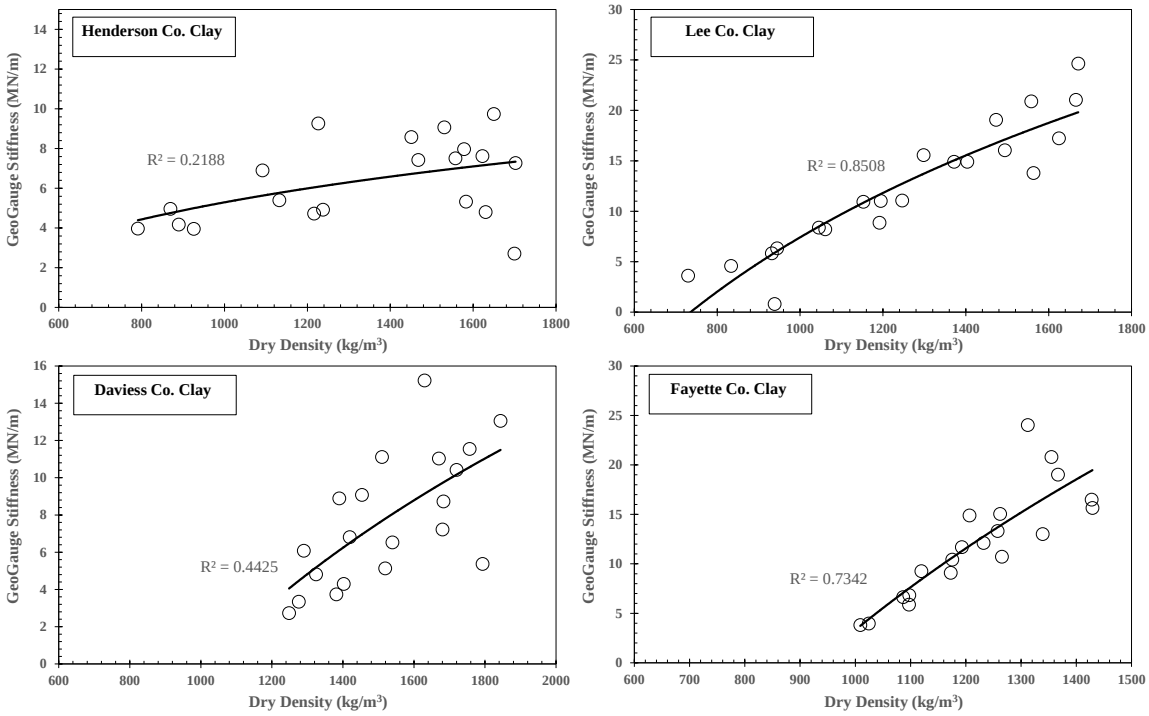

Figure 4.3: Dry unit weight versus GeoGauge Stiffness for the four clays tested

The Henderson County clay showed the least correlation between dry unit weight and GeoGauge stiffness. The general behavior was seen which showed an increasing stiffness with an increasing dry unit weight. The Lee County clay showed a stronger correlation between dry unit weight and GeoGauge stiffness than the Henderson County clay. The Daviess County clay showed a better correlation between dry unit weight and GeoGauge stiffness the Henderson County clay, but a weaker correlation than the Lee County clay. The Fayette County clay showed a strong correlation between dry unit weight and GeoGauge stiffness. However in this case, the trend was strongest with an exponential trend. For all of the soils, a general behavior was observed showing an increase in GeoGauge stiffness as the soil's dry unit weight increased, with the exception of some outliers. All of the trends for dry density versus GeoGauge stiffness were found using logarithmic trend lines. The GeoGauge stiffness showed a much stronger trend in terms of

density, but both the stiffness and the shear wave velocity measured after rebound showed an increasing trend with soil density. There is a strong indicator that a correlation can be made between stiffness and shear wave velocity, which can both be used to determine a shear modulus.

4.3 Effects of Void Ratio

An increasing void ratio is an indication of an increasing density gradient. The void ratio made a significant impact on shear wave travel time and shear modulus. The void ratio is an extremely important parameter when analyzing soil stiffness and behavior. The mechanical properties (e.g. strength and stiffness) of soil depend heavily on the nature and microscopic composition of the soil structure as well as the state of stress, water content, and unit weight. The void ratio can be used to describe the orientation of the soil grains, which are heavily affected by pore water pressure. The expression to calculate the void ratio is given in Equation 12.

$$e = \left[\frac{G_S * \gamma_w}{\gamma_{Dry}} \right] - 1 \tag{12}$$

where G_S is the specific gravity, γ_w is the unit weight of water, and γ_{Dry} is the dry unity weight of the soil. For all four of the test soils, a correlation was seen that showed a decreasing shear modulus with an increasing void ratio (or increase in density). This trend was expected since one of the main goals of this research was to compact the test soils to their maximum dry densities, which is the density at which the soils experience their highest strengths and bearing capacities. Figure 4.4 shows the void ratio versus the shear modulus calculated from the shear wave velocity measurements after the soil had

rebounded for all of the four clays. The trend lines from Figure 4.4 were all found using logarithmic equations.

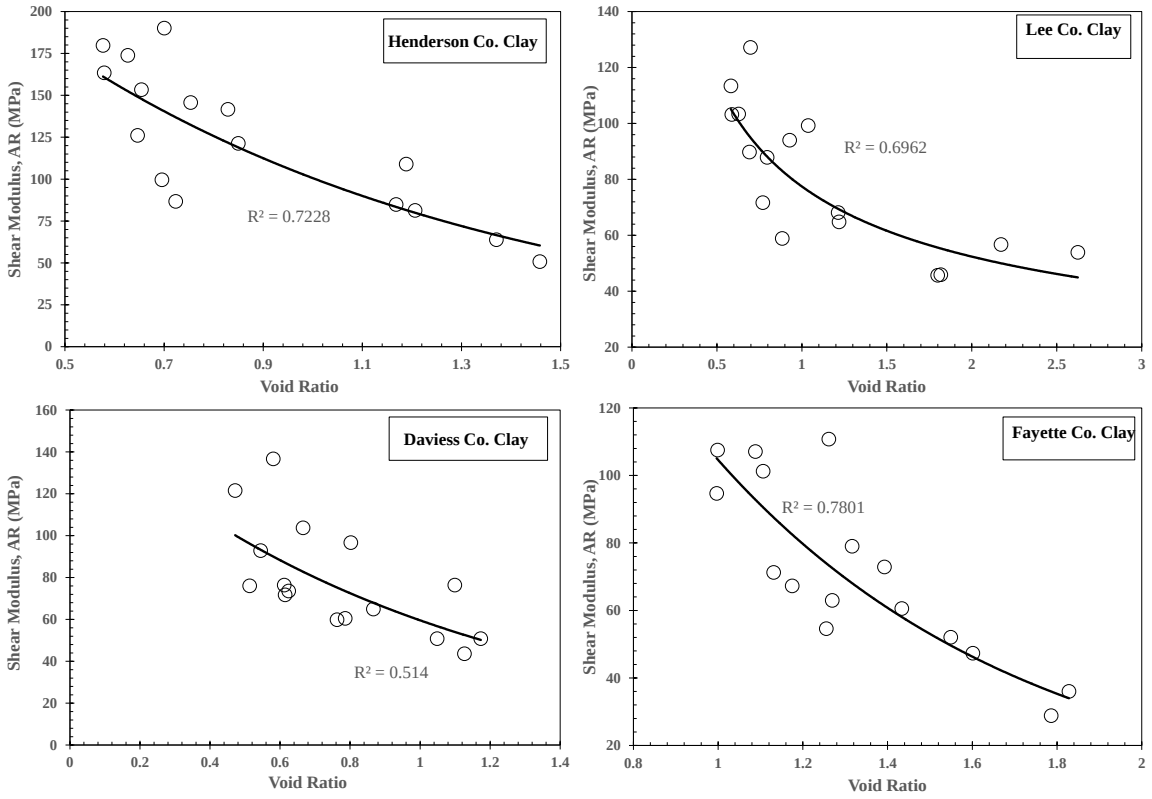

Figure 4.4: The void ratio versus the shear modulus after rebound

4.3.1 The void ratio function

To analyze the impact of the void ratio on the soils behavior and shear modulus, a term referred to as the void ratio function, $f(e)$, was developed to create a standard means of measurement when comparing the void ratio to other soil parameters. The expression for the void ratio function is given in Equation 13.

$$f(e) = \frac{e^3}{1+e} \qquad (13)$$

There are many different variations that have previously been used in geotechnical engineering research (e.g. Hardin and Black, 1968). However, for this particular application, the void ratio function was taken from the Kozeny-Carman Equation, which accounts for the reaction of soil particles based on orientation or the soil pore space. The Kozeny-Carman Equation utilizes the void ratio function provided in Equation 13, and also uses soil parameters including seepage velocity, tortuosity (or diffusion of a porous specimen), hydraulic gradient, and a shape factor (Das, 2008). The void ratio function is plotted against the shear modulus value produced by the GeoGauge as well as the shear wave velocities in Figure 4.5.

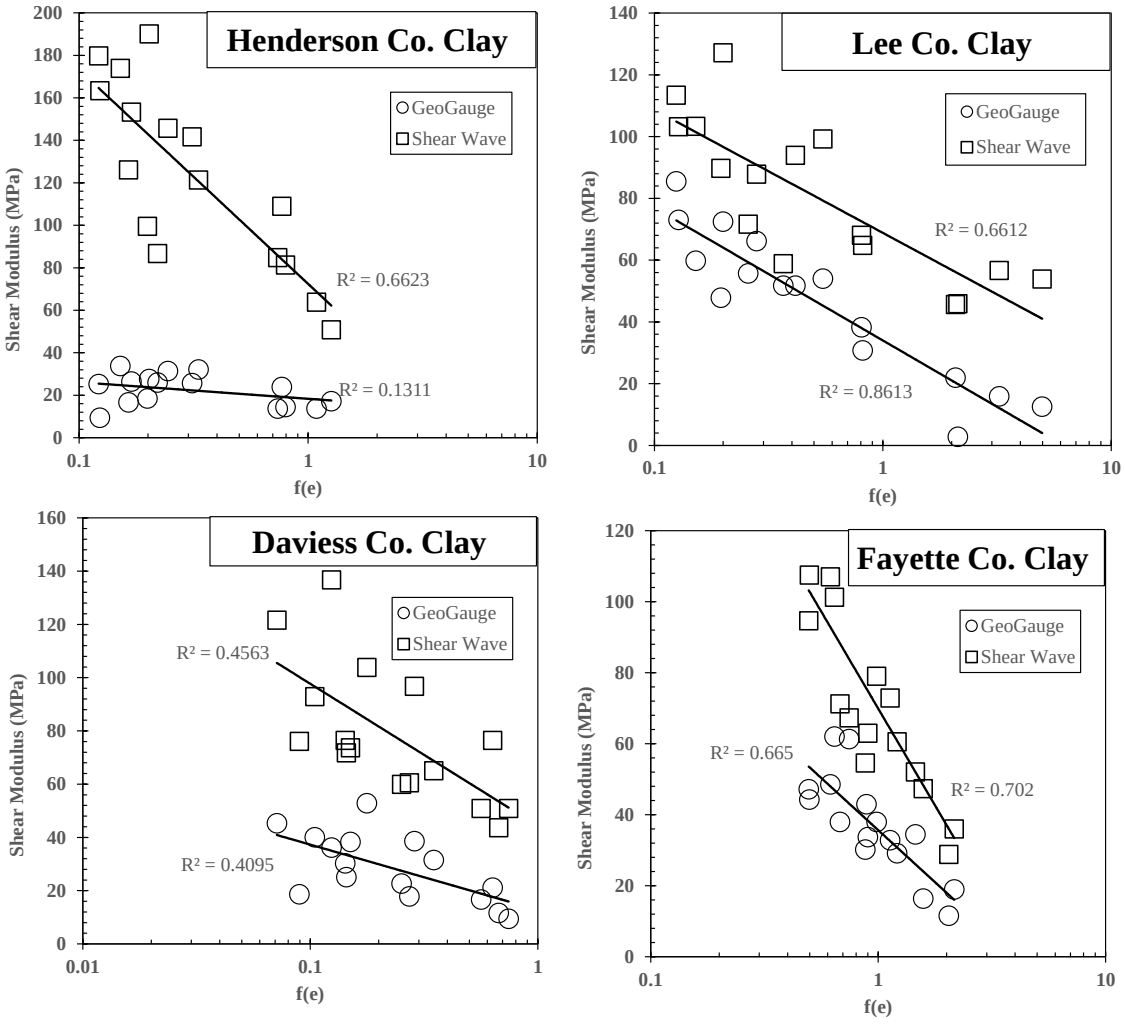

Figure 4.5: Shear modulus versus void ratio function

The $f(e)$ axis was plotted on a logarithmic scale, and a logarithmic function was used to determine the trends. For all four of the clays, the shear modulus produced by the GeoGauge was lower than the shear modulus value from the shear wave velocities. This may have been due to the fact that the shear wave velocities took the depth of the soil into account, or the shear waves may have made a better contact with the soil particles. Both methods used to calculate the shear modulus showed a somewhat steady trend that the shear modulus decreased as the void ratio function increased.

4.4 Variation of Matric Suction with a Density Gradient

Due to the fact there was no physical measurement of the soil suction available during the testing, an empirical approach was used to investigate the relationship between the degree of saturation and the initial void ratio. This approach, which was presented by Zhou et al. (2012) presented a method to quantify the effect of initial density on the soil-water characteristic curve for a three-phase unsaturated soil mixture of pore air, pore water, and solid soil particles.

A new parameter was presented, ζ, which was referred to as a fitting parameter, and is calibrated through experimentation. The effective degree of saturation was calculated based on known values of the initial effective degree of saturation, void ratio, and a dry density. Void ratio values used to represent a density gradient were taken from four stages of soil compaction. At each point of compaction, the void ratio, degree of saturation, and net normal stress were all recorded from testing data. To apply the Zhou et al. (2012) method to this research specifically, a void ratio was calculated for each stage of compaction (or increase in density gradient), and four of these void ratios were used to calculate four matric suction values using the initial data provided by the SWCC at maximum dry density based on data from Kidd (2012).

The fitting parameter, ζ, typically was said to require a minimum of two soil water characteristic curves for calibration. One of which is referred to as the reference SWCC, and the other being the SWCC at a new density (or different void ratio). Equation 14 gives the expression provided by Zhou et al. (2012) to calibrate the fitting parameter for a given void ratio based on reference data.

$$\ln\frac{e_{Ref}}{e_i} \approx \frac{\left(S_e - S_e^{Ref}\right)}{6}\left[f\left(S_e^{Ref}\right) + 4f\left(\frac{S_e^{Ref} + S_e}{2}\right) + f\left(S_e\right)\right] \quad (14)$$

where e^{Ref} is the void ratio at maximum dry density, e_i is the void ratio at a specified stage of compaction, S_e^{Ref} is the effective degree of saturation at maximum dry density, and S_e is the effective degree of saturation at the same stage of compaction as e_i.

In Equation 14, there are three functions inside the brackets on the right hand side of the equation. These function are referred to as $f(x)$, which is a function of soil saturation, and three different values of x are used. These values of x are either functions of the reference degree of saturation, the effective degree of saturation, or both for the middle term. Equation 15 provides the expression for $f(x)$, which is a factor or the specific value of x in Equation 14, and the fitting parameter, ζ.

$$f(x) = \frac{1}{x(1-x)^{\varsigma}} \quad (15)$$

where x refers to the three values contained in the $f(x)$ term from Equation 14.

Unfortunately there was only one available SWCC for each of the soil samples being tested, each of which were created by Kidd (2011), and were found using the Fredlund and Xing Method, presented in Equation 8. This made it impossible to determine the second value of ζ needed to calibrate the exact value needed, and for that reason, a value of 0.5 was used for ζ due to the fact that it was readily available, and was also near the mean value of ζ values determined through testing performed by Zhou et al. (2012). However, with

the one available SWCC, which was conveniently evaluated at each soils' maximum dry density, and an assumed value of ζ, all of the required parameters for the Zhou et al., (2012) method were known. The form of Equation 13 with an assumed fitting parameter value of 0.5, shown in Equation 16.

$$\frac{1-\sqrt{1-S_e}}{1+\sqrt{1-S_e}} = \frac{e_i^{Ref}}{e_i}\frac{1-\sqrt{1-S_e^{Ref}}}{1+\sqrt{1-S_e^{Ref}}} \quad (16)$$

The reference SWCC provided the degree of saturation as well as the residual degree of saturation, S_e^{Res}, which was described in Section 2.3. Due to the fact that the degree of saturation remains constant, irrespective of any change in volume for unsaturated soil at the residual degree of saturation, the value of S_e^{Res} was considered constant for each soil. This allowed for a simple way to calculate the degree of saturation for all four of the test soils at various void ratios. The effective degree of saturation for the reference SWCC was determined using Equation 17.

$$S_e^{Ref} = \frac{S^{Ref} - S^{Res}}{1-S^{Res}} \quad (17)$$

MathCAD was used to evaluate Equation 16 to solve for the effective degree of saturation based on the three required parameters (e_i, e^{Ref}, S_e^{Ref}), and is shown in Equation 18. The corresponding values of X_1, X_2 and Y_1 through Y_3 are provided in Equation 19 through Equation 23.

$$S_e = \frac{4*\left[X_1 + X_2\right]}{Y_1 + Y_2 + Y_3} \quad (18)$$

$$X_1 = -S_e^{Ref\,2} e_i^{Ref\,3} e_i + 2S_e^{Ref\,2} e_i^{Ref\,2} e_i^{\,2} - S_e^{Ref\,2} e_i^{Ref} e_i^{\,3} \quad (19)$$

$$X_2 = 2\sqrt{1 - S_e^{Ref}}\, S_e^{Ref} e_i^{Ref\,3} + 2S_e^{Ref} - 2S_e^{Ref} S_e^{Ref} + 2S_e^{Ref} e_i^{Ref} e_i^{\,3} \quad (20)$$

$$Y_1 = S_e^{Ref} e_i^{Ref\,4} - 4S_e^{Ref\,2} e_i^{Ref\,3} e_i + 6S_e^{Ref\,2} e_i^{Ref\,2} e_i^{\,2} \quad (21)$$

$$Y_2 = -4S_e^{Ref\,2} e_i^{Ref} e_i^{\,3} + S_e^{Ref\,2} e_i^{\,4} + 8S_e^{Ref} e_i^{Ref\,3} e_i \quad (22)$$

$$Y_3 = -16S_e^{Ref} e_i^{Ref\,2} e_i^{\,2} + 8S_e^{Ref} e_i^{Ref} e_i^{\,3} + 16 e_i^{Ref\,2} e_i^{\,2} \quad (23)$$

After the effective degree of saturation was calculated, the degree of saturation was then determined by rearranging Equation 17 to solve for the degree of saturation, S_i (note that the "Ref" terms have been removed from the S terms, since the equation is no longer only referring to the reference SWCC values). Equation 24 provides the expression to solve for the degree of saturation with a density gradient based on the effective degree of saturation and the residual degree of saturation.

$$S_i = S_e\left(1 - S^{Res}\right) + S^{Res} \quad (24)$$

With the reference SWCC known, showing the relationship between the degree of saturation and matric suction at each soil's maximum dry density, the Zhou et al. (2012)

method was used to create a table showing the relationship between the decrease in saturation at the reference void ratio, the decrease in saturation at the void ratio, e_i, and the corresponding matric suction. The data was then plotted to create a new SWCC for each of the test soils at four different void ratio values, which corresponded to an increasing density gradient.

Each value of e_i corresponded to a net normal stress and a degree of Saturation, which was physically calculated based on the gravimetric water content, w, the void ratio, e_i, and the specific gravity, G_S. The matric suction was then found for each value of S_i by means of interpolation of the matric suction versus degree of saturation data. Figure 4.6 shows the SWCC for the Henderson County clay at the first moisture content of 11.4 percent, and all of the soil-water characteristic curves generated for the other four clays and the four moisture contents that each were tested are located in Appendix D.

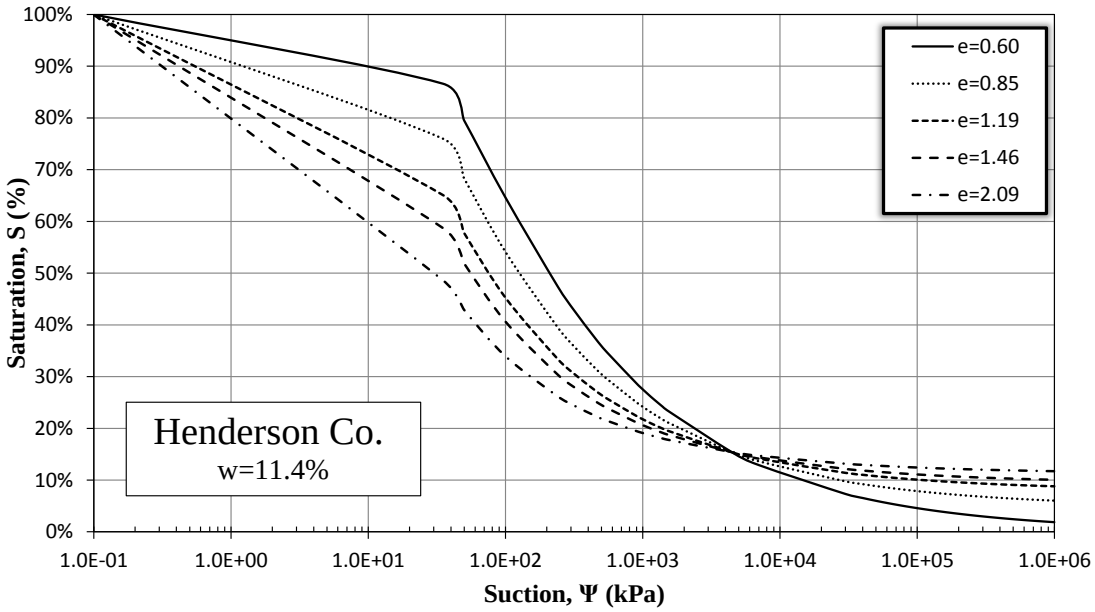

Figure 4.6: Soil Water Characteristic Curve for Henderson County at w=11.4%

4.4.1 Relationship between Matric Suction and Net Normal Stress

A trend was seen between the matric suction derived using the Zhou et al. equation and the net normal stress, p. The net normal stress was calculated by taking the average value of the three pressure plate stress readings, and is provided in Equation 25.

$$p = \frac{\sigma_1 + \sigma_2 + \sigma_3}{3} \qquad (25)$$

where σ_1, σ_2, and σ_3 represent the three stresses recorded by the pressure plates. The net normal stress was plotted against the net normal stress under loading, p_{UL}, which required the load frame to be paused and the net normal stress after rebound, p_{AR}, which was the stress on the pressure plates after the soil had been given enough time to fully

rebound. Naturally, p_{AR} was much smaller than p_{UL} . Figure 4.7 shows the results of the suction versus net normal stress (under load) for all four of the clays.

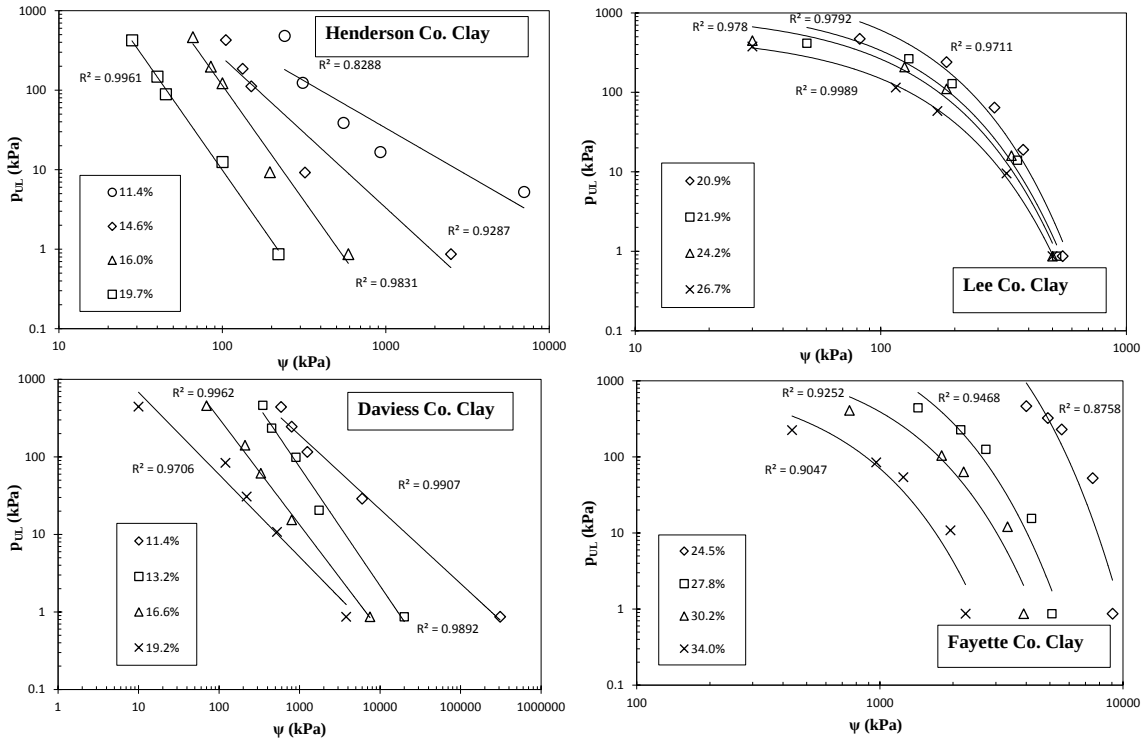

Figure 4.7: Matric suction versus net normal stress under loading

From Figure 4.7, it is apparent that for all four of the clays, the net normal stress under loading was directly proportional to the matric suction. The Henderson County and Daviess Counties showed a strong linear trend, and the Lee and Fayette County clays showed a strong trend using a logarithmic function. As expected, at higher net normal stresses, lower suction values were observed and a highly predictable trend was seen between the net normal stress under loading and the matric suction. Figure 4.8 shows the same plots for the matric suction versus the net normal stress on the four clays after they had been given time to rebound once the load was released.

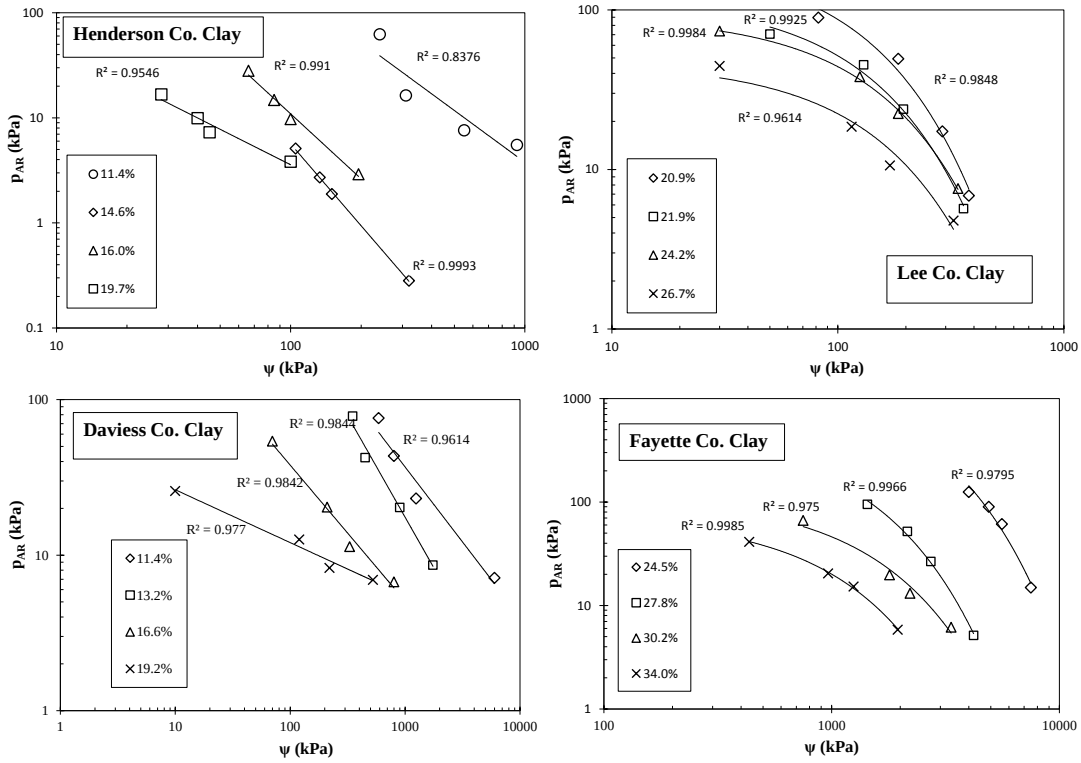

Figure 4.8: Matric suction versus net normal stress after rebound

In Figure 4.7 and Figure 4.8, an extremely strong trend was seen between the matric suction and net normal stress both while under the controlled loading and after the removal of the load. This remarkably strong trend between soil suction and net normal stress brought attention to the fact that these closely related parameters could most likely be used in some combination to form a relationship with soil stiffness and therefore could impact the shear modulus. The Henderson County and Daviess Counties showed a strong linear trend, and the Lee and Fayette County clays showed a strong trend using a logarithmic function.

From Figure 4.7 and Figure 4.8, the lean clays (Henderson Co. and Daviess Co.) showed a very strong trend with a power function, and the fat clays (Lee Co. and Fayette Co.) showed the most accuracy when an exponential function was used. The general

expression for a power function is given in Equation 26 and Equation 27 provides the general expression for an exponential function. Table 4.2 and Table 4.3 provide the constants used for the “m” and “b” terms for each of the four clay samples.

$$y = m * x^{b} \quad (26)$$

$$y = m * e^{b*x} \quad (27)$$

Table 4.2: Parameters for net normal stress under loading versus matric suction

		Moisture Content	m	b
Lean Clays	**Henderson County**	11.4%	121719	-1.187
		14.6%	2000000	-1.889
		16.0%	70000000	-2.905
		19.7%	8000000	-2.941
	Daviess County	11.4%	143787	-0.958
		13.2%	3000000	-1.533
		16.6%	172128	-1.37
		19.2%	7873.3	-1.062
Fat Clays	**Lee County**	20.9%	2364.9	-0.014
		21.9%	1282.3	-0.013
		24.2%	995.92	-0.013
		26.7%	530.44	-0.013
	Fayette County	24.5%	106463	-0.001
		27.8%	7385.9	-0.002
		30.2%	2399.1	-0.002
		34.0%	1170	-0.003

Table 4.3: Parameters for net normal stress under loading versus matric suction

		Moisture Content	m	b
Lean Clays	**Henderson County**	11.4%	304998	-1.636
		14.6%	843247	-2.587
		16.0%	139426	-2.053
		19.7%	625.57	-1.121
	Daviess County	11.4%	29023	-0.965
		13.2%	141219	-1.302
		16.6%	2126	-0.874
		19.2%	57.588	-0.34
Fat Clays	**Lee County**	20.9%	208.85	-0.009
		21.9%	118.49	-0.008
		24.2%	92.141	-0.007
		26.7%	460877	-0.007
	Fayette County	24.5%	1739.3	0.0006
		27.8%	478.1	-0.001
		30.2%	114.78	-0.0009
		34.0%	72.385	-0.001

5 RELATIONSHIP BETWEEN SHEAR WAVE VELOCITY AND GEOGAUGE STIFFNESS

5.1 An Empirical Method to Estimate Matric Suction from GeoGauge Stiffness Measurements

With the matric suction of the soils calculated using the Zhou et al. (2012) method, a relationship between matric suction and GeoGauge stiffness measurements would potentially show a prediction model for the matric suction of a soil by simply taking a stiffness reading using the GeoGauge to some basic soil parameters.

The strength and stiffness of saturated soils mainly depends on the effective stresses on the soil. However, the behavior of unsaturated soils depends mainly on both the matric suction as well as the net normal stresses action on the soil specimen. Parameters such as void ratio, degree of saturation, matric suction, and net normal stress were known for all four of the clay samples. Due to the fact that matric suction and the net normal stress play a significant factor in the stiffness behavior of unsaturated soils, vigorous attempts were made to identify a function of these two parameters that would correlate with a function of the shear modulus values produced from both the GeoGauge and the shear wave velocity calculations. A strong relationship was eventually observed by taking the square root of the sum of the net normal stress, p, and the matric suction, ψ, and plotting that value against the shear modulus calculated from the GeoGauge, $G_{SSG,}$ divided by the void ratio function, $f(e)$. A logarithmic trend line provided the most accuracy with strong indicators of predictable behavior for all four of the clay samples.

The plots for the Henderson County clay are provided in Figure 5.1. Plots of $(p+\psi)^{1/2}$ versus $G_{SSG}/f(e)$ for the other three clay samples are provided in Appendix C.

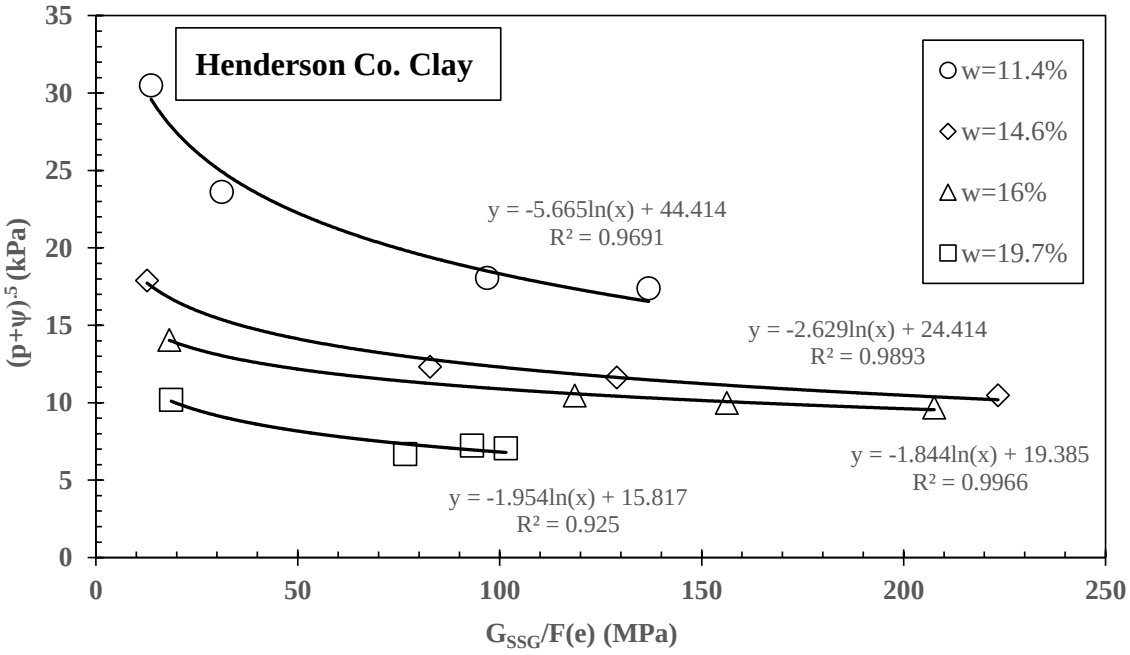

Figure 5.1: $(p+\psi)^{1/2}$ vs. G_{SSG} / F(e) for the Henderson County Clay

Based on logarithmic trend line data from plotting $(p+\psi)^{1/2}$ versus $G_{SSG}/f(e)$, a logarithmic relationship was found for each of the four soils at the four moisture contents. This relationship is provided in Equation 28, where A_1 is the x intercept, and A_2 is the y intercept.

$$(p+\psi)^{1/2} = A_1 * Ln\left[\frac{G_{SSG}}{f(e)}\right] + A_2 \qquad (28)$$

When analyzing the data for $(p+\psi)^{1/2}$ versus $G_{SSG}/f(e)$, it was important to observe a trend of either increasing or decreasing values of A_1 and A_2 with each of the four moisture contents plotted on the chart. After a relationship was found between A_1 , A_2 , and the moisture content, w , for all of the samples, the values were plotted graphically. The

plots of A_1 and A_2 versus gravimetric moisture content were again used to form trend lines (which were linear), and are provided in Equation 29 and Equation 30.

$$A_1 = C_1 * (w + C_2) \quad (29)$$

$$A_2 = C_3 * (w + C_4) \quad (30)$$

The plots for A_1 and A_2 versus w for the Henderson County clay are provided in Figure 5.2, and plots for all of the other samples are located in Appendix C.

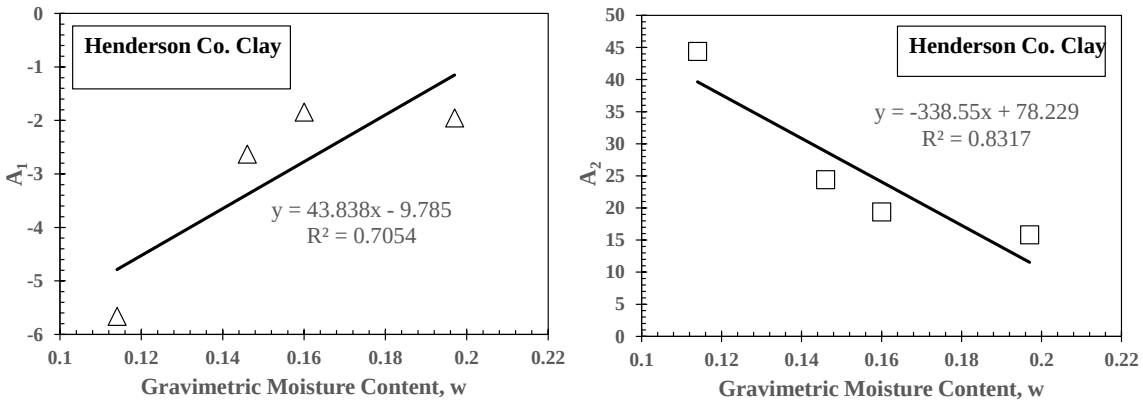

Figure 5.2: A1 and A2 versus gravimetric moisture content for Henderson Co.

A new expression was created using Figure 5.1 and Figure 5.2, which in theory would provide accurate matric suction values based on GeoGauge stiffness with known values for the void ratio, net normal stress, and the gravimetric moisture content. Equation 31 provides the long form of the expression by combining Equation 29 and Equation 30 with Equation 28.

$$(p+\psi)^{1/2} = C_1(w+C_2)*Ln\left[\frac{G_{SSG}}{f(e)}\right]+C_3(w+C_4) \quad (31)$$

Equation 32 provides a simplified version of Equation 31, by solving for only the matric suction. Using Equation 32, the matric suction can theoretically be determined by knowing the stiffness gauge shear modulus, void ratio, gravimetric water content, net normal stress, and constants C_1-C_4.

$$\psi = \left[C_1(w+C_2)*Ln(\frac{G_{SSG}}{f(e)})+C_3(w+C_4)\right]^2 - p \quad (32)$$

Figure 5.3 shows a plot of the matric suction from the Zhou et al. (2012), referred to as the actual matric suction, ψ_{act} versus the matric suction which was calculated using Equation 32, referred to as ψ_{calc}. The charts in Figure 5.3 show the two different suction values on the x and y axis and by setting both maximum axis values the same and with equal increments, the variation between values can be seen. The dashed line represents the median, and the data points would theoretically lie on that line for the best possible accuracy between the two suction values.

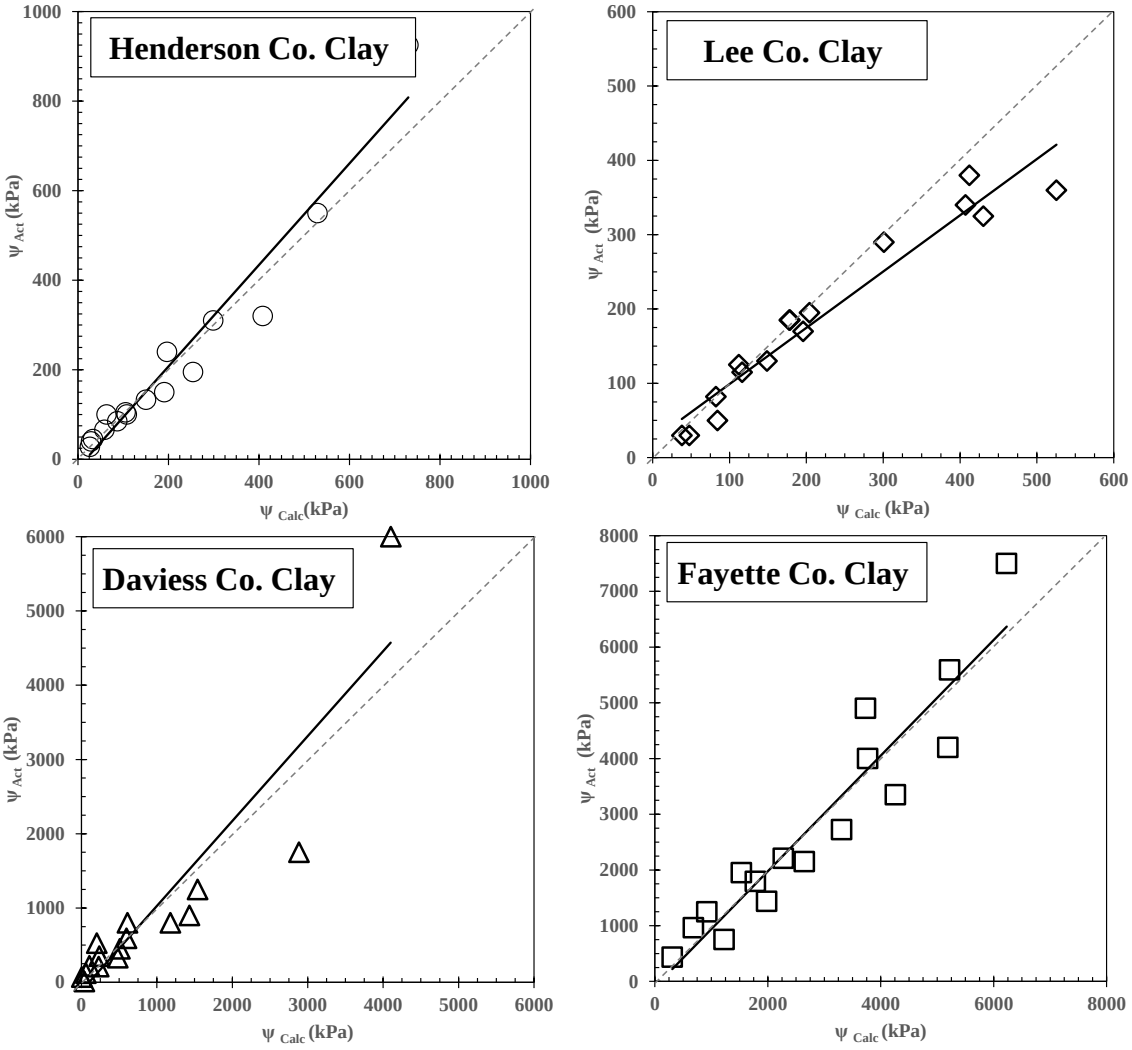

Figure 5.3: Matric suction from Zhou et al. vs. matric suction from Equation 30

It can be seen from Figure 5.3 that there is a very strong relationship between the Zhou et al. equation and the values for matric suction from Equation 32. All of the clays produced an R^2 value of 0.97 or higher, which gives the expression from Equation 32 a very strong amount of reliability for predicting a soil's matric suction if the net normal stress, void ratio, and shear modulus from the GeoGauge are known. Henderson and Fayette counties showed a very high R squared value, and the least reliable trend was given by the Lee

County clay, which clearly showed the most offset from the median line on the top right chart of Figure 5.3.

5.2 An Empirical Method to Estimate Matric Suction from Shear Wave Velocity Measurements

The next objective for this research was to find an expression to relate the shear modulus value derived from shear wave velocity measurements (after rebound), and the same function of $(p+\psi)^{1/2}$ that the shear modulus from the GeoGauge was compared to. The same methodology was used to relate the $(p+\psi)^{1/2}$ term to the shear modulus produced from shear wave velocities.

In this case, however, a better relationship was seen when the degree of saturation, S, was multiplied by the shear modulus, making a new term, $G_{AR} * S/f(e)$. A logarithmic trend was observed for the data, and the constants were referred to as *B*, as opposed to *A* in Section 5.1. Equation 33 provides the expression derived from the plots.

$$(P+\psi)^{1/2} = B_1 * Ln\left[\frac{G_{AR} * S}{f(e)}\right] + B_2 \qquad (33)$$

The plot for $(p+\psi)^{1/2}$ versus $G_{AR} * S/f(e)$ for the Henderson County clay is provided in Figure 5.4, and the plots for the other three clay soils can be found in Appendix C.

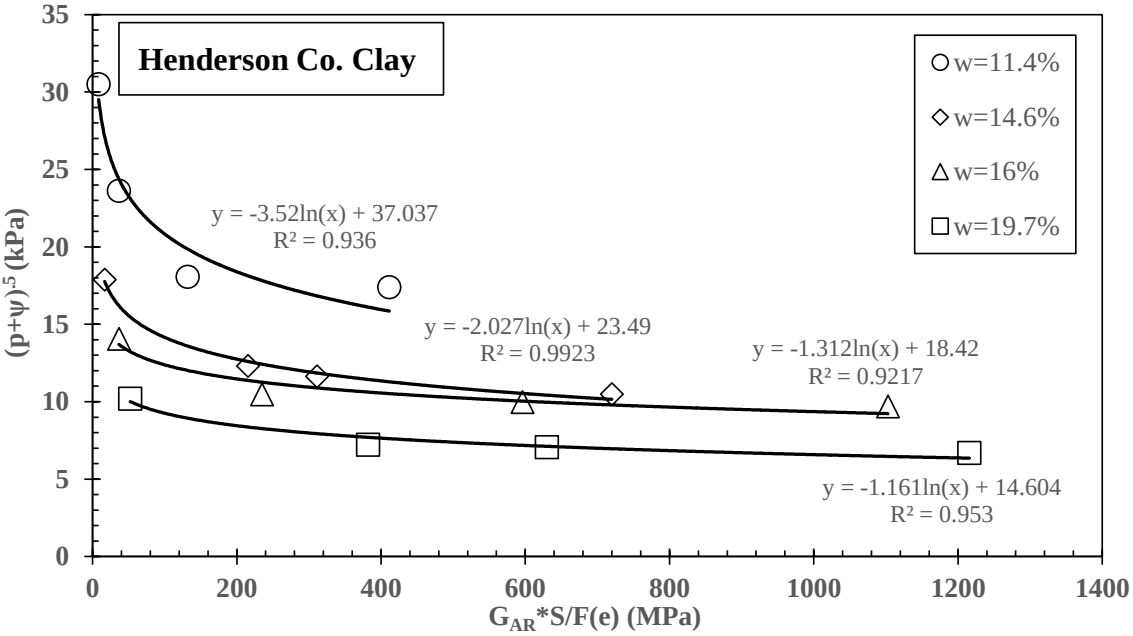

Figure 5.4: $(p+\psi)^{1/2}$ vs. $G_{AR}*S$ / f(e) for the Henderson County Clay

Similarly to the A parameters in Section 5.1, a trend was seen for the B values, where B_1 and B_2 were seen either increase or decrease steadily based on the gravimetric moisture content. Equation 34 and Equation 35 show the linear relationship between B_1 and B_2, and the gravimetric moisture content.

$$B_1 = D_1 * (w + D_2) \tag{34}$$

$$B_2 = D_3 * (w + D_4) \tag{35}$$

The plots of B_1 and B_2 versus gravimetric moisture content for the Henderson County clay are provided in Figure 5.5, and these plots for the remaining three soils can be found in Appendix C.

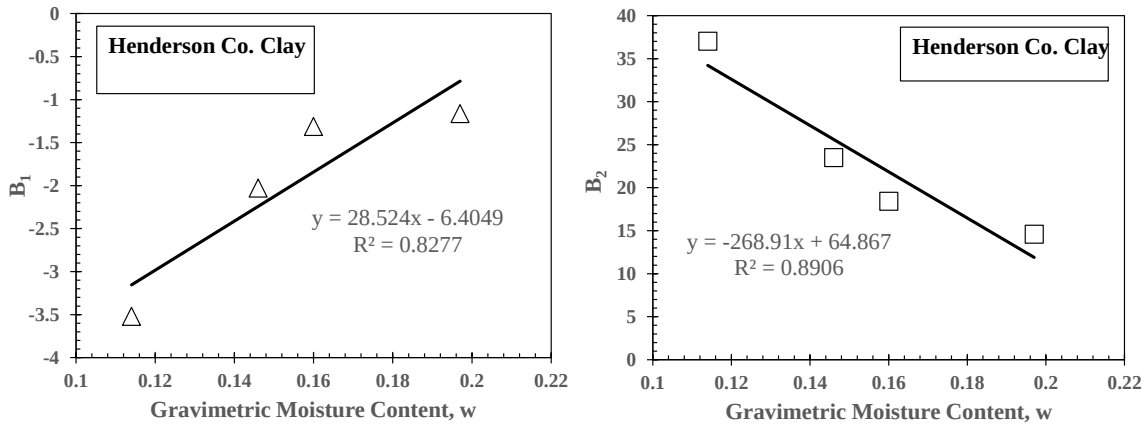

Figure 5.5: B_1 and B_2 versus gravimetric moisture content

Equation 36 provides the expression that is created when Equation 34 and Equation 35 are combined with Equation 33.

$$\left(P+\psi\right)^{1/2} = D_1\left(w+D_2\right)* Ln\left[\frac{G_{AR}*S}{f(e)}\right] + D_3\left(w+D_4\right) \qquad (36)$$

Table 5.1 provides a summary of all of the "A" and "B" parameters for the four clay samples, and Table 5.2 provides the "C" and "D" parameters of each sample.

Table 5.1: Summary "A" and "B" parameters for all soils.

	Moisture Content	A_1	A_2	B_1	B_2
Henderson County	11.4%	-5.665	44.414	-3.52	37.037
	14.6%	-2.629	24.414	-2.027	23.49
	16.0%	-1.844	19.385	-1.312	18.42
	19.7%	-1.954	15.817	-1.161	14.604
Lee County	20.9%	-1.556	23.453	-0.848	20.757
	21.9%	-1.218	19.732	-1.023	20.456
	24.2%	-1.76	21.754	-1.024	19.384
	26.7%	-1.859	20.045	-1.082	17.713
Daviess County	11.4%	-22.83	154.92	-18.5	136.27
	13.2%	-8.427	69.621	-7.149	64.16
	16.6%	-4.8	41.29	-4.418	40.682
	19.2%	-5.391	37.131	-4.4885	39.834
Fayette County	24.5%	-14.52	130.68	-11.73	118.56
	27.8%	-11.42	92.117	-10.95	93.836
	30.2%	-9.728	76.821	-8.239	75.552
	34%	-9.313	64.861	-7.972	62.585

Table 5.2: Summary of "C" and "D" parameters for all soils

	C Constant		*D* Constant	
Henderson County	C_1	43.8380	D_1	28.5240
	C_2	-0.2232	D_2	-0.2245
	C_3	-338.5500	D_3	-268.9100
	C_4	-0.2311	D_4	-0.2412
Lee County	C_1	-8.3179	D_1	-3.1750
	C_2	-0.0421	D_2	0.0789
	C_3	-33.9700	D_3	-52.7980
	C_4	-0.8597	D_4	-0.6050
Daviess County	C_1	195.7600	D_1	156.7700
	C_2	-0.2039	D_2	-0.2061
	C_3	-1351.2000	D_3	-1105.0000
	C_4	-0.2071	D_4	-0.2146
Fayette County	C_1	54.9810	D_1	43.7710
	C_2	-0.4958	D_2	-0.5134
	C_3	-681.6900	D_3	-595.7300
	C_4	-0.4249	D_4	-0.4384

5.3 Relationship between GeoGauge and Shear Wave Velocity Shear Modulus Values

Finally, an equation to solve for (and predict) the shear modulus that would be found based on shear wave velocity measurements (after loading and allowing for the soil to rebound), G_{AR}, was determined by setting Equation 31 and Equation 36 equal to one another, and is presented in Equation 37.

$$C_1(w+C_2)*Ln\left[\frac{G_{SSG}}{f(e)}\right]+C_3(w+C_4)=D_1(w+D_2)*Ln\left[\frac{G_{AR}*S}{f(e)}\right]+D_3(w+D) \qquad (37)$$

Equation 37 can be rearranged to solve for the Shear Modulus based on the shear wave velocity measurements. Equation 38 provides the expression to determine G_{AR} based on known soil parameters of void ratio, and the degree of saturation, and gravimetric moisture content.

$$G_{AR}=\frac{f(e)}{S}*\exp\left[\frac{C_1(w+C_2)*Ln\left[\frac{G_{SSG}}{f(e)}\right]+C_3(w+C_4)-D_3(w+D_4)}{D_1(w+D_2)}\right] \qquad (38)$$

5.4 Fidelity of the Constant Parameters

The results from Equation 38, were used to calculate the shear modulus from the shear wave velocity measurements (after rebound). G_{Emp} was compared to the actual shear modulus values from testing, G_{Calc}. The results from the comparison are shown in Figure 5.6.

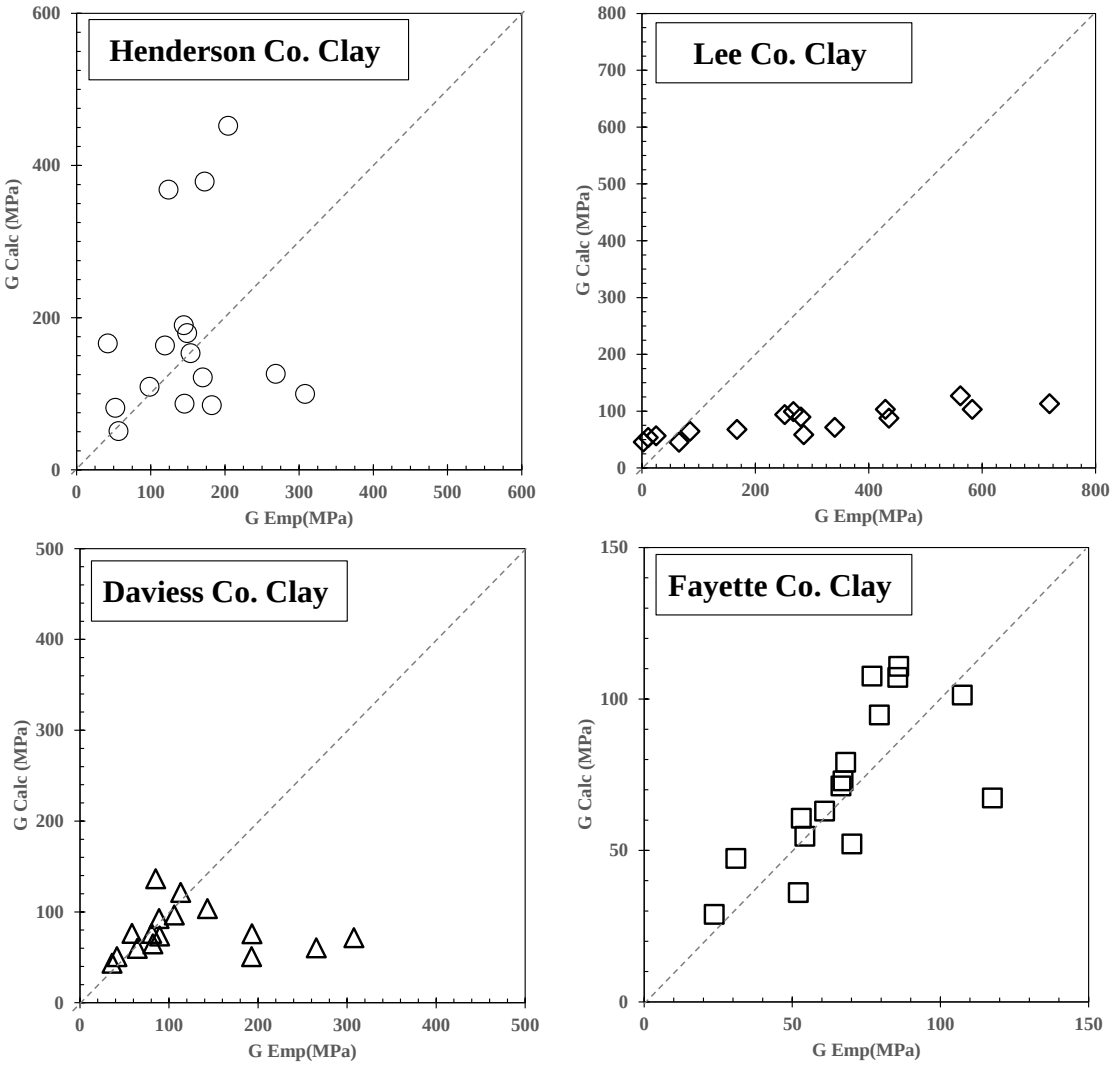

Figure 5.6: Calculated versus actual shear modulus values

The best correlation between the calculated shear modulus and the empirical shear modulus was seen in the Fayette County clay. The Lee County clay was by far the worst trend out of all of the clays. For the Lee County clay, the empirical value of the shear modulus was much higher than the actual shear modulus from test data. The Lee County clay had the lowest percent fines value and the highest clay fraction, and showed the worst relationship for predicting matric suction from Figure 5.3. The Lee County clay also showed the lowest R squared value when A_1 and A_2 were plotted against the gravimetric moisture content used to derive $C_1 - C_4$

5.5 Relationship between Constant Parameters and Material Properties

Further investigation was conducted in an attempt to relate the "C" and "D" parameters to the clays' material properties. A relationship between those parameters and material properties would yield an empirical method that would allow the parameters to be predicted, therefore making it possible to predict the shear modulus from shear wave velocity measurements based on material properties, soil-state parameters, and the GeoGauge shear modulus. A strong relationship was found between C_4 and the percent fines, as well as D_4 and the percent fines. Unfortunately, no other correlation was found, and all attempted plots can be found in Appendix E. The parameters for each of the clay soils were plotted against the percent fines and liquid limit. If a relationship does exist, it would most likely require a linear regression to be determined.

5.6 An Alternative Approach to Relate G_{AR} and G_{SSG}

Another attempt was made to investigate the relationship between the shear modulus values produced by the GeoGauge and the shear wave velocities. The functions used in Figure 5.1 and Figure 5.4 were used, and plotted against each other, neglecting the $(p+\psi)^{1/2}$ term. The plots for $G_{SSG}/f(e)$ versus $G_{AR}*S/f(e)$ are provided in Figure 5.7.

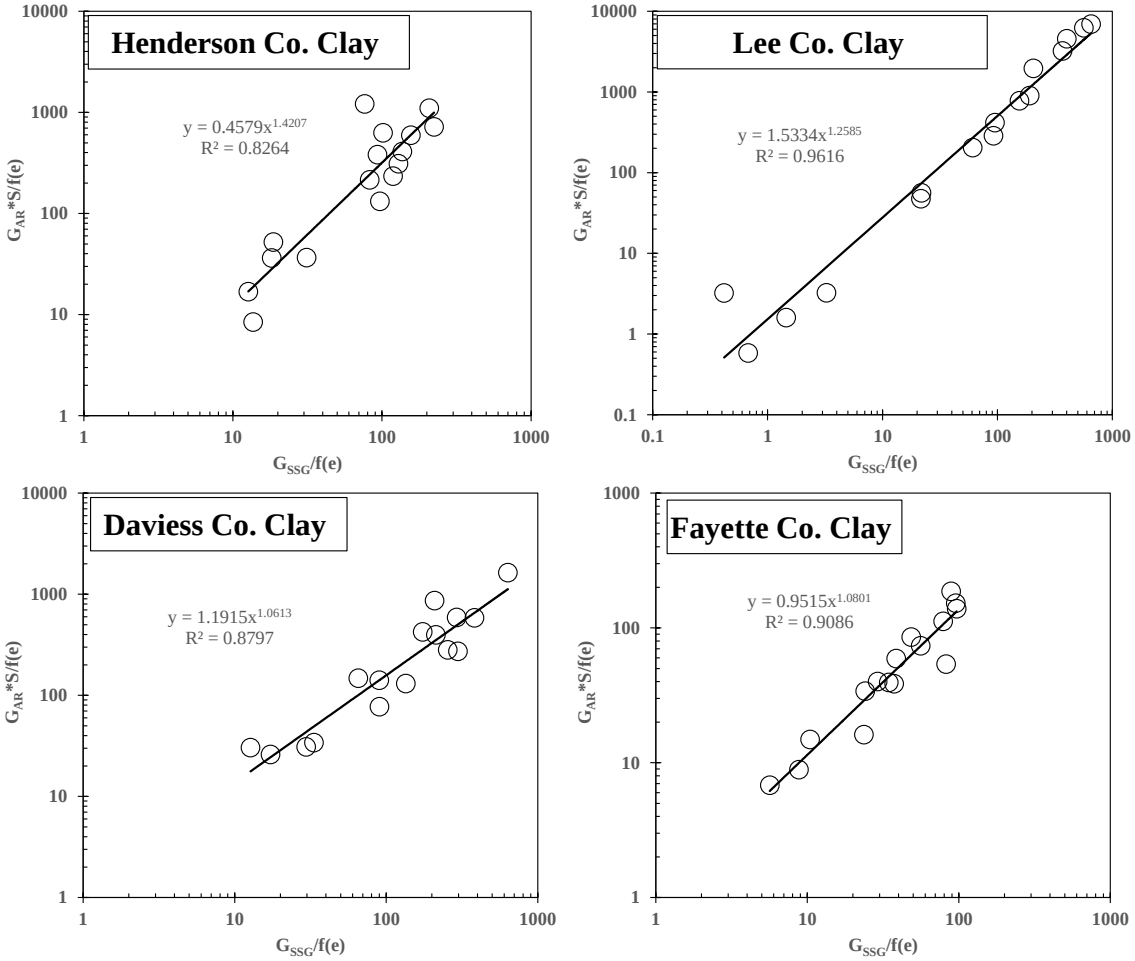

Figure 5.7: Relationship between the shear modulus functions

In Figure 5.7, both axes were plotted on a logarithmic scale, and a power function was found to provide a strong trend between the values. The power function used to relate $G_{AR} * S / f(e)$ to $G_{SSG} / f(e)$ is provided in Equation 39, and is simplified to solve for G_{AR} in Equation 40.

$$\frac{G_{AR} * S}{f(e)} = A_3 * \frac{G_{SSG}}{f(e)}^{B_3} \quad (39)$$

$$G_{AR} = \frac{A_3 * f(e) * \left[\frac{G_{SSG}}{f(e)}\right]^{B_3}}{S} \quad (40)$$

A_3 and B_3 represent the slope and intercept of the power function from Equation 39. Table 5.3 provides the values of A_3 and B_3 for all four of the clay samples.

Table 5.3: Values of A_3 and B_3 for all four of the clay soils.

	A_3	**B_3**
Henderson Co.	**0.4579**	**1.4207**
Lee Co.	**1.5334**	**1.2585**
Daviess Co.	**1.1915**	**1.0613**
Fayette Co.	**0.9515**	**1.0801**

The values of A_3 and B_3 were also examined for any relationship with the material properties of the four clay samples. They were plotted against the percent fines, clay fraction, plasticity index, activity (PI/CF), and the liquid limit. There was no strong trend found when these constants were plotted against the soil material properties. The plots created to attempt to find a relationship between A_3, B_3 and the material properties can be found in Appendix E.

6 CONCLUSIONS

The soil samples used for this research were carefully prepared to ensure that each test followed the same procedure as possible. Each clay was thoroughly mixed to ensure homogeneity by evenly distributing the water for a uniform moisture content and grain size distribution. Regardless of all attempts to simulate field behavior or unsaturated soils, there will always be non-uniform soil conditions present that cannot be perfectly duplicated, which could easily affect the outcome or shear wave velocities and GeoGauge readings. Despite the uncontrollable variations which exist in soil mechanics outside of the laboratory, the findings from this research provided a direct relationship between the GeoGauge stiffness readings and the shear modulus values computed from the elastic theory equation from shear wave velocity measurements. The overall conclusion of this research is that soil parameters and material properties have a significant effect on the stiffness behavior of unsaturated soils.

The findings form this research have shown that:

- The maximum dry density (MDD) was very closely approached, if not reached for all of the tests.
- The results of the three-layer box tests were not used in the data analysis of this research, because more data was available from the single-compression tests, and the single-compression tests were able to adequately reach the maximum dry density for all of the soils.
- The shear wave velocities did not show much variation based on the depth in which they were measured. However, the shear waves did show a steady

increase in travel time after each compression increment (or increase in dry density), which was expected. It has been noted that the shear wave travel times were found based on human interpretation of the PicoScope charts. Suggested further research could include a more advanced computer program to measure the shear wave travel times, or measure multiple aspects of the waves, such as peak-to-peak distances.

- The matric suction of the four Kentucky clays was calculated using the Zhou et al. (2012) method, and provided a model to analyze the behavior of each soil's suction under a density gradient. Suggested further research in this area would be to apply a matric suction probe to physically measure the soil suction, and compare those findings to the Zhou et al. (2012) expression, or to develop a minimum of two SWCCs for each soil so that a more accurate fitting parameter, ζ,, could be determined through means of calibration.
- Based on the results of the box testing on four Kentucky clays, a relationship was found between the values of the two methods for the shear modulus, G, which were observed from the GeoGauge and shear wave velocity measurements. This relationship showed a high factor of reliability.
- A generalized expression (provided in Equation 21) was developed to determine the matric suction based on known values of the void ratio, gravimetric moisture content, net normal stress, and basic material properties in order to determine the constants $C_1 - C_4$.
- When the shear modulus from the shear wave velocity measurements was compared to the shear modulus from Equation 38, most of the clays had a good

relationship between the two values. The Lee County clay had the lowest correlation between the calculated and tested shear modulus values, and most of the soils had a good correlation at lower degrees of saturation and lower density values which indicated the early stages of compaction.

- The attempt to find empirical equations to predict the "C" and "D" parameters was unsuccessful. There was no direct relationship between all of the parameters and the material properties. The only direct relationship was seen between C_4, D_4 and the percent fines value. All of the parameters were plotted against the percent fines and liquid limit, and the results are shown in Appendix E. Suggested further research into this subject would be to conduct a regression analysis to attempt every possibly combination of material properties and parameter values to find any possibly relationship between them. The absence of a relationship between G_{AR} and G_{SSG} with the soils' material properties from this method indicated that the initial gravimetric moisture content did not have much (if any) influence on the relationship between the shear modulus values.
- A second attempt was made to evaluate a relationship between G_{AR} and G_{SSG} by plotting the functions of $G_{AR} * S / f(e)$ and $G_{SSG} / f(e)$ against each other, and neglecting the $(p+\psi)^{1/2}$ term. A power function in the form of $\frac{G_{AR} * S}{f(e)} = A_3 * \frac{G_{SSG}}{f(e)}^{B_3}$ was found, producing a strong R-squared value. However, when the values of A_3 and B_3 were plotted against the material properties of the clay samples, no strong relationship was seen.

APPENDIX A

PicoScope Specifications

Table A.1: PicoScope technical specifications (Pico Technology Ltd., 2007)

Variant	3204	3205	3206	3224	3424
Vertical resolution	8 bits			12 bits	
Analog bandwidth	50 MHz	100 MHz	200 MHz	10 MHz	
Max. sampling rate One channel in use Two channels in use 3 or 4 channels in use Repetitive signals	 50 MS/s 50 MS/s - 2.5 GS/s	 100 MS/s 100 MS/s - 5 GS/s	 200 MS/s 100 MS/s - 10 GS/s	 20 MS/s 10 MS/s - -	 20 MS/s 10 MS/s 5 MS/s -
Trigger bandwidth	50 MHz	100 MHz	150 MHz	10 MHz	
Buffer size (samples per channel) One channel in use Two channels in use 3 or 4 channels in use	 256 K 128 K -	 512 K 256 K -	 1 M 512 K -	 512 K 256 K -	 512 K 256 K 128 K
Inputs	2 BNC channels				4 BNC channels
	1 MΩ impedance AC/DC coupling 20 pF capacitance				
Outputs Signal generator	Fixed (Note 1)	Variable (Note 2)		None	
External trigger	1 BNC input shared with signal generator Variable trigger threshold ± 20 V Rising/falling 12.2 mV resolution 1 MΩ impedance			None	
Voltage ranges	± 100 mV to ± 20 V in 8 ranges			± 20 mV to ± 20 V in 10 ranges	
Accuracy	3% voltage 50 ppm time			1% voltage 50 ppm time	
Operating environment Temperature range Humidity	 0°C to 70°C (25°C for quoted accuracy) 25% to 75% RH			 0°C to 70°C (20°C to 30°C for quoted accuracy) 25% to 75% RH	
Overload protection Channels External trigger	 ± 100 V ± 30 V			 ± 100 V -	
PC connection	USB 2.0 Compatible with USB 1.1				
Power supply	From USB port: 4.6 to 5.25 V 500 mA External power supply is not required			From USB port	
Dimensions	140 mm x 200 mm x 45 mm				
Compliance	CE standard; FCC Part 15				

APPENDIX B

GeoGauge Specifications

Table B.1: GeoGauge technical specifications (Humboldt, 2007)

Conforms to ASTM D6758		
Soil Measurement Range	**From**	**To**
	MN/m (klbf/in)	MN/m (klbf/in)
Stiffness	3 (17)	70 (399)
	MPa (kpsi)	MPa (kpsi)
Young's Modulus	26.2 (3.8)	610 (89)
Measurement Precision (typ., Coefficient of Variation)	< 10 %	
Depth of Measurement (from surface)	220 to 310 mm (9 to 12 in.)	
Calibration	Laboratory	
Accuracy (% of actual mass)	$< \pm$ 1%	
Electrical		
Power Source	(6) D size disposable cells	
Battery Life	Sufficient for 500 to 1,500 measurements	
Mechanical		
External Materials	Aluminum case & foot, rubber isolators & seal	
Vibration	$<1.27 \times 10^{-6}$ m (<0.0005 in.) @ 125 Hz	
Level re Vertical	± 5 °	
Operating Temperature	0°C to 38°C (ambient)	
Storage Temperature	-20°C to 50°C	
Humidity	98%, without condensation	
Gauge Dimension	280 mm (11") Diameter, 255 mm (10") Height (without handle)	
Weight	Net: 10 kg (22 lbs), Shipping: with case, 17.7 kg (39 lbs)	
Standard Accessories		
Transit Case, 6 'D' Batteries, User Guide		
Optional Accessories		
* Infrared (IR) serial interface adapter cable with software template (3.5" floppy, PC only)		
* Verifier Mass		

APPENDIX C

Data used to determine "C" and "D" parameters for Lee, Daviess, and Fayette Counties

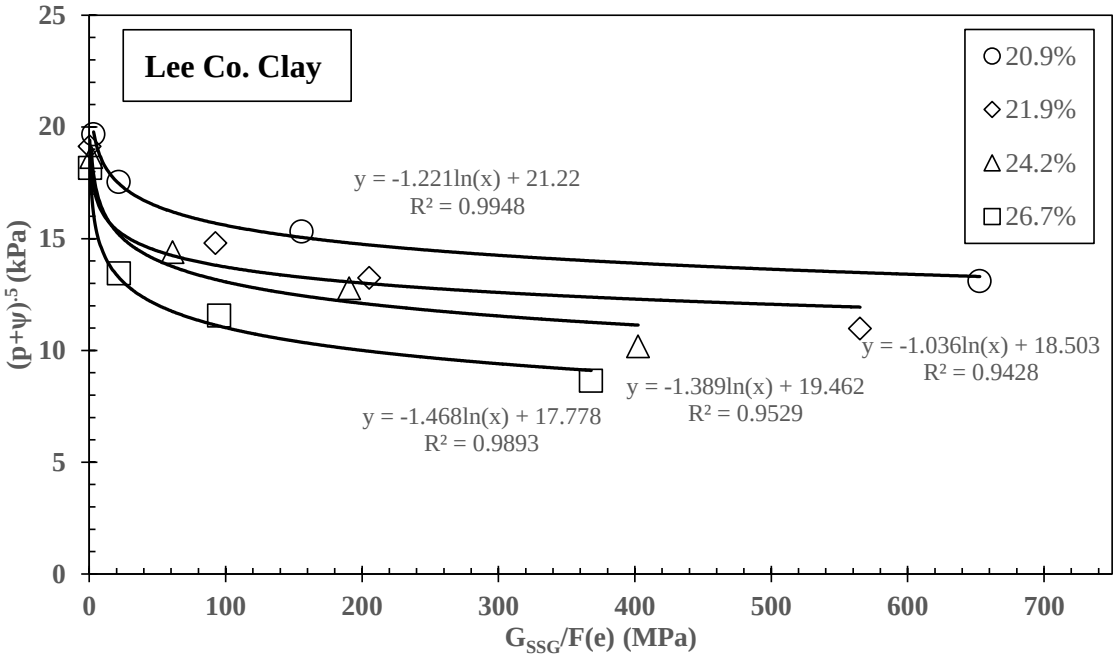

Figure C.1: $(p+\psi)^{1/2}$ vs. GSSG / f(e) for Lee County

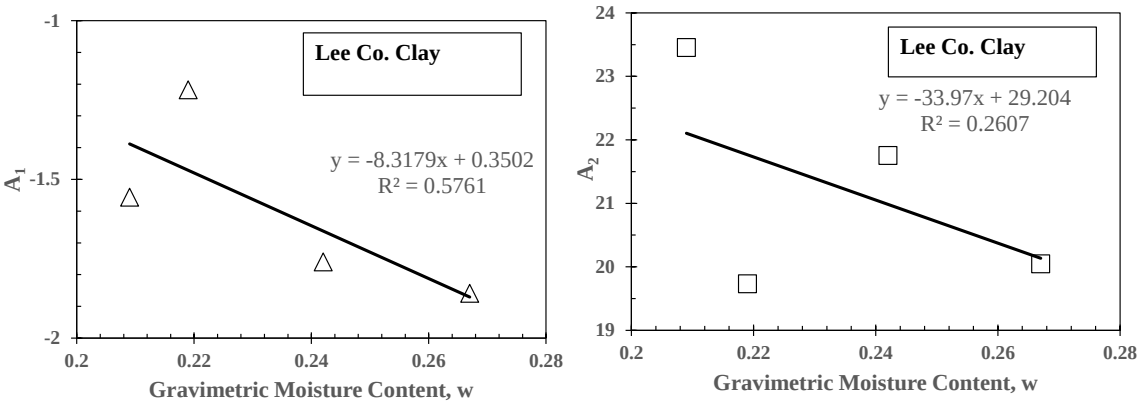

Figure C.2: A_1 and A_2 versus gravimetric moisture content for Lee County

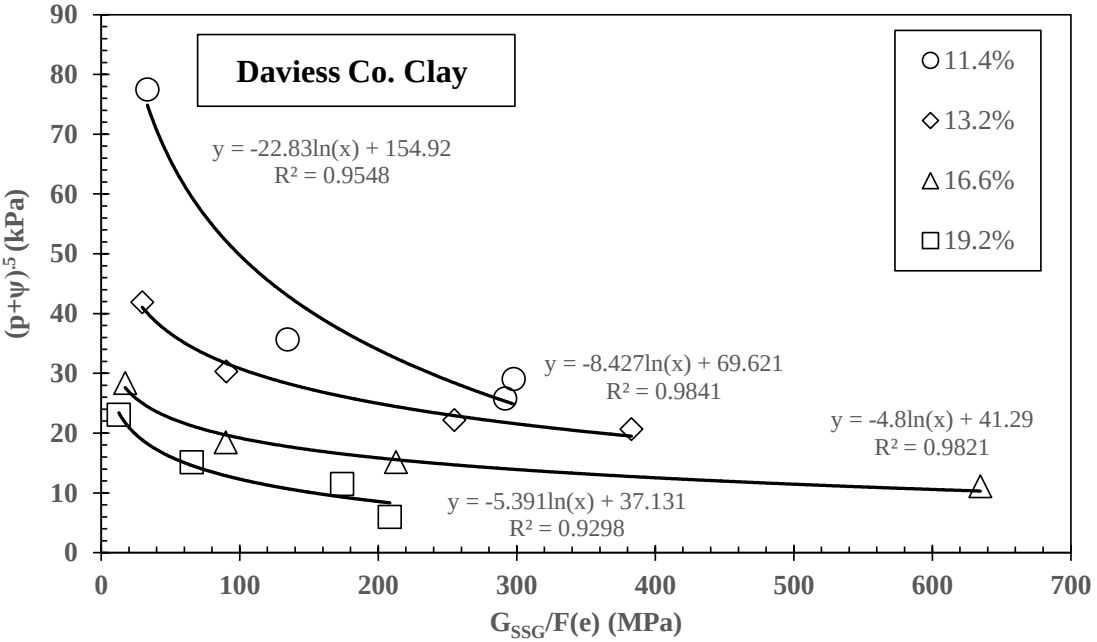

Figure C.3: $(p+\psi)^{1/2}$ vs. GSSG / f(e) for Daviess County

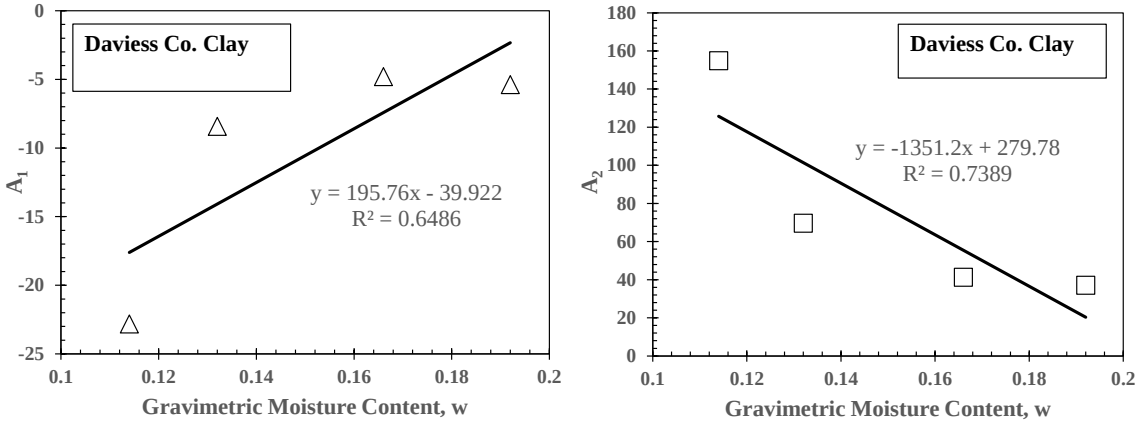

Figure C.4: A_1 and A_2 versus gravimetric moisture content for Daviess Co.

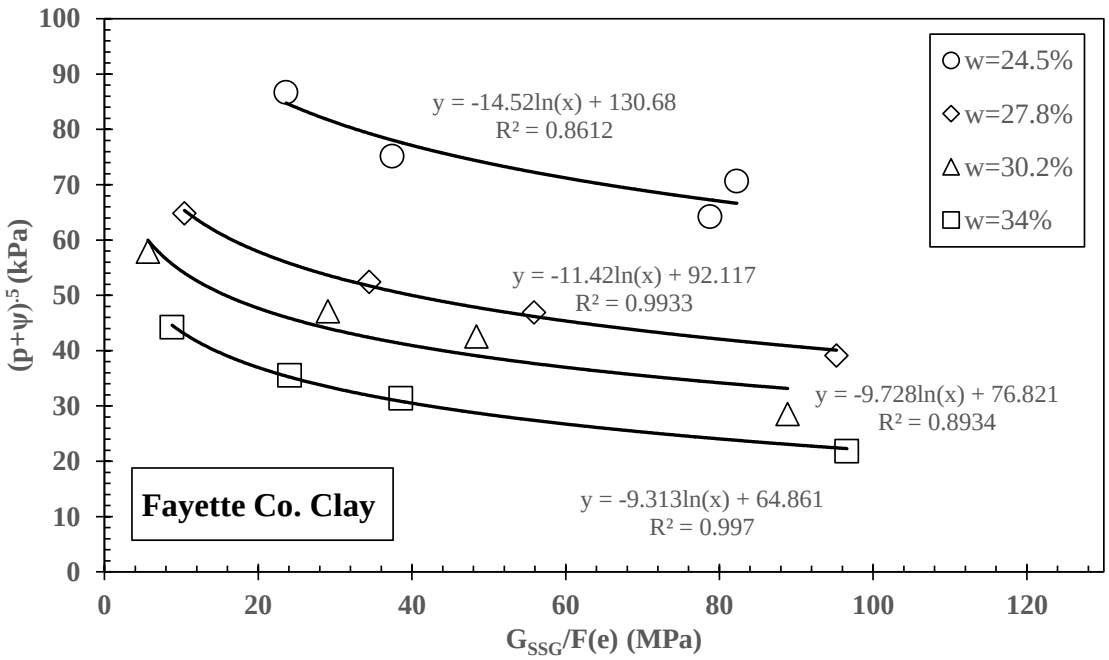

Figure C.5: $(p+\psi)^{1/2}$ vs. GSSG / f(e) for Fayette County

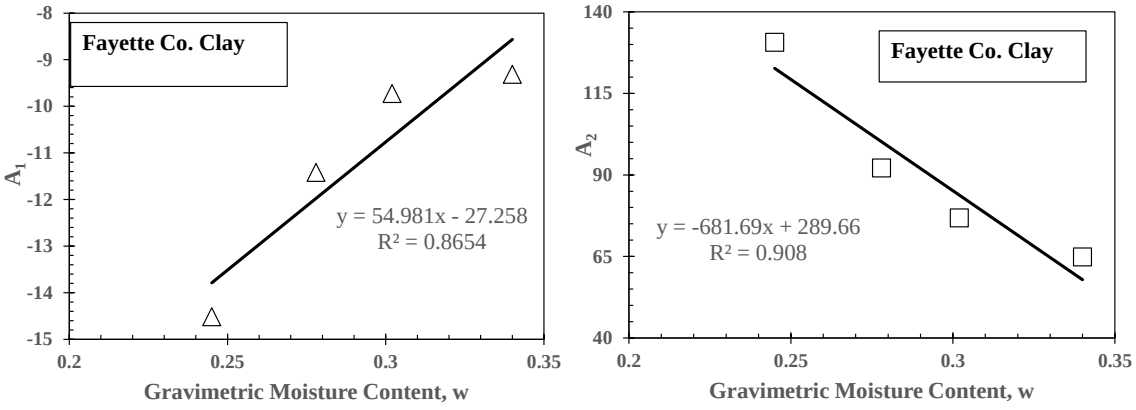

Figure C.6: A_1 and A_2 versus gravimetric moisture content for Fayette Co.

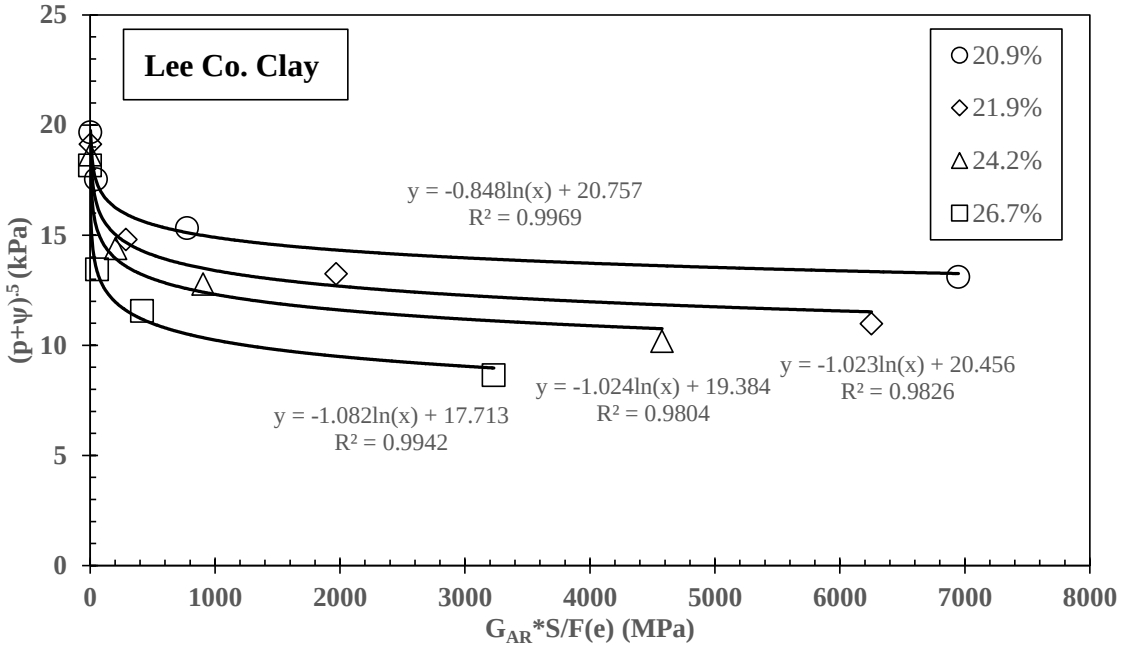

Figure C.7: $(p+\psi)^{1/2}$ vs. $G_{AR}*S / f(e)$ for Lee County

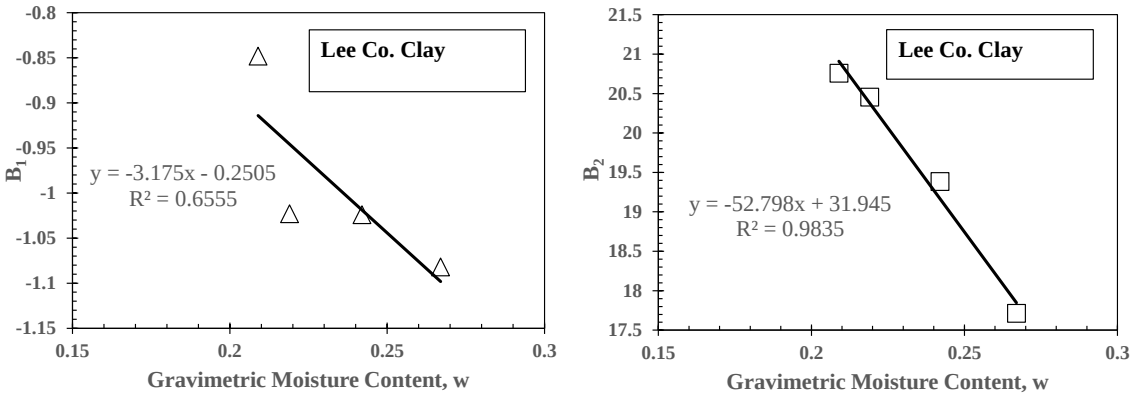

Figure C.8: B_1 and B_2 versus gravimetric moisture content for Lee County

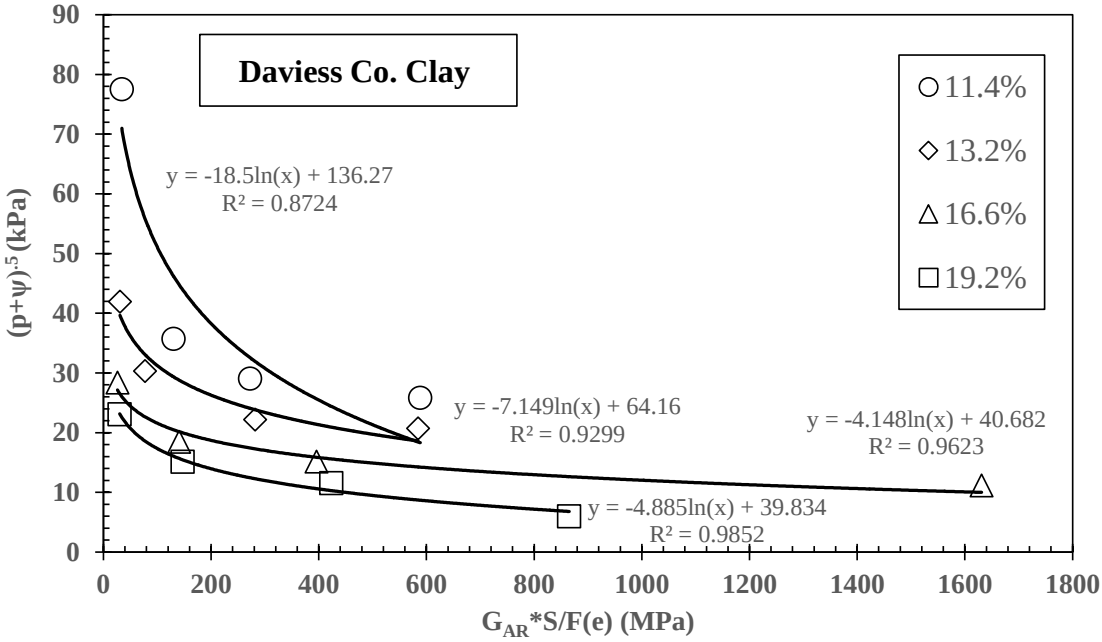

Figure C.9: $(p+\psi)^{1/2}$ vs. $G_{AR}*S / f(e)$ for Daviess County

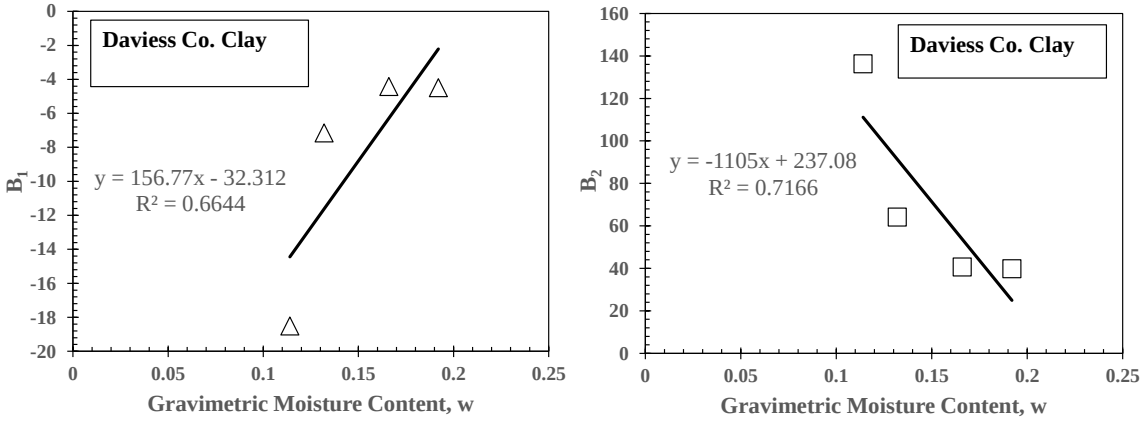

Figure C.10: B_1 and B_2 versus gravimetric moisture content for Daviess Co.

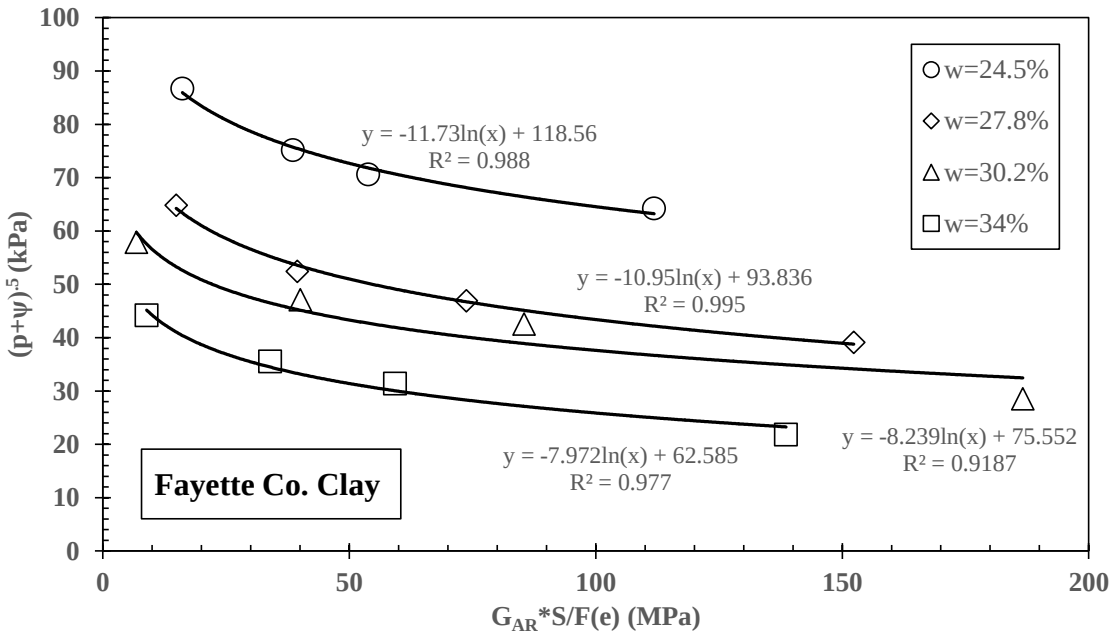

Figure C.11: $(p+\psi)^{1/2}$ vs. $G_{AR}*S / f(e)$ for Fayette County

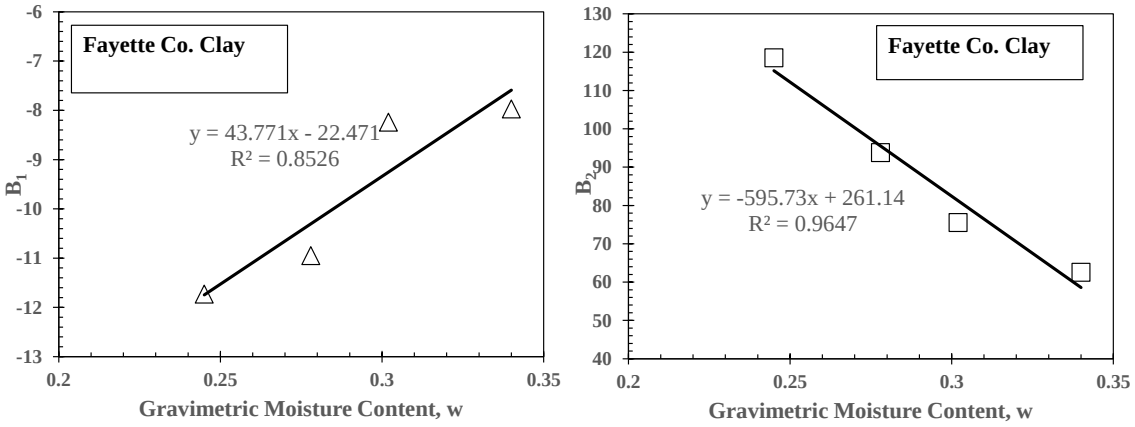

Figure C.12: B_1 and B_2 versus gravimetric moisture content for Fayette Co.

APPENDIX D

Soil Water Characteristic Curves

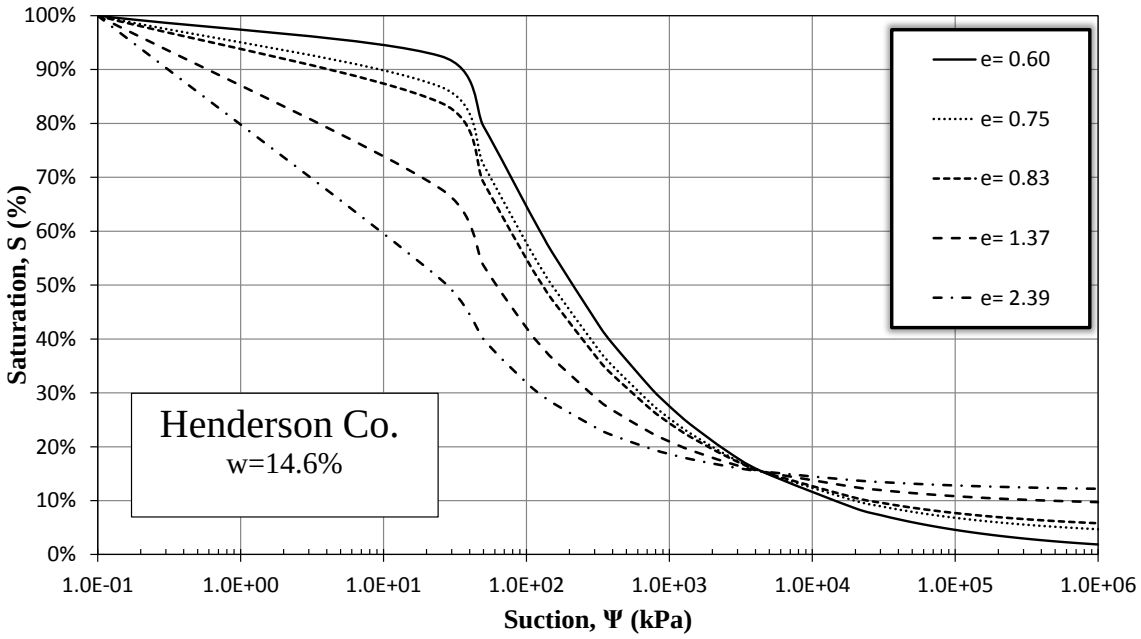

Figure D.1: Soil Water Characteristic Curve for Henderson County Clay at w=14.6%

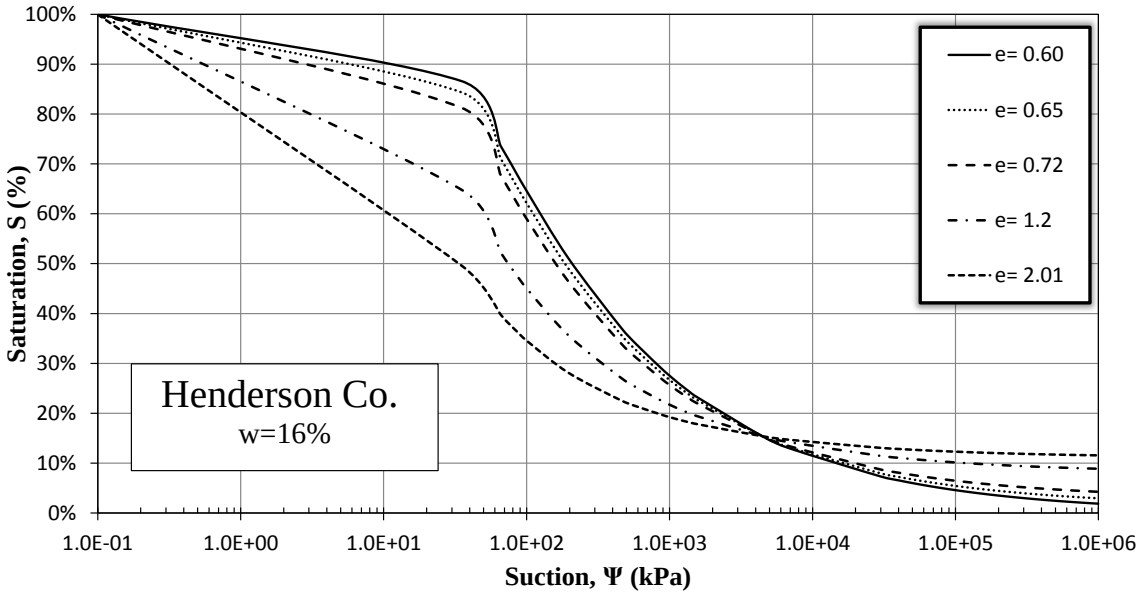

Figure D.2: Soil Water Characteristic Curve for Henderson County Clay at w=16%

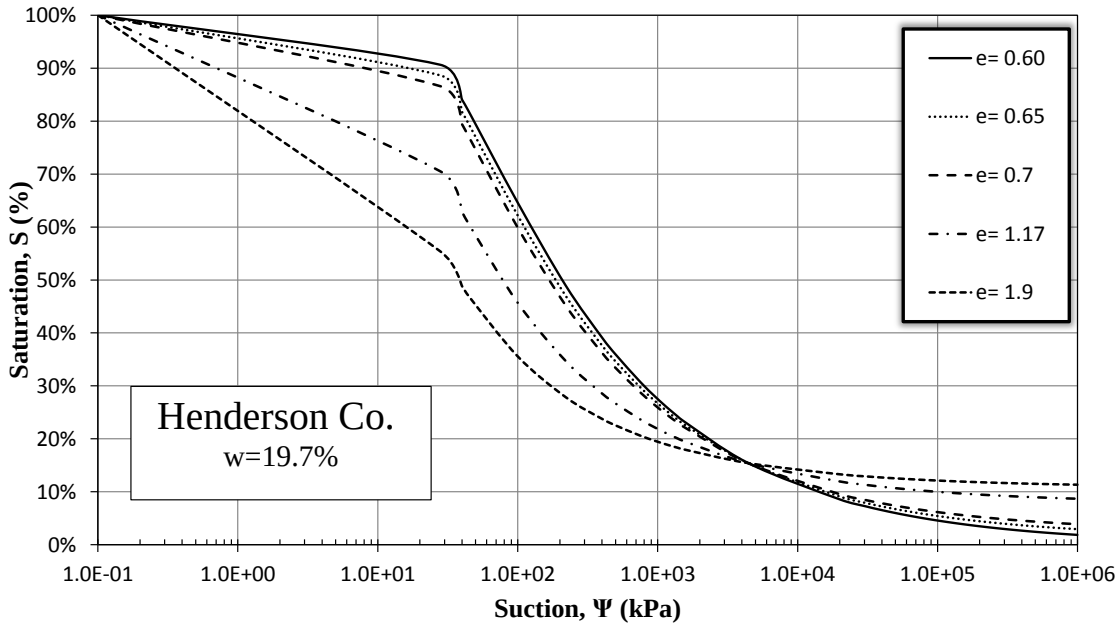

Figure D.3: Soil Water Characteristic Curve for Henderson County Clay at w=19.7%

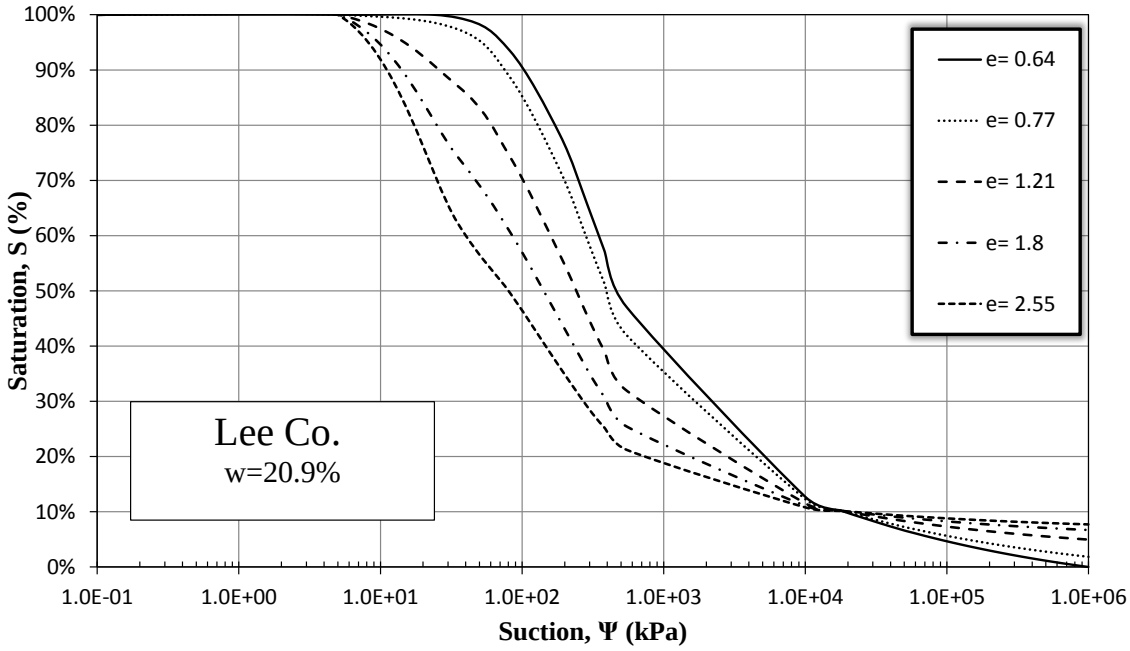

Figure D.4: Soil Water Characteristic Curve for Lee County Clay at w=20.9%

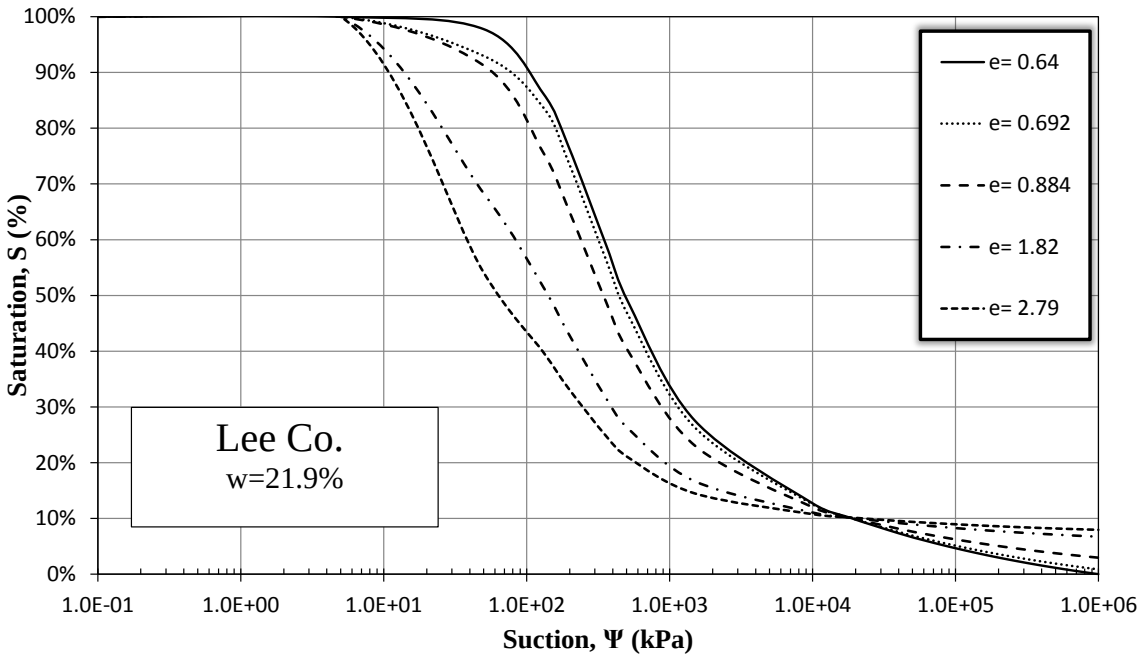

Figure D.5: Soil Water Characteristic Curve for Lee County Clay at w=21.9%

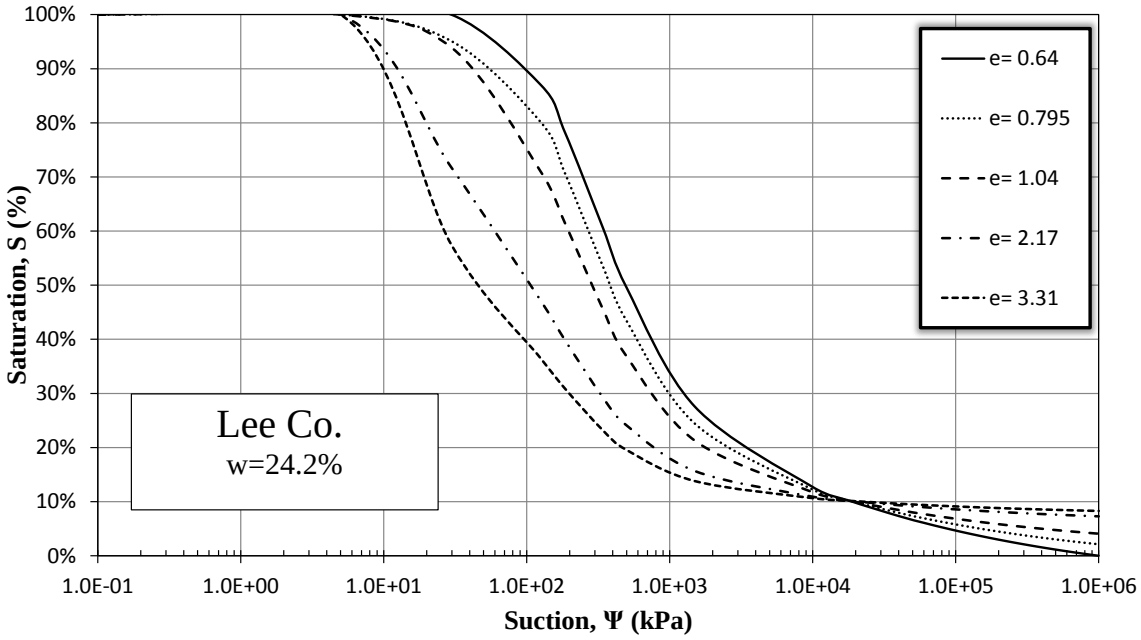

Figure D.6: Soil Water Characteristic Curve for Lee County Clay at w=24.2%

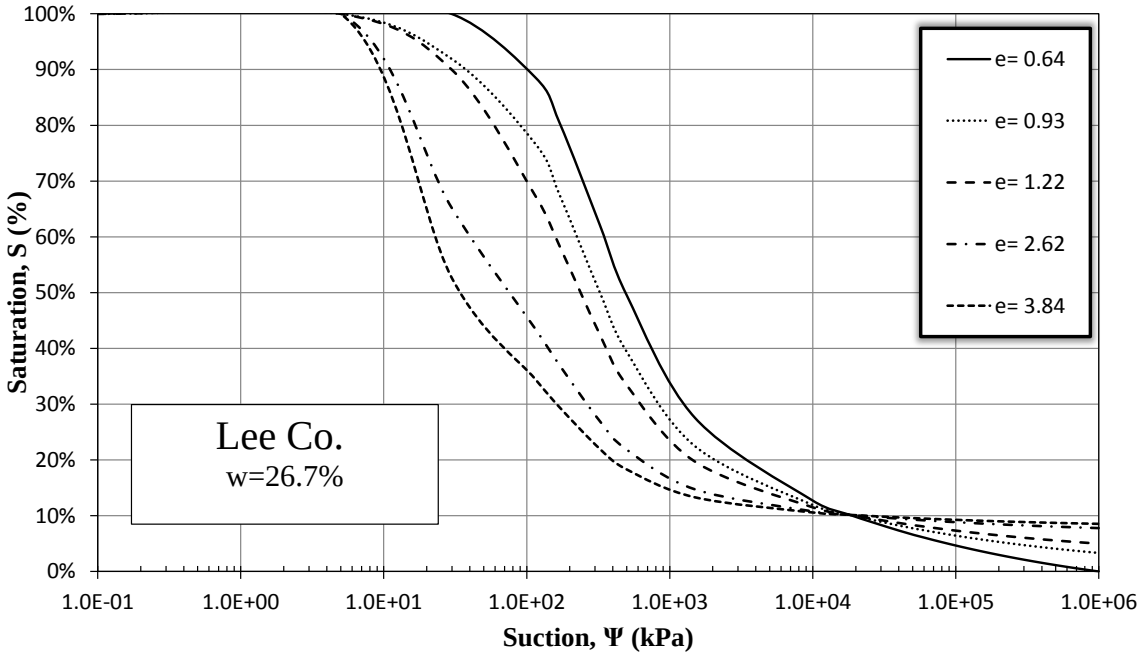

Figure D.7: Soil Water Characteristic Curve for Lee County Clay at w=26.7%

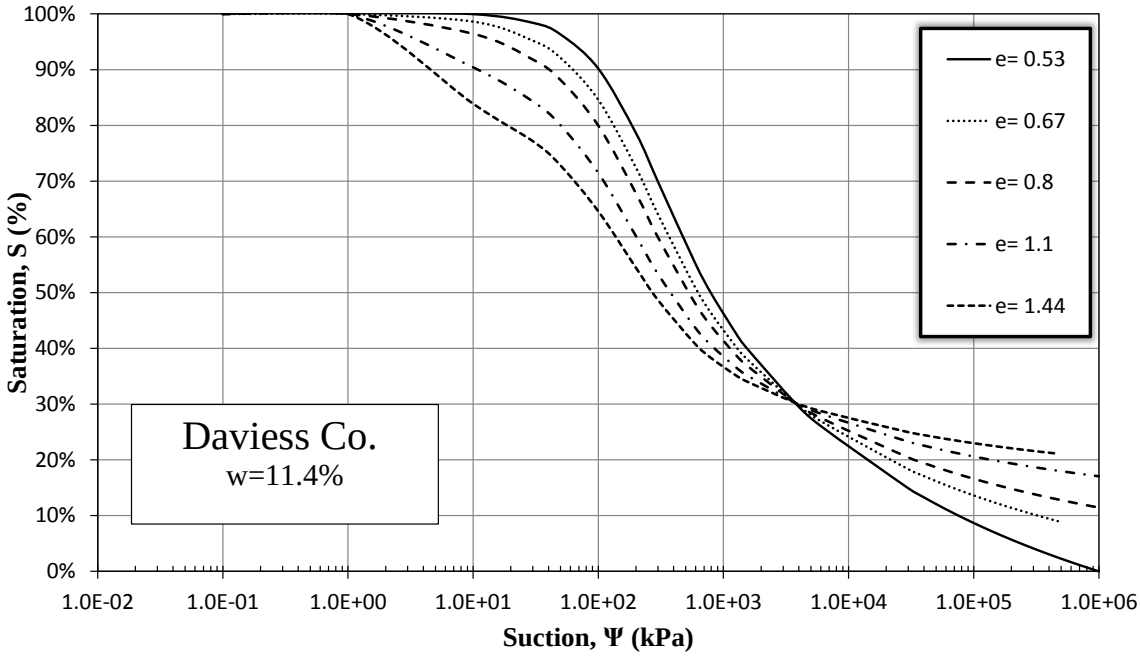

Figure D.8: Soil Water Characteristic Curve for Daviess County Clay at w=11.4%

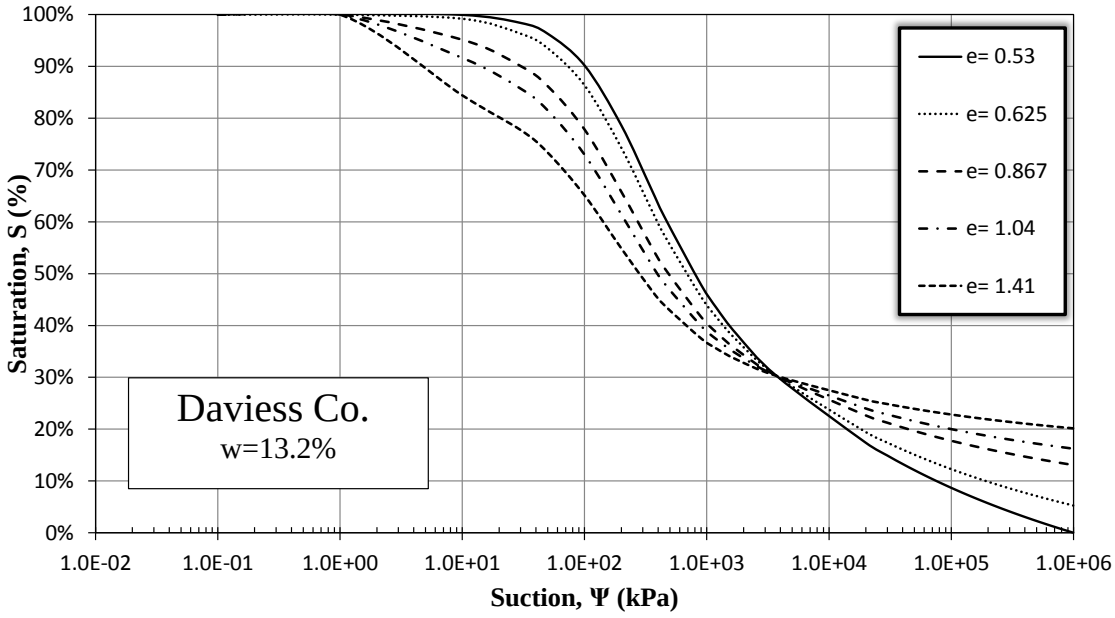

Figure D.9: Soil Water Characteristic Curve for Daviess County Clay at w=13.2%

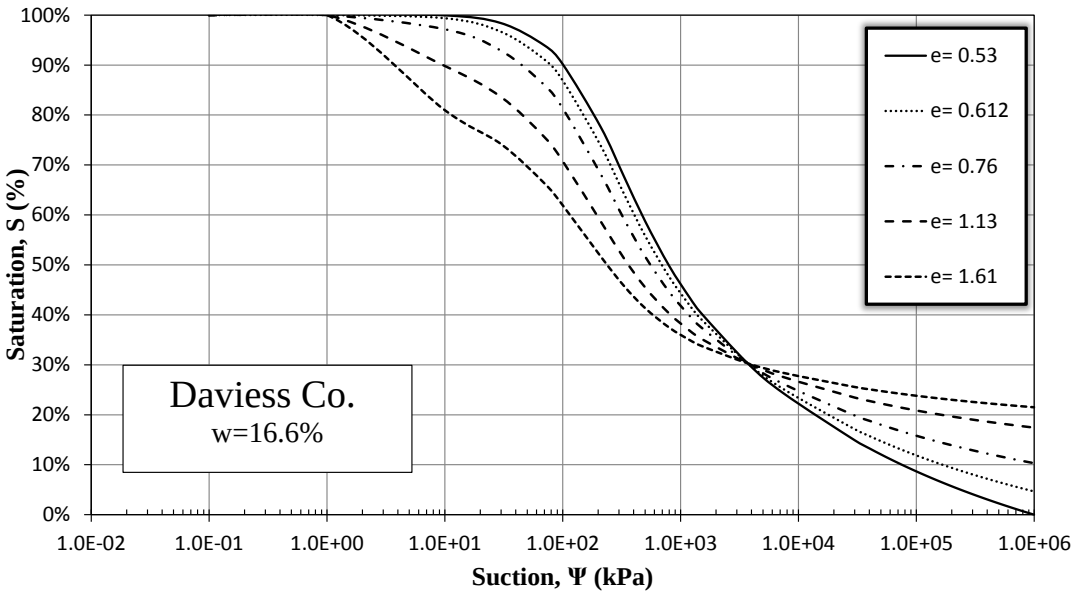

Figure D.10: Soil Water Characteristic Curve for Daviess County Clay at w=16.6%

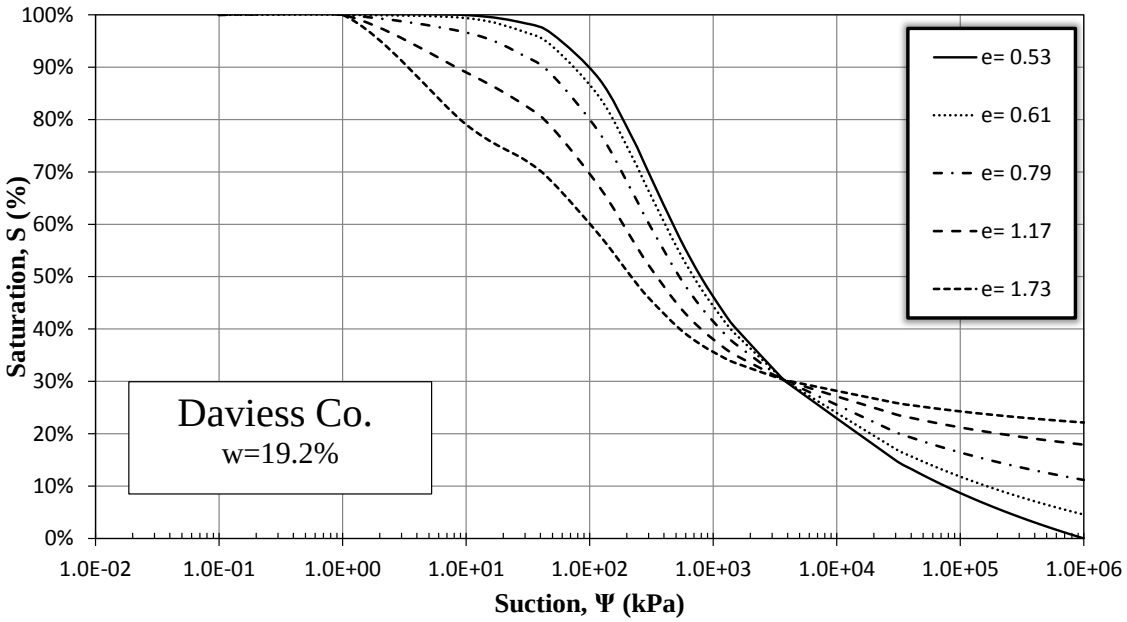

Figure D.11: Soil Water Characteristic Curve for Daviess County Clay at w=19.2%

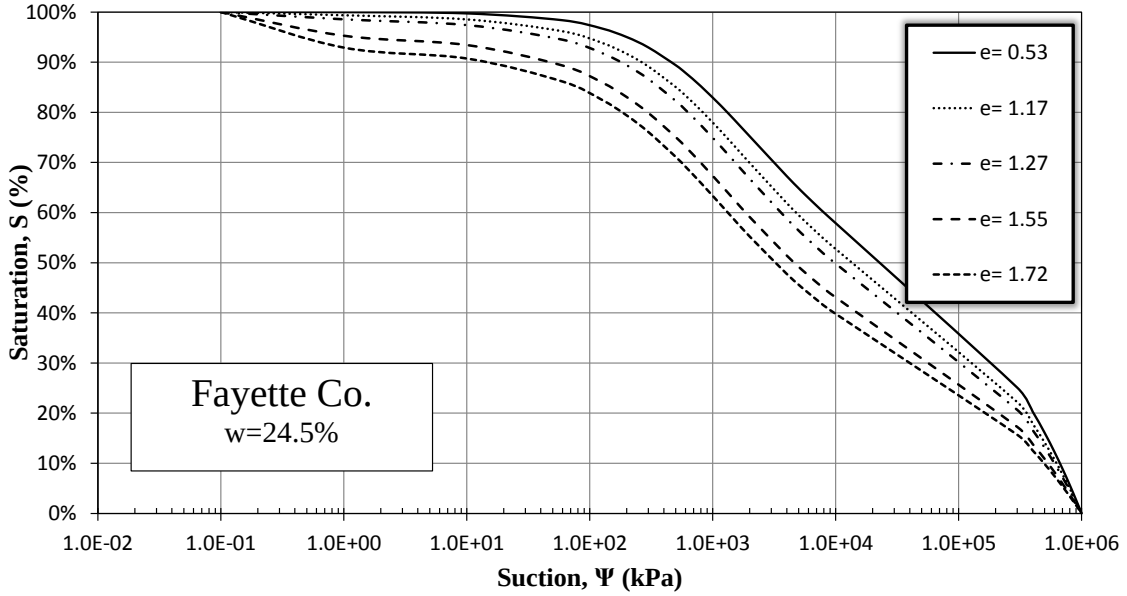

Figure D.12: Soil Water Characteristic Curve for Fayette County Clay at w=24.5%

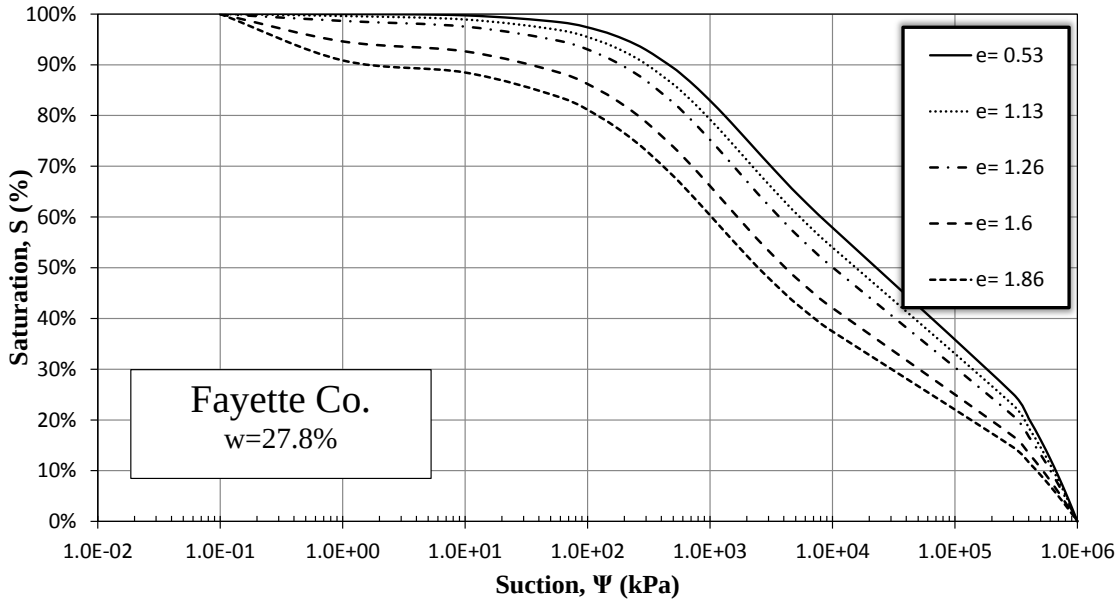

Figure D.13: Soil Water Characteristic Curve for Fayette County Clay at w=27.8%

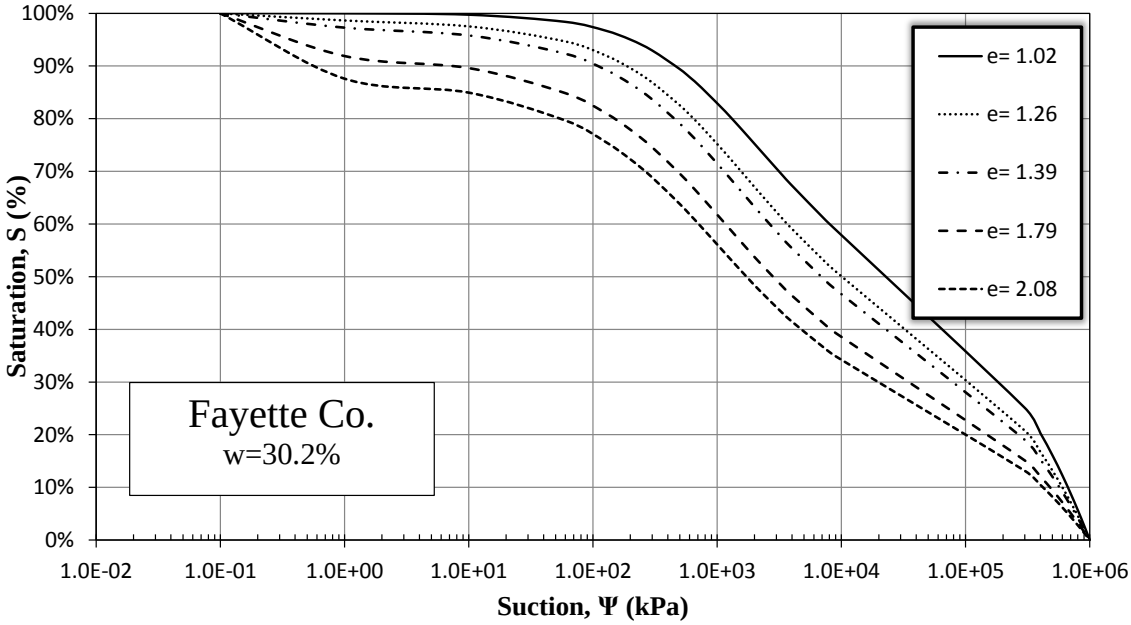

Figure D.14: Soil Water Characteristic Curve for Fayette County Clay at w=30.2%

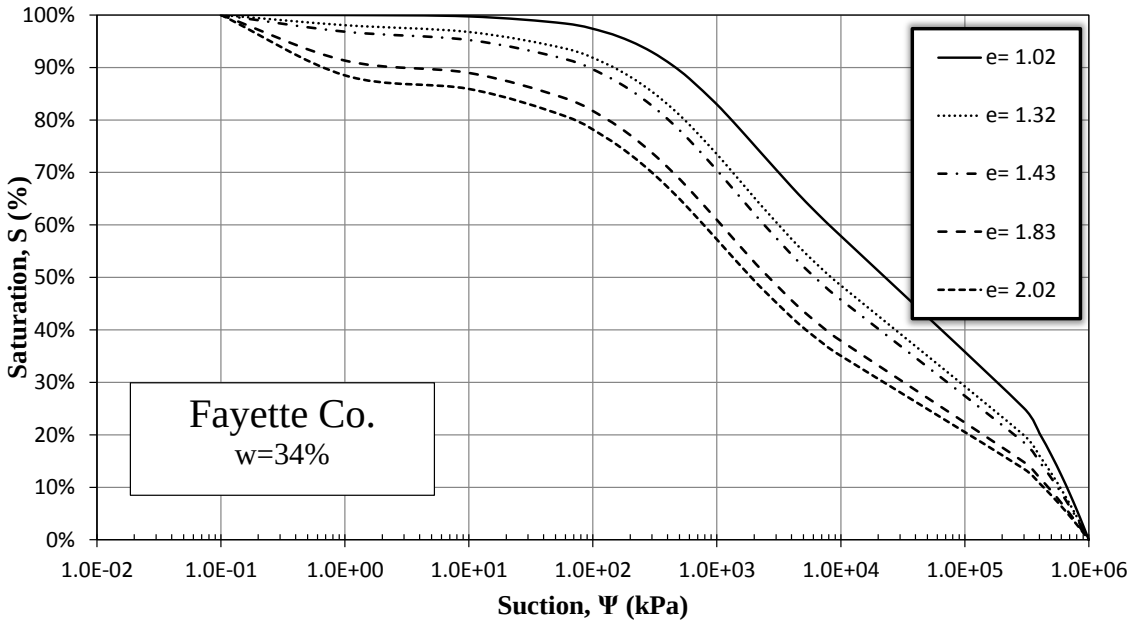

Figure D.15: Soil Water Characteristic Curve for Fayette County Clay at w=34%

APPENDIX E

Attempt to relate empirical testing parameters to soil material properties

The "C" and "D" parameters were examined to look for a possible relationship between those constants and the clay material properties. The values of C_4 and D_2 were the only two parameters that showed a strong relationship to the material properties of the clays. They are provided in Figures E.1 and E.2. The other "C" and "D" parameters showed very weak relationships to material properties.

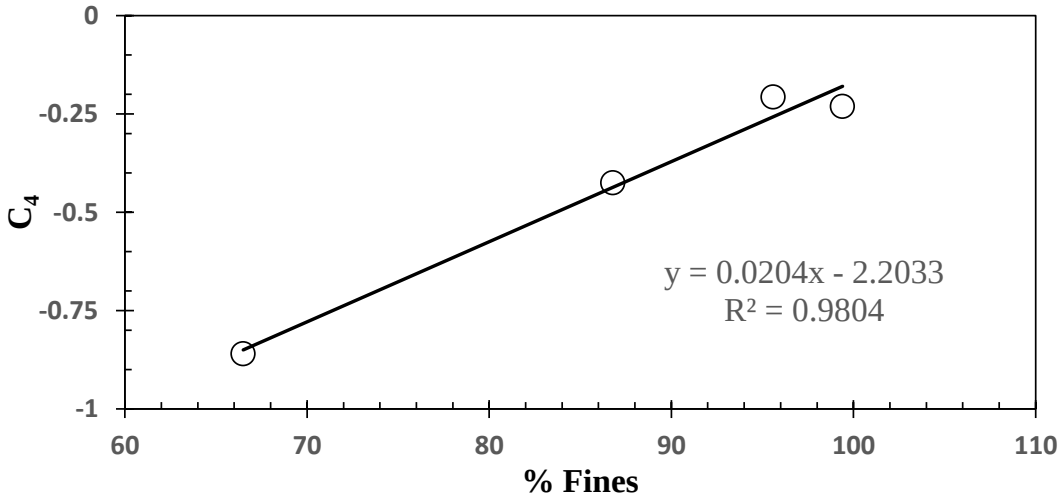

Figure E.1: C_4 plotted against the percent fines for all four of the soils.

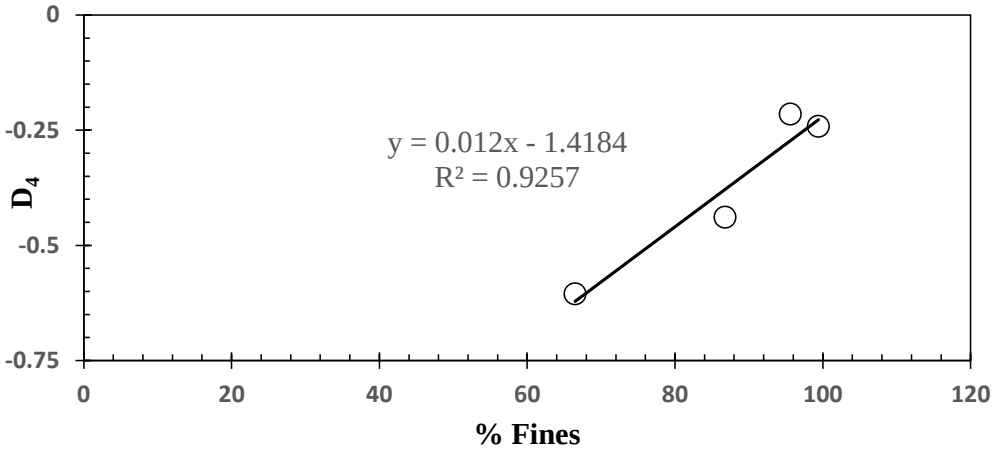

Figure E.2: D2 plotted against the Clay Fraction for all four test clays.

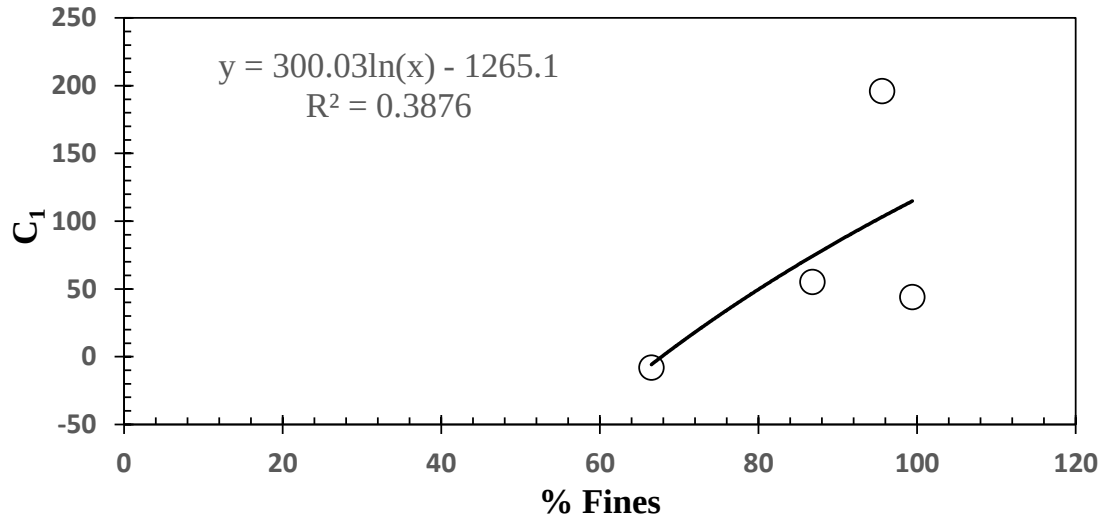

Figure E.3: C_1 plotted against the percent fines for all four of the soils.

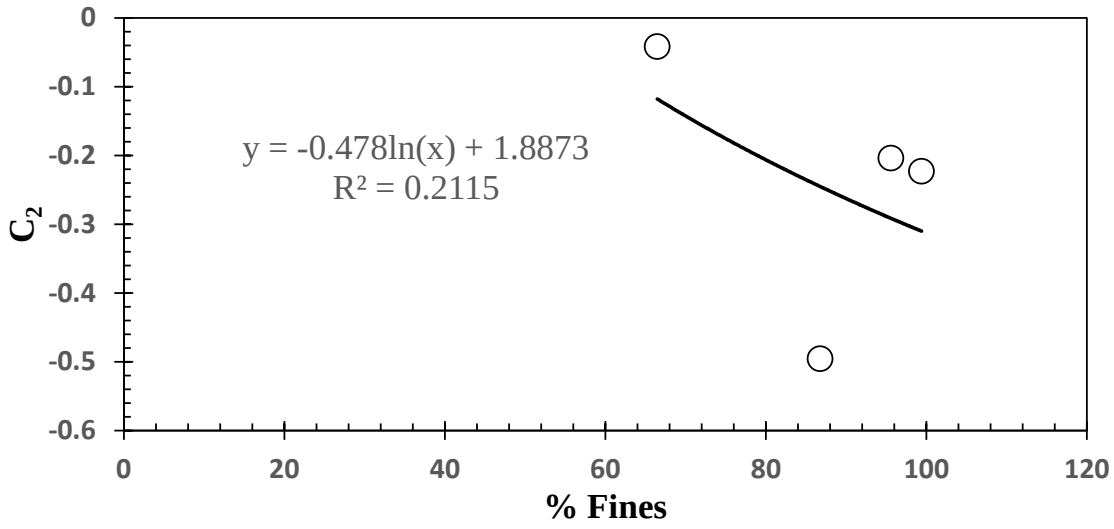

Figure E.4: C_2 plotted against the percent fines for all four of the soils.

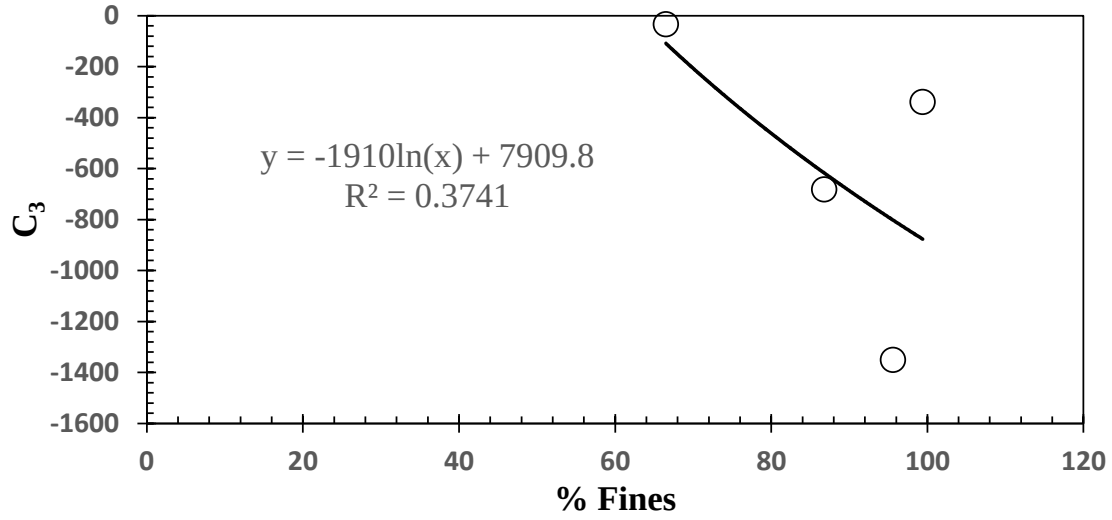

Figure E.5: C_3 plotted against the percent fines for all four of the soils.

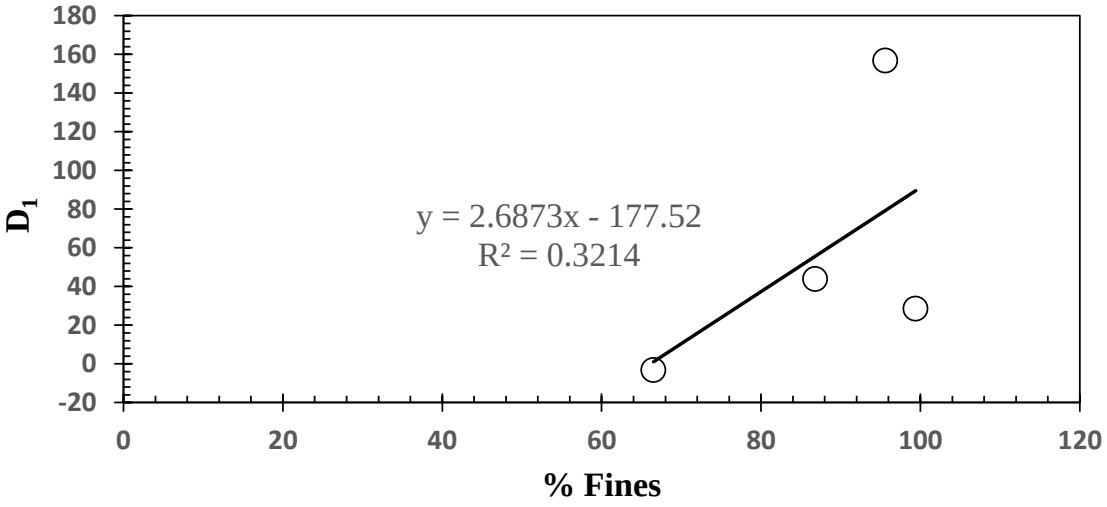

Figure E.6: D_1 plotted against the percent fines for all four of the soils.

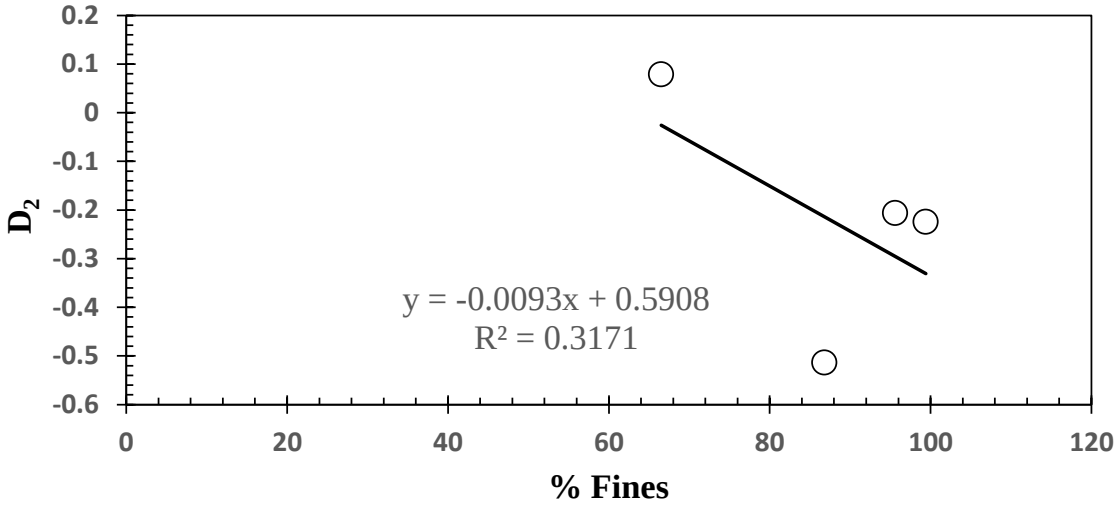

Figure E.7: D_2 plotted against the percent fines for all four of the soils.

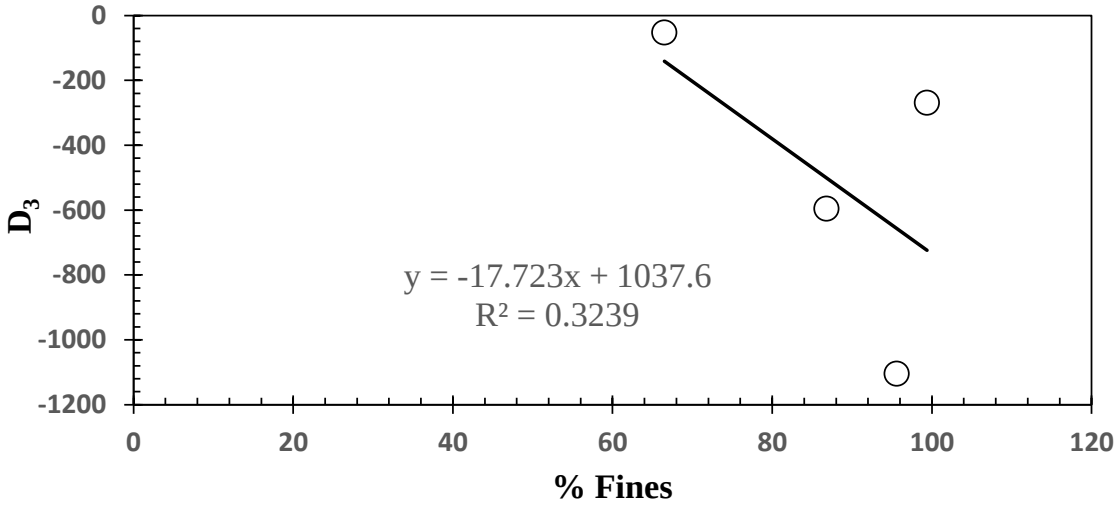

Figure E.8: D_3 plotted against the percent fines for all four of the soils.

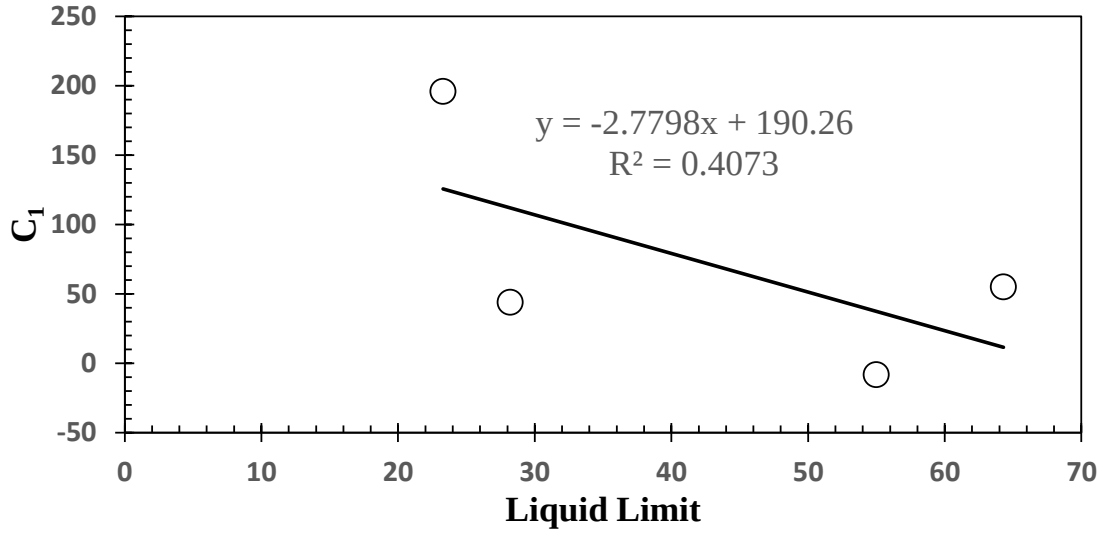

Figure E.9: C_1 plotted against the liquid limit for all four of the soils.

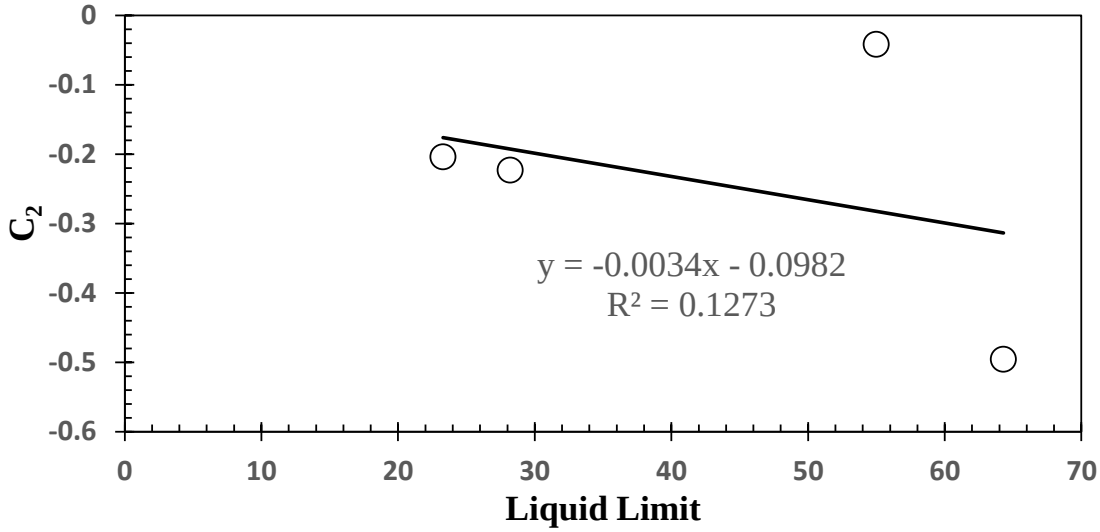

Figure E.10: C_2 plotted against the liquid limit for all four of the soils.

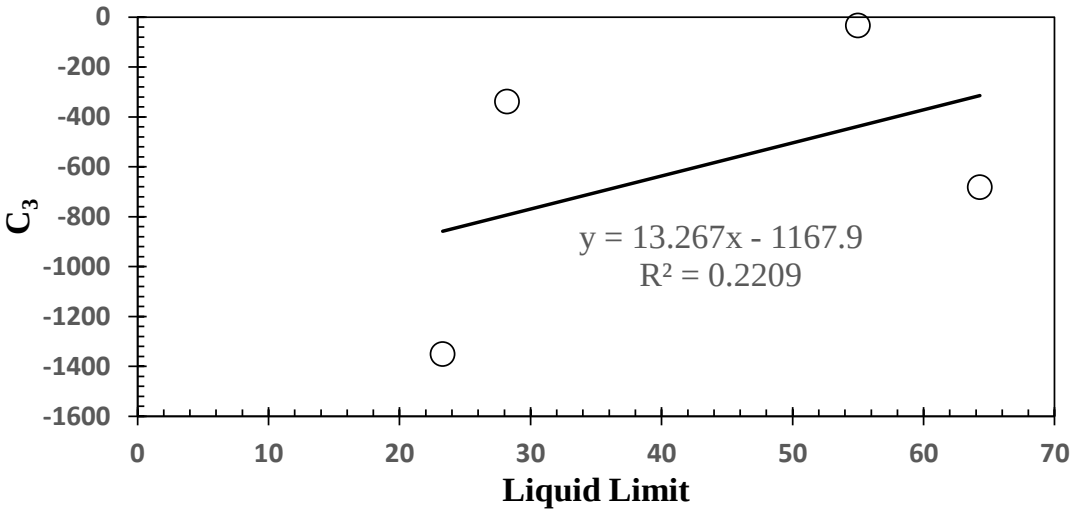

Figure E.11: C_3 plotted against the liquid limit for all four of the soils.

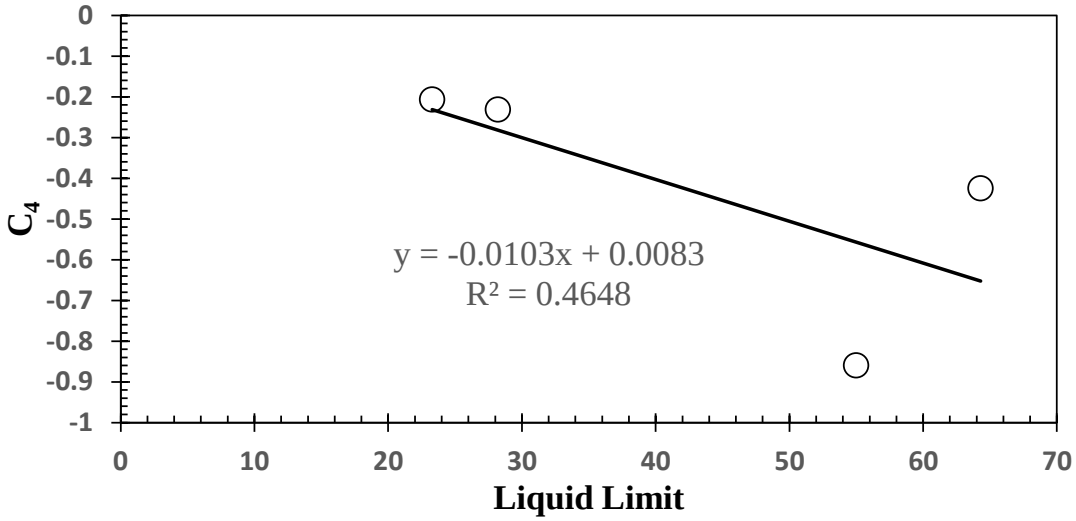

Figure E.12: C_4 plotted against the liquid limit for all four of the soils.

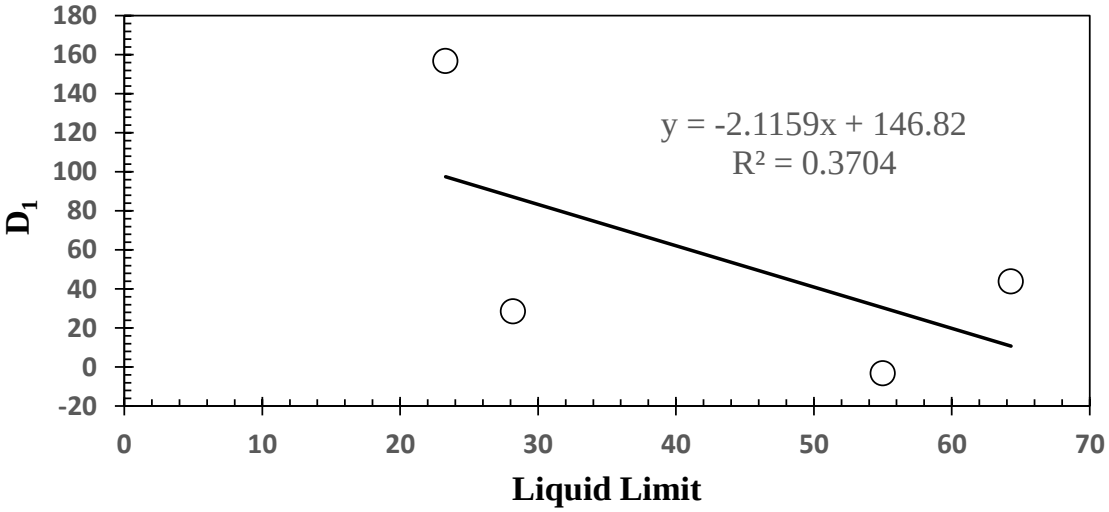

Figure E.13: D_1 plotted against the liquid limit for all four of the soils.

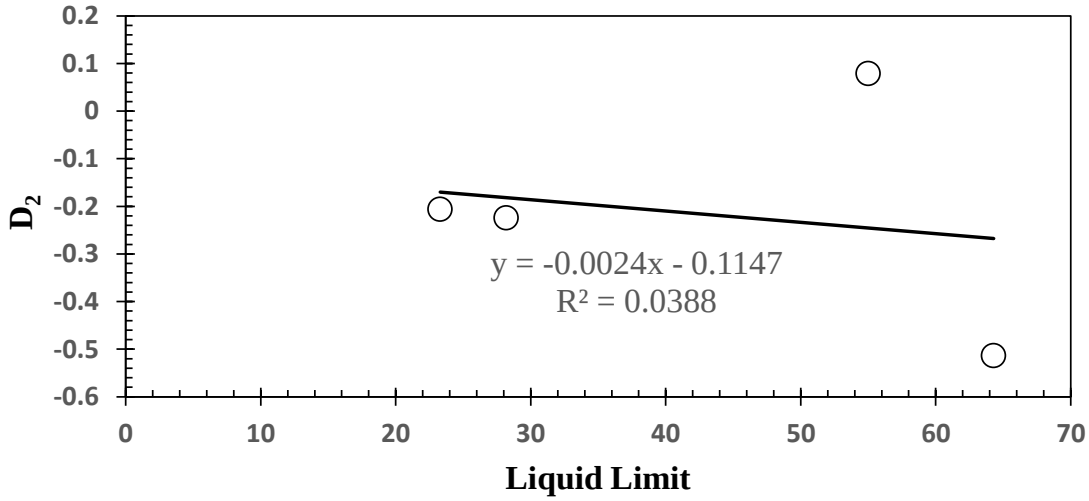

Figure E.14: D_2 plotted against the liquid limit for all four of the soils.

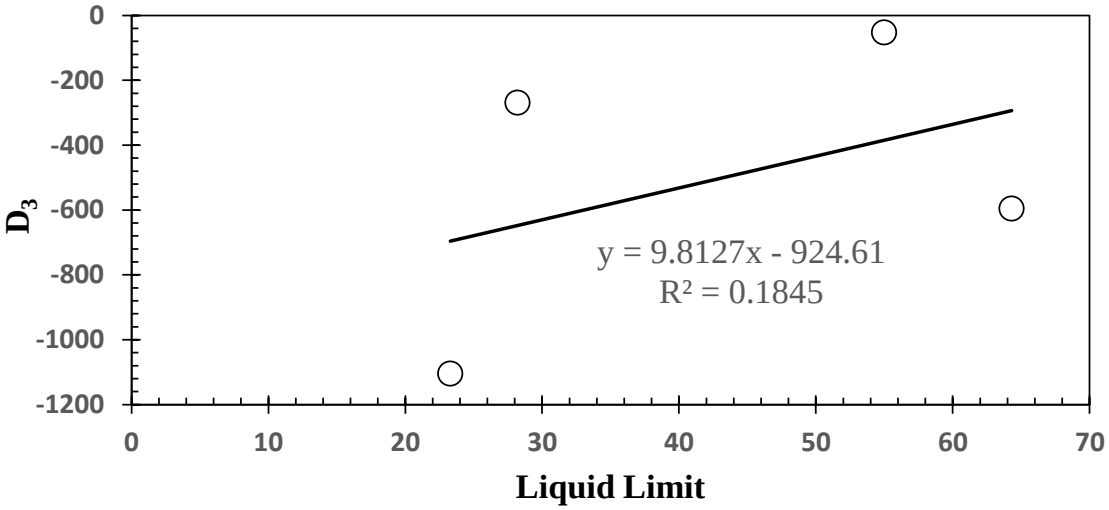

Figure E.15: D_3 plotted against the liquid limit for all four of the soils.

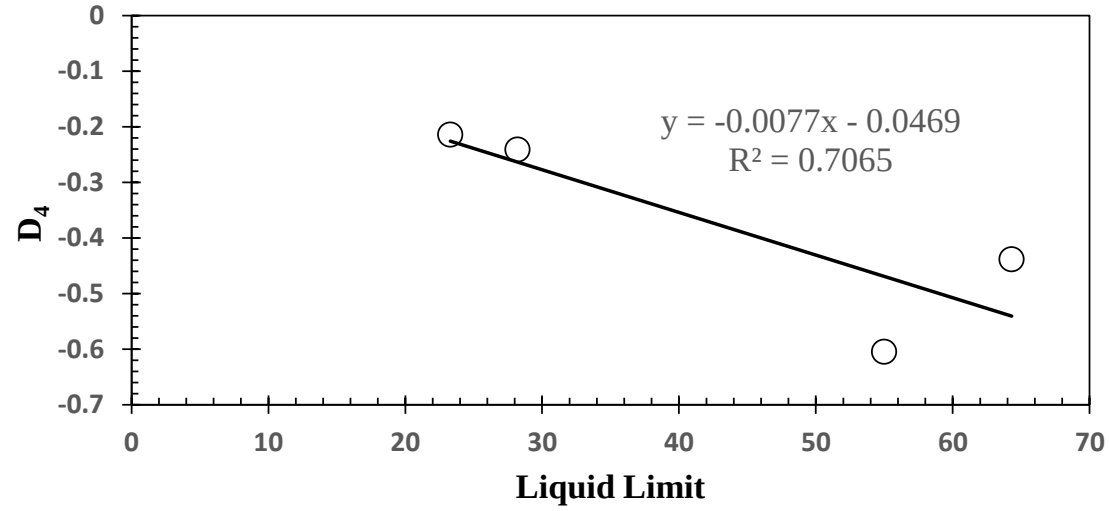

Figure E.16: D_4 plotted against the liquid limit for all four of the soils.

The values of A_3 and B_3 were also plotted against the material properties of the clays.

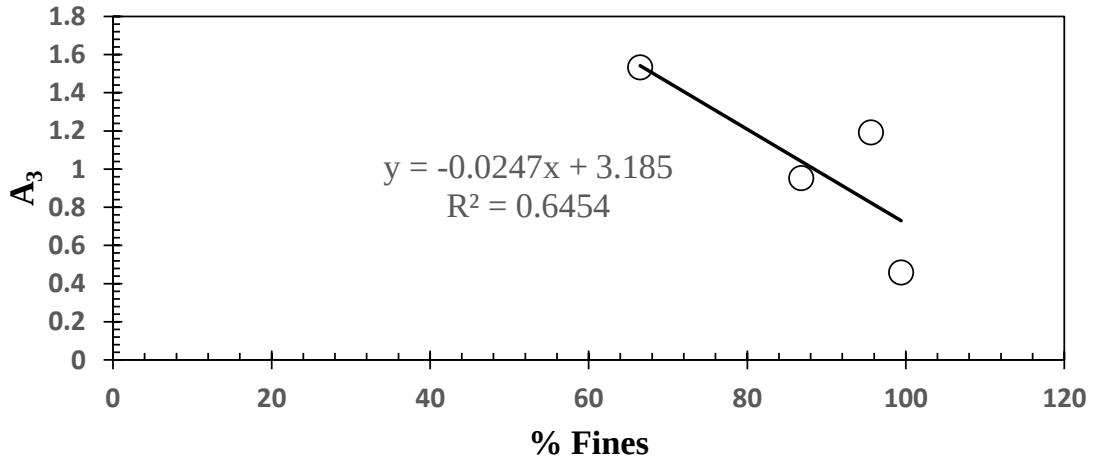

Figure E.17: A_3 versus the percent fines values

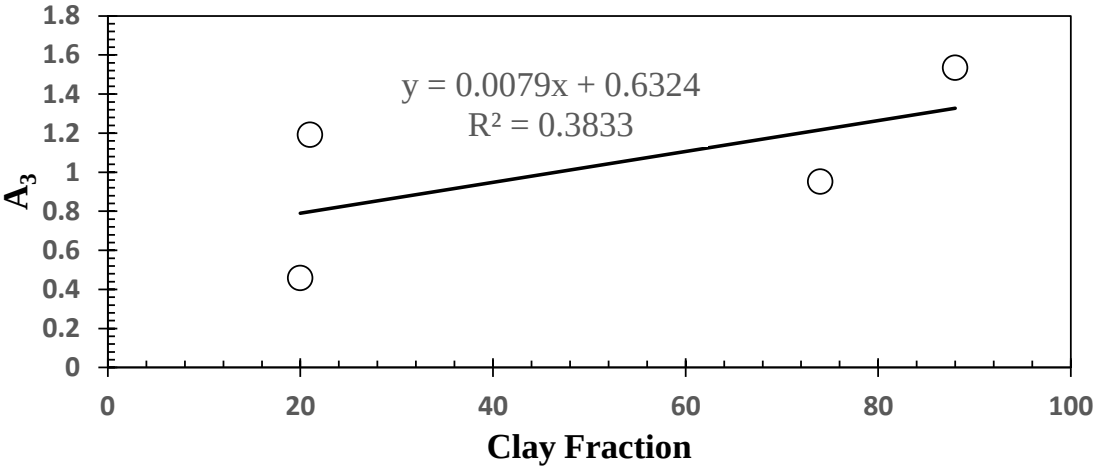

Figure E.18: A_3 versus the clay fraction

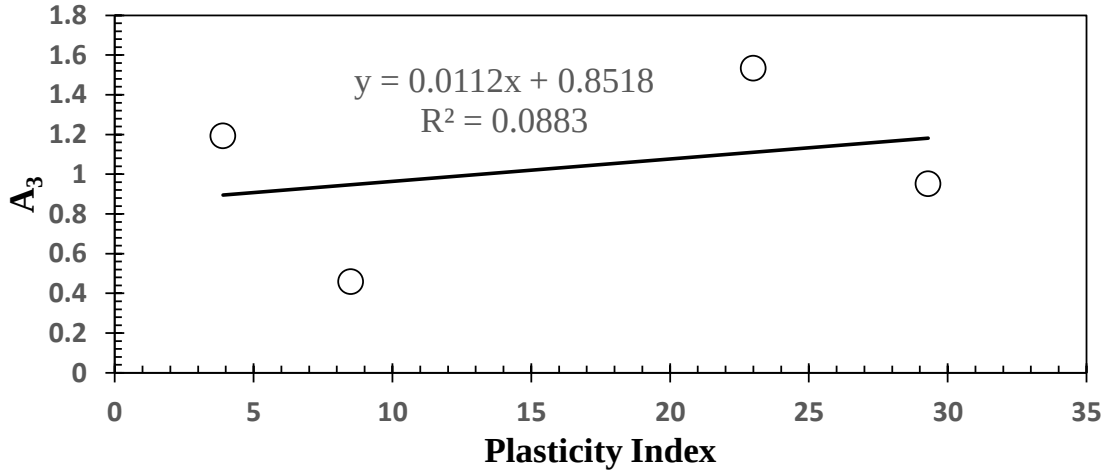

Figure E.19: A_3 versus the plasticity index

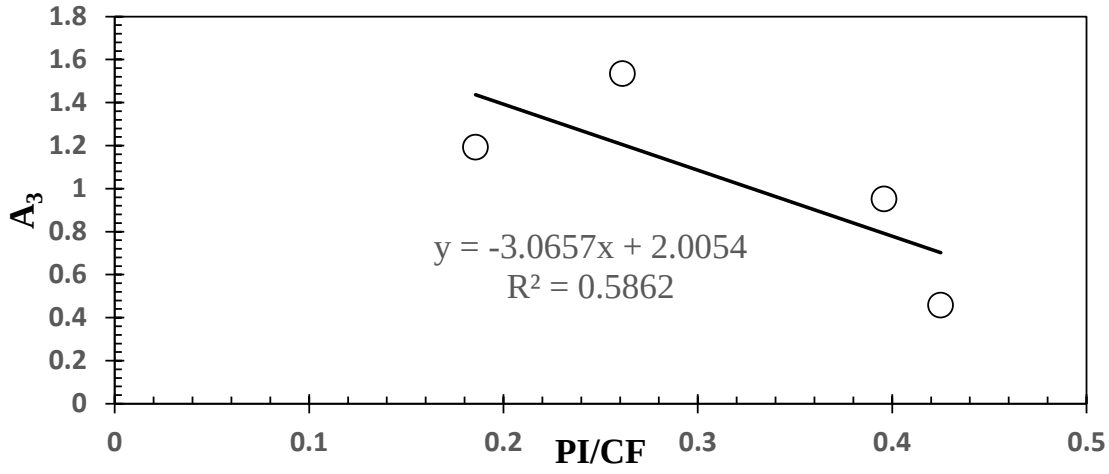

Figure E.20: A_3 versus the activity (PI/CF)

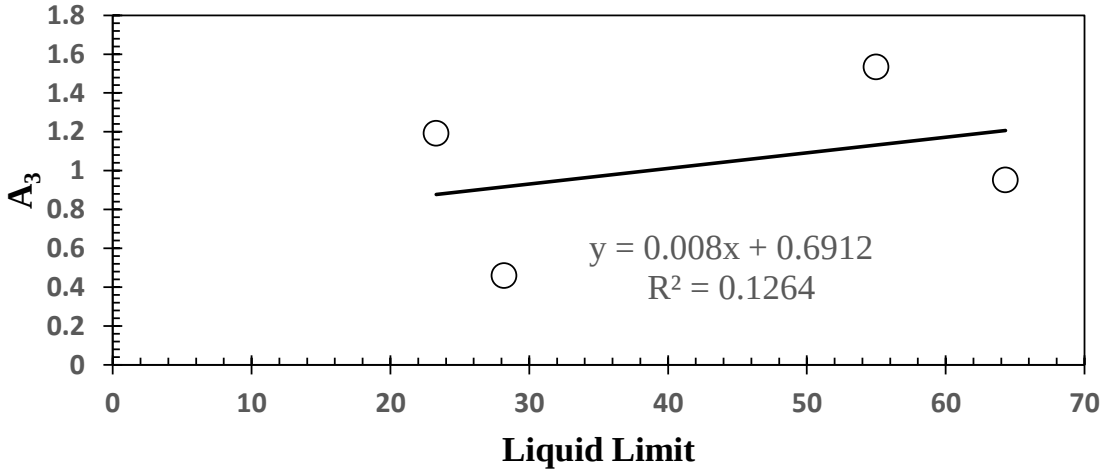

Figure E.21: A_3 versus the liquid limit

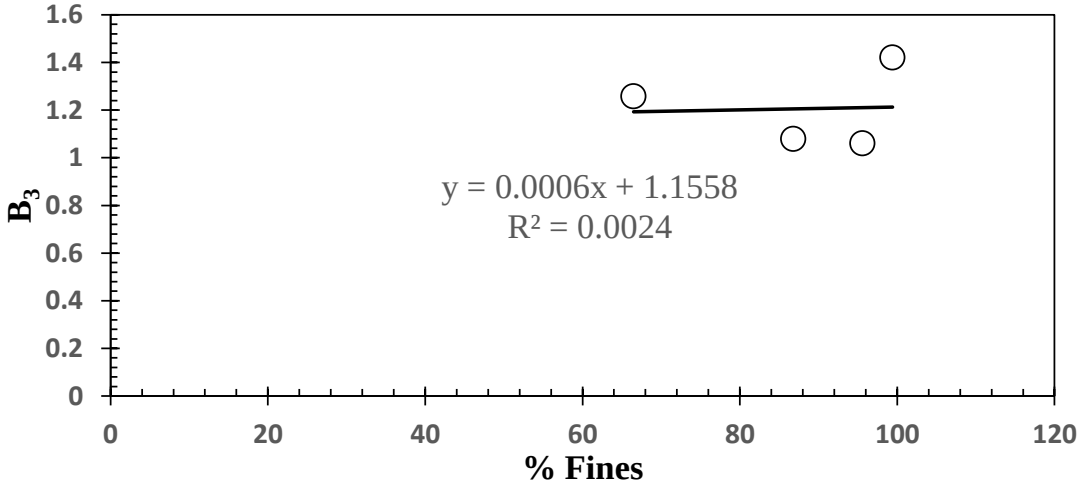

Figure E.22: B_3 versus the percent fines values

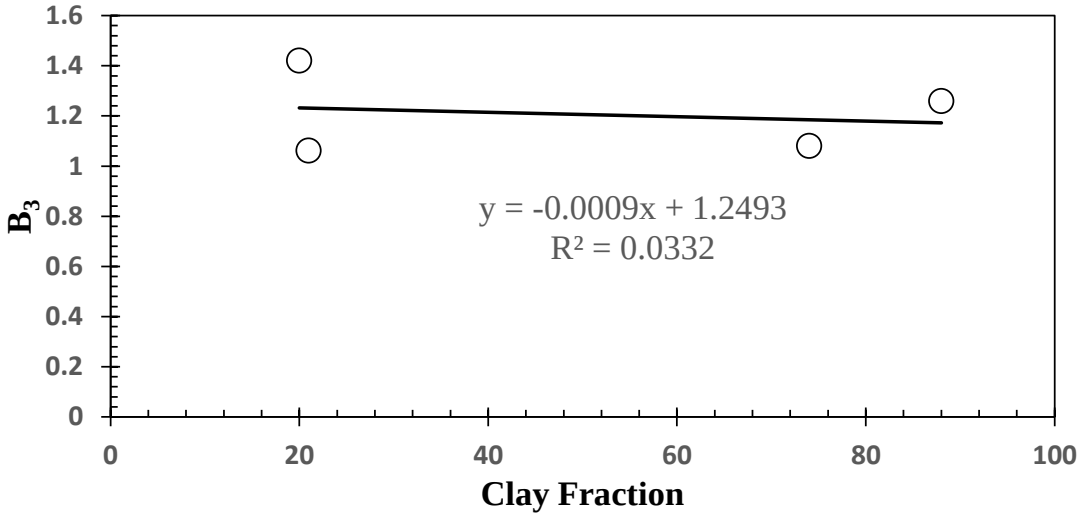

Figure E.23: B_3 versus the clay fraction

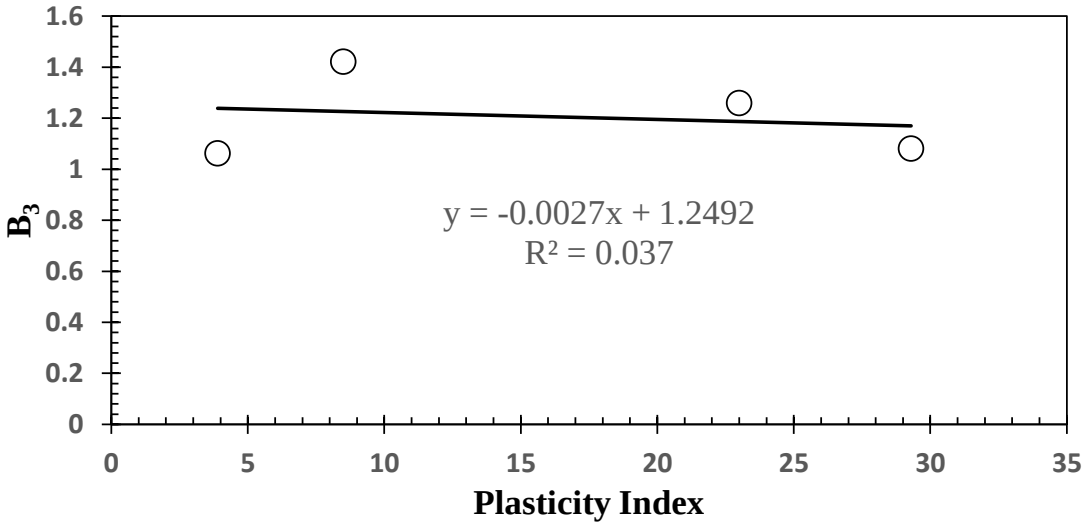

Figure E.24: B_3 versus the plasticity index

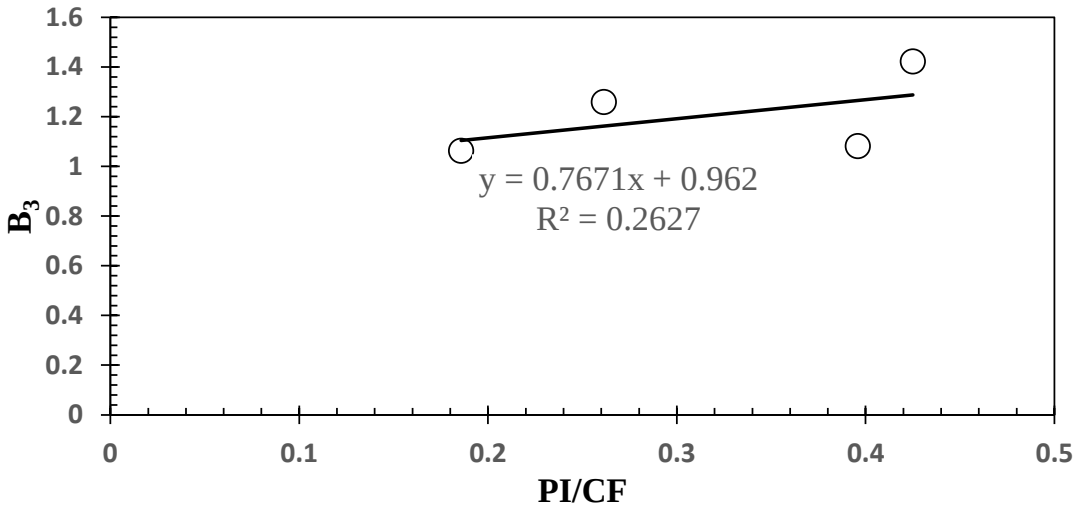

Figure E.25: B_3 versus the activity (PI/CF)

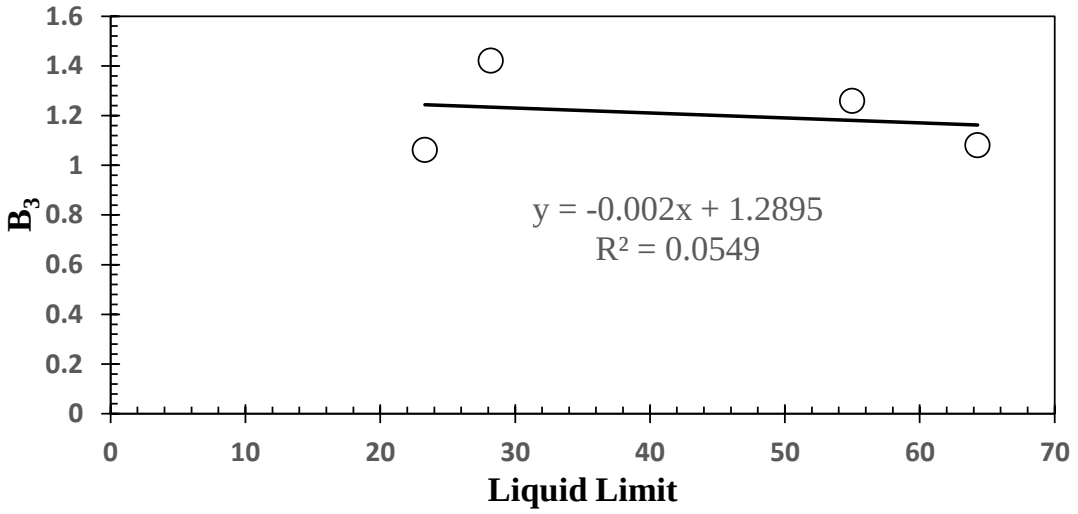

Figure E.26: B_3 versus the liquid limit

APPENDIX F

Raw Data Tables for Test Clays

Henderson County Clay Raw Data

Table F.1: Henderson County Clay test data (1/4)

MC Target	MC Actual	e	f(e)	θ (%)	S (%)	ψ kPa
12	w=11.4%	2.09	2.94	11.07	14.70	7000
		1.46	1.26	13.90	21.03	925
		1.19	0.77	15.61	25.80	550
		0.85	0.33	18.47	36.08	310
		0.70	0.20	20.09	43.78	240
15	w=14.6%	2.39	4.04	13.26	16.41	2500
		1.37	1.09	18.99	28.66	320
		0.83	0.31	24.61	47.38	150
		0.75	0.24	25.67	52.12	133
		0.63	0.15	27.67	62.67	105
17	w=16%	2.02	2.72	16.55	21.34	590
		1.21	0.80	22.63	35.67	195
		0.72	0.22	28.97	59.48	100
		0.65	0.17	30.18	65.79	85
		0.58	0.12	31.67	74.64	66
19	w=19.7%	1.90	2.36	21.88	27.91	220
		1.17	0.74	29.26	45.36	100
		0.70	0.20	37.41	76.17	45
		0.65	0.16	38.53	81.97	40
		0.58	0.12	40.17	91.50	28

Table F.2: Henderson County Clay test data (2/4)

Load Frame									
Under Load			After Rebound						
p (kPa)	ln(p)	q (kPa)	p (kPa)	ln(p)	q (kPa)	v	M (kPa)	E (MPa)	Glf (MPa)
5.25	1.66	8.15	5.25	1.66	8.15	0.30			
16.68	2.81	26.54	5.54	1.71	7.95	0.30	349.15	0.26	0.10
38.73	3.66	55.63	7.63	2.03	7.53	0.30	475.73	0.35	0.14
123.45	4.82	158.90	16.36	2.79	5.22	0.30	938.46	0.70	0.27
480.72	6.18	503.34	62.51	4.14	41.96	0.30	2061.68	1.53	0.59
0.87	-0.14	1.70				0.30			
9.19	2.22	12.44	0.28	-1.27	0.68	0.30	321.85	0.24	0.09
111.61	4.72	131.61	1.89	0.64	1.21	0.30	872.74	0.65	0.25
185.40	5.22	244.98	2.71	1.00	2.19	0.30	1166.48	0.87	0.33
425.61	6.05	543.81	5.11	1.63	4.88	0.30	1956.77	1.45	0.56
0.87	-0.14	1.70				0.30			
9.26	2.23	10.28	2.91	1.07	2.20	0.30	311.59	0.23	0.09
121.80	4.80	164.54	9.74	2.28	0.50	0.30	1110.71	0.83	0.32
197.71	5.29	292.85	14.80	2.69	2.23	0.30	1476.00	1.10	0.42
462.70	6.14	718.50	28.07	3.33	11.38	0.30	2486.19	1.85	0.71
0.87	-0.14	1.70				0.30			
12.51	2.53	13.97	3.83	1.34	3.72	0.30	260.47	0.19	0.07
88.76	4.49	88.17	7.29	1.99	0.42	0.30	751.91	0.56	0.21
148.05	5.00	135.62	9.96	2.30	3.90	0.30	901.29	0.67	0.26
423.60	6.05	244.83	16.75	2.82	16.15	0.30	1749.73	1.30	0.50

Table F.3: Henderson County Clay test data (3/4)

Shear Wave				
Under Load		After Rebound		
GuL (MPa)	E (MPa)	Gar (MPa)	Gar*S/f(e) (MPa)	E (MPa)
32.81	85.31	32.81	1.64	
55.20	143.51	50.80	8.47	132.08
97.44	253.35	108.96	36.65	283.31
96.63	251.24	121.36	131.99	315.54
144.53	375.78	190.10	411.62	494.25
85.03	221.08	63.87	16.85	166.05
100.20	260.52	141.66	215.60	368.32
165.23	429.60	145.69	311.17	378.80
173.89	452.10	173.89	720.12	452.10
100.94	262.45	81.32	36.45	211.43
169.11	439.69	86.76	234.81	225.58
233.15	606.20	153.34	595.97	398.68
158.50	412.11	179.76	1103.02	467.37
64.58	167.90	84.86	52.36	220.64
123.64	321.45	99.60	382.05	258.97
158.79	412.85	126.15	629.99	327.98
248.50	646.10	163.43	1215.62	424.93

Table F.4: Henderson County Clay test data (4/4)

SSG		
After Rebound		
k (MN/m)	Gssg (MPa)	Gssg/f(e) (MPa)
4.97	17.24	13.67
6.90	23.95	31.22
9.27	32.15	96.88
7.98	27.67	136.87
3.97	13.78	12.69
7.43	25.76	82.75
9.07	31.47	128.96
9.74	33.80	223.39
4.18	14.49	18.21
7.51	26.06	118.58
7.62	26.45	156.24
7.28	25.25	207.59
3.96	13.74	18.69
5.33	18.51	93.19
4.81	16.67	101.58
2.72	9.42	76.60

Lee County Clay Raw Data

\

Table F.5: Lee County Clay test data (1/4)

MC Target	MC Actual	e	f(e)	θ (%)	S (%)	ψ kPa
21	20.9	2.55	4.68	18.86	21.71	550
		1.80	2.08	23.92	30.79	380
		1.21	0.81	30.25	45.64	290
		0.77	0.26	37.84	71.97	185
		0.58	0.12	42.33	95.16	82
23	21.9	2.79	5.75	18.65	20.77	520
		1.82	2.13	25.11	31.94	360
		0.88	0.37	37.55	65.65	195
		0.69	0.20	41.82	83.91	130
		0.59	0.13	44.56	98.79	50
25	24.2	3.31	8.41	18.48	19.38	500
		2.17	3.23	25.11	29.53	340
		1.04	0.55	39.11	61.86	185
		0.80	0.28	44.37	80.66	125
		0.63	0.15	48.94	102.18	30
27	26.7	3.85	11.76	18.49	18.39	500
		2.62	4.98	24.74	26.97	325
		1.22	0.82	40.40	58.05	170
		0.93	0.41	46.50	76.27	115
		0.70	0.20	52.81	101.45	30

Table F.6: Lee County Clay test data (2/4)

Load Frame									
Under Load			After Rebound						
p (kPa)	ln(p)	q (kPa)	p (kPa)	ln(p)	q (kPa)	v	M (kPa)	E (MPa)	Glf (MPa)
0.87	-0.14	1.70				0.30			
18.94	2.94	14.58	6.86	1.93	1.48	0.30	479.89	0.36	0.14
64.23	4.16	53.30	17.34	2.85	1.73	0.30	647.69	0.48	0.19
239.90	5.48	216.23	49.43	3.90	30.91	0.30	1154.18	0.86	0.33
471.70	6.16	367.32	89.55	4.49	77.06	0.30	1570.45	1.17	0.45
0.87	-0.14	1.70				0.30			
14.03	2.64	11.52	5.68	1.74	2.57	0.30	334.82	0.25	0.10
128.65	4.86	113.56	23.89	3.17	10.82	0.30	803.33	0.60	0.23
264.79	5.58	211.51	45.33	3.81	34.00	0.30	1100.96	0.82	0.31
414.20	6.03	269.93	70.63	4.26	62.09	0.30	1371.49	1.02	0.39
0.87	-0.14	1.70				0.30			
16.01	2.77	23.30	7.60	2.03	9.95	0.30	226.74	0.17	0.06
110.76	4.71	143.68	22.39	3.11	18.05	0.30	533.47	0.40	0.15
208.52	5.34	219.45	38.16	3.64	15.06	0.30	765.78	0.57	0.22
446.35	6.10	330.85	73.62	4.30	21.31	0.30	1157.36	0.86	0.33
0.87	-0.14	1.70				0.30			
9.56	2.26	5.86	4.79	1.57	2.50	0.30	177.65	0.13	0.05
58.19	4.06	31.87	10.62	2.36	3.90	0.30	344.42	0.26	0.10
114.66	4.74	52.88	18.55	2.92	10.23	0.30	500.22	0.37	0.14
377.56	5.93	128.35	44.55	3.80	35.90	0.30	929.44	0.69	0.27

Table F.7: Lee County Clay test data (3/4)

Shear Wave				
Under Load		After Rebound		
GuL (MPa)	E (MPa)	Gar (MPa)	Gar*S/f(e) (MPa)	E (MPa)
53.75	139.75	45.68	3.25	118.76
68.09	177.04	68.09	47.66	177.04
148.40	385.85	71.66	777.72	186.33
243.83	633.95	113.43	6949.37	294.91
71.54	186.01	45.88	3.23	119.28
91.79	238.66	58.86	287.49	153.04
98.74	256.73	89.77	1969.95	233.41
143.26	372.48	103.21	6251.94	268.35
56.66	147.31	56.66	1.60	147.31
80.80	210.09	99.24	205.08	258.03
171.24	445.23	87.86	904.03	228.43
183.16	476.22	103.36	4577.80	268.75
80.59	209.54	53.90	0.59	140.13
71.27	185.29	64.78	56.48	168.42
146.88	381.88	94.00	417.94	244.40
181.50	471.91	127.14	3229.87	330.57

Table F.8: Lee County Clay test data (4/4)

SSG		
After Rebound		
k (MN/m)	**Gssg (MPa)**	**Gssg/f(e) (MPa)**
6.34	21.98	0.39
11.03	38.28	9.91
16.06	55.72	235.46
24.65	85.52	3229.42
0.80	2.79	0.05
14.91	51.74	84.69
13.80	47.86	536.87
21.05	73.04	2600.09
4.59	15.92	0.16
15.57	54.01	69.70
19.07	66.16	376.34
17.24	59.81	1722.65
3.62	12.55	0.05
8.87	30.76	12.06
14.91	51.74	150.12
20.90	72.50	1625.48

Daviess County Clay Raw Data

Table F.9: Daviess County Clay test data (/14)

MC Target	MC Actual	e	f(e)	θ (%)	S (%)	ψ kPa
13	11.4	1.44	1.22	14.15	21.53	310000
		1.10	0.63	16.45	28.21	6000
		0.80	0.29	19.17	38.65	1250
		0.67	0.18	20.73	46.56	800
		0.58	0.12	21.85	53.38	590
14	13.2	1.41	1.17	16.83	25.38	20000
		1.05	0.56	19.83	34.22	1750
		0.87	0.35	21.77	41.42	900
		0.62	0.15	25.01	57.47	450
		0.54	0.10	26.31	65.90	350
16	16.6	1.61	1.60	20.17	28.04	7500
		1.13	0.67	24.75	40.07	800
		0.76	0.25	29.86	59.19	330
		0.61	0.14	32.66	73.75	210
		0.47	0.07	35.77	95.71	70
19	19.2	1.73	1.89	22.84	30.26	3800
		1.17	0.74	28.64	44.50	525
		0.79	0.27	34.85	66.41	220
		0.61	0.14	38.55	84.94	120
		0.51	0.09	41.13	101.70	10

Table F.10: Daviess County Clay test data (2/4)

Load Frame									
Under Load			After Rebound						
p (kPa)	ln(p)	q (kPa)	p (kPa)	ln(p)	q (kPa)	v	M (kPa)	E (MPa)	Glf (MPa)
0.87	-0.14	1.70				0.30			
28.92	3.36	35.66	7.15	1.97	3.01	0.30	749.25	226.94	0.75
116.46	4.76	122.03	23.18	3.14	13.80	0.30	1030.36	392.30	1.03
246.37	5.51	276.90	43.49	3.77	37.10	0.30	1465.51	997.84	1.47
441.07	6.09	490.50	76.17	4.33	77.81	0.30	1967.17	1579.82	1.97
0.87	-0.14	1.70				0.30			
20.60	3.03	14.38	8.65	2.16	7.58	0.30	486.35	223.13	0.49
99.28	4.60	74.38	20.27	3.01	3.41	0.30	801.61	399.23	0.80
235.99	5.46	192.69	42.40	3.75	28.66	0.30	1326.33	938.11	1.33
462.92	6.14	381.39	78.43	4.36	75.23	0.30	1934.73	1611.47	1.94
0.87	-0.14	1.70				0.30			
15.46	2.74	15.57	6.75	1.91	9.99	0.30	260.32	69.43	0.26
61.61	4.12	58.75	11.34	2.43	8.20	0.30	479.50	213.21	0.48
141.91	4.96	131.65	20.39	3.02	7.13	0.30	818.15	600.38	0.82
460.11	6.13	382.69	54.13	3.99	48.91	0.30	1693.01	1518.12	1.69
0.87	-0.14	1.70				0.30			
10.79	2.38	16.44	6.95	1.94	11.55	0.30	199.96	62.80	0.20
30.85	3.43	36.32	8.28	2.11	12.24	0.30	318.79	101.24	0.32
83.91	4.43	72.77	12.62	2.54	9.67	0.30	555.58	193.06	0.56
447.11	6.10	87.90	25.87	3.25	10.48	0.30	1310.81	829.33	1.31

Table F.11: Daviess County Clay test data (3/4)

Shear Wave				
Under Load		After Rebound		
GuL (MPa)	E (MPa)	Gar (MPa)	Gar*S/f(e) (MPa)	E (MPa)
57.67	149.94	76.43	34.07	198.72
72.64	188.86	96.71	130.42	251.44
130.36	338.94	103.79	272.63	269.87
153.86	400.04	136.69	588.44	355.38
87.65	227.89	50.86	30.89	132.22
95.20	247.52	64.99	77.17	168.98
135.44	352.15	73.62	281.88	191.42
159.60	414.95	92.86	584.65	241.44
50.71	131.85	43.63	25.98	113.43
84.93	220.82	59.91	140.79	155.76
140.54	365.41	76.40	395.92	198.64
171.86	446.85	121.56	1630.93	316.07
59.82	155.53	50.84	30.42	132.18
60.49	157.28	60.49	147.56	157.28
66.25	172.24	71.74	423.44	186.53
121.09	314.84	76.09	864.95	197.83

Table F.12: Daviess County Clay test data (4/4)

SSG		
After Rebound		
k (MN/m)	Gssg (MPa)	Gssg/f(e) (MPa)
6.08	21.09	33.34
11.12	38.57	134.58
15.22	52.81	297.89
10.42	36.16	291.62
4.81	16.69	29.62
9.08	31.49	90.27
11.03	38.27	254.98
11.55	40.06	382.72
3.34	11.59	17.23
6.53	22.64	89.91
8.72	30.26	212.66
13.05	45.27	634.60
2.73	9.46	12.72
5.13	17.81	65.41
7.22	25.04	174.01
5.37	18.64	208.31

Fayette County Clay Raw Data

Table F.13: Fayette County Clay test data (1/4)

MC Target	MC Actual	e	f(e)	θ (%)	S (%)	ψ kPa
25	24.5	1.72	1.87	32.06	40.70	9050
		1.55	1.46	34.22	45.24	7500
		1.27	0.90	38.44	55.20	5590
		1.17	0.75	40.12	59.65	4900
		1.09	0.62	41.78	64.41	4000
28	27.8	1.86	2.25	35.55	42.78	5100
		1.60	1.58	39.06	49.65	4200
		1.26	0.88	45.06	63.34	2725
		1.13	0.68	47.68	70.29	2150
		1.00	0.50	50.89	79.78	1435
31	30.2	2.08	2.91	36.55	41.58	3900
		1.79	2.05	40.36	48.36	3350
		1.39	1.13	47.00	62.02	2210
		1.26	0.89	49.73	68.48	1795
		1.00	0.50	56.27	86.49	750
34	34	2.02	2.74	43.11	48.08	2250
		1.83	2.16	46.08	53.19	1950
		1.43	1.21	53.55	67.84	1248
		1.32	0.98	56.26	73.88	965
		1.11	0.64	61.87	87.92	435

Table F.14: Fayette County Clay test data (2/4)

Load Frame									
Under Load			After Rebound						
p (kPa)	ln(p)	q (kPa)	p (kPa)	ln(p)	q (kPa)	v	M (kPa)	E (MPa)	Glf (MPa)
0.87	-0.14	1.70				0.25			
52.33	3.96	55.90	14.97	2.71	9.54	0.25	897.50	105.06	0.91
229.32	5.44	238.41	61.37	4.12	41.89	0.25	1265.92	216.05	1.27
322.97	5.78	305.52	90.01	4.50	68.93	0.25	1438.20	368.59	1.44
464.26	6.14	419.90	125.15	4.83	107.39	0.25	1661.52	512.83	1.67
0.87	-0.14	1.70				0.25			
15.49	2.74	12.68	5.15	1.64	0.87	0.25	379.79	31.45	0.38
125.26	4.83	125.10	26.75	3.29	19.80	0.25	704.97	113.01	0.71
227.12	5.43	194.77	52.14	3.95	46.49	0.25	964.27	261.57	0.97
441.36	6.09	332.00	95.05	4.55	95.58	0.25	1361.55	616.46	1.36
0.87	-0.14	1.70				0.25			
12.07	2.49	20.13	6.17	1.82	10.91	0.25	243.18	18.25	0.25
63.40	4.15	84.51	13.15	2.58	9.14	0.25	398.82	38.49	0.40
104.01	4.64	126.66	19.79	2.98	4.51	0.25	501.65	67.96	0.51
407.29	6.01	282.47	66.48	4.20	54.89	0.25	1037.50	168.99	1.04
0.87	-0.14	1.70				0.25			
10.84	2.38	13.37	5.85	1.77	10.07	0.25	230.44	32.84	0.23
54.11	3.99	37.67	15.31	2.73	3.03	0.25	398.37	73.34	0.40
84.47	4.44	60.12	20.50	3.02	1.99	0.25	468.26	93.28	0.47
224.08	5.41	140.41	41.24	3.72	25.09	0.25	752.59	193.68	0.76

Table F.15: Fayette County Clay test data (3/4)

Shear Wave				
Under Load		After Rebound		
GuL (MPa)	E (MPa)	Gar (MPa)	Gar*S/f(e) (MPa)	E (MPa)
57.01	142.53	52.06	16.15	130.15
83.82	209.55	62.96	38.57	157.39
126.63	316.59	67.28	53.84	168.20
152.82	382.05	107.05	111.84	267.62
39.88	99.71	47.33	14.89	118.32
78.64	196.59	54.61	39.44	136.52
134.12	335.31	71.26	73.77	178.14
224.88	562.19	94.65	152.36	236.64
35.99	89.97	28.83	6.82	72.08
46.74	116.84	72.88	40.04	182.21
66.22	165.56	110.73	85.44	276.83
79.93	199.82	107.51	186.63	268.78
69.74	174.36	36.03	8.87	90.07
90.54	226.36	60.55	33.94	151.38
98.09	245.22	79.02	59.31	197.56
127.16	317.91	101.25	138.58	253.12

Table F.16: Fayette County Clay test data (4/4)

SSG		
After Rebound		
k (MN/m)	Gssg (MPa)	Gssg/f(e) (MPa)
9.27	34.45	23.63
13.32	33.73	37.43
24.03	61.31	82.26
19.01	48.59	78.80
5.87	16.42	10.41
10.72	30.21	34.44
13.01	37.96	55.90
15.65	47.21	95.25
3.97	11.56	5.65
11.69	32.82	29.07
15.04	42.94	48.39
16.50	44.29	88.88
3.82	18.98	8.79
9.10	29.18	24.11
12.11	37.97	38.57
20.80	62.04	96.57

REFERENCES

ASTM Standard 2487/2488, 2011, "Standard Practice for Classification of Soils for Engineering Purposes (Unified Soil Classification System)" ASTM International, West Conshohocken, PA, 2011, DOI: 10.1520/D2487-11, www.astm.org

ASTM Standard 4318, 2010, "Standard Test Methods for Liquid Limit, Plastic Limit, and Plasticity Index of Soils" ASTM International, West Conshohocken, PA, 2010, DOI: 10.1520/D4318-10, www.astm.org

ASTM Standard D4428, 2007, "Standard Test Methods for Crosshole Seismic Testing" ASTM International, West Conshohocken, PA, 2007, DOI: 10.1520/D4428_D4428M-07, www.astm.org

ASTM Standard D558, 2011, "Standard Test Methods for Moisture-Density (Unit Weight) Relations of Soil-Cement Mixtures" ASTM International, West Conshohocken, PA, 2011, DOI: 10.1520/D0558-11, www.astm.org

ASTM Standard D6758, 2008, "Standard Test Method for Measuring Stiffness and Apparent Modulus of Soil and Soil-Aggregate In-Place by Electro-Mechanical Method" ASTM International, West Conshohocken, PA, 2008, DOI: 10.1520/D6758-08, www.astm.org

Carman, P.E. 1956. Flow of Gases Through Porous Media, Academic, New York.

Das, B.M. 2008. Advanced Soil Mechanics. Taylor and Francis, Abington, Oxon, United Kingdom.

Environmental Protection Agency (EPA). 2012. General Crosshole Procedures. <www.epa.gov/esd/cmb/GeophysicsWebsite/pages/reference/methods/Borehole_Geophysical_Methods/General_Crosshole_Procedures.htm> (May, 2013)

Fredlund, D.G., and Rahardjo, H. 1993. Soil mechanics for unsaturated soils. John Wiley and Sons, Inc., New York.

Fredlund, D.G. 1995. Predictions of Unsaturated Soil Functions Using the Soil-Water Characteristic Curve. *Bengt B. Broms Symposium in Geotechnical Engineering*, Singapore, Malaysia, December 13-16.

Fredlund, D.G., and Xing, A. 1994. Equations for the soil-water characteristic curve. Canadian Geotechnical Journal, 31(3), 521–532.

GeoVision. 2012. SASW Method. Corona, CA. <www.geovision.com> (May, 2013)

Hardin, B.O. 1965. Dynamic versus Static Shear Modulus for Dry Sand. Materials Research and Standards, ASTM. 5: 232-235. Lanham, MD.

Hardin, B.O., and Black, W.L. 1968. Vibration Modulus of Normally Consolidated Clay. *Journal of the Soil Mechanics and Foundations Division.* ASCE. 95(2): 1531-1537.

Hardin, B.O., and Black, W.L. 1969. Closure to Vibration Modulus of Normally Consolidated Clay. *Journal of the Soil Mechanics and Foundations Division.* ASCE. 98(2):1531-1537.

Hardin, B.O., and Richarrt, F.E. 1963. Elastic Wave Velocities in Granular Soils. *Journal of the Soil Mechanics and Foundations Division,* ASCE. 89(1): 33-65.

Huff, J. 2010. Investigation of Humboldt GeoGauge for Quality Control of Compacted Subgrades. *Master's Thesis*. University of Kentucky, Lexington, KY.

Humboldt Manufacturing Company. 2007. *GeoGauge User Guide.* User Guide, Norridge: Humboldt Mfg. Co.

Kidd, B. 2011. Constitutive Mechanical Relationship for Compacted Unsaturated Soils. *Master's Thesis*. University of Kentucky, Lexington, KY.

Larsson, R., and Mulabdic, M. 1991. Shear moduli in Scandinavian clays; measurement of initial shear modulus with seismic cones, Report No 40. Swedish Geotechnical Institute. Linkoping. 127.

Lenke, L.R., McKeen, G., Grtush, M.P. (1999). Evaluation of the Humboldt GeoGauge on Dry Cohesionless Silica Sand in a Cubical Test Bin. ATR Institute. University of New Mexico. Albuquerque, NM.

Lenke, L.R., McKeen, G., Grtush, M.P. (2003). Laboratory Evaluation of the GeoGauge for Compaction Control. Transportation Research Board Annual Meeting. Washington D.C.

Nazzal, M.D. (2002). Field Evaluation of In-Situ Test Technology for Q_C/Q_A During Construction of Pavement Layers and Embankments. Thesis. Louisiana State University. Baton Rouge, LA.

Ng, C.W., and Menzies, B. 2007. Advanced Unsaturated Soil Mechanics and Engineering. Taylor and Francis, New York, NY.

Ng, C.W.W., and Yung, S.Y. 2007. Determination of anisotropic shear stiffness of an unsaturated decomposed soil. *Géotechnique*, 58(1), 23-35.

Pico Technology Limited. 2007. PicoScope 3000 Series PC Oscilloscopes. User's Guide.

Salem, M. A. 2006. Stiffness of Unsaturated Compacted Clays at Small Strains. *Ph.D. Dissertation*. The University of Texas at Austin. Austin, TX.

Sawangsuriya, A., Edil, T.B., Bosscher, P. J. 2005. Evaluating Stiffness and Strength of Pavement Materials. *Geotechnical Engineering*. I58:217-230

Schneider, J. A., Hoyos, L., Mayne, P., Macari, E., Rix, G. 1999. Field and Laboratory Measurements of Dynamic Shear Modulus of Piedmont Residual Soils. Behavioral Characteristics of Residual Soils, GSP 92. ASCE. Reston, VA. 12-25

Takkabutr, P. 2006. Experimental Investigations on Small-Strain Striffness Properties of Partially Saturated Soils via Resonant Column and Bender Element Testing. *Ph.D. Dissertation*. The University of Texas at Austin. Austin, TX.

Vanapalli, S.K., Fredlund, D.G., and Pufahl, D.E. 1996. The relationship between the soil-water characteristic curve and the shear strength of a compacted glacial till. *Geotechnical Testing Journal*, 19 (3): 259-268.

Zhou, A.N., Sheng, D, and Carter, J.P. 2012. Modeling the effect of initial density on soil-water characteristic curves. *Géotechnique.* 62 (8), 669-680.

VITA

Jason Michael Curd grew up in Lexington Kentucky and obtained a Bachelor of Science Degree in Civil Engineering in 2011. He sat for the Engineer in Training (EIT/FE) exam in 2011. He is a professional member of the American Society of Civil Engineers (ASCE) and the United States Society on Dams (USSD). He is also a student member of the Kentucky Society of Professional Engineers.

Professional Publications

Curd, J., Bryson, L.S., and Kalinski, M. (2012), "Sonar for Protection of Maritime Structures", United States Society on Dams 2012 Annual Meeting Conference, USSD, New Orleans, LA, 23-27 April, 2012.

Curd, J., Kirkendoll, J., Dennison, D., Walton-Macaulay, C., Bryson, L.S., Kalinski, M., and Lusk, B. (2012), "Waterside Attacks on Dams; Detect and Track Technologies," *Technical Report*, submitted to the National Institute for Hometown Security, Somerset, KY, June 2012, For Official Use Only (FOUO).